MARTIN MARIETTA ENERGY SYSTEMS LIBRARIES
3 4456 0049392 7

CENTRAL RESEARCH LIBRARY
DOCUMENT COLLECTION
CD

[redacted]

ORNL-3226

AEC RESEARCH AND DEVELOPMENT REPORT

C-84 – Reactors–Special Features of Aircraft Reactors

DECLASSIFIED
CLASSIFICATION CHANGED TO
BY AUTHORITY OF AEC 5-6-70
BY: Joe Gray 12-9-70

AIRCRAFT NUCLEAR PROPULSION PROGRAM

PROGRESS REPORT

FOR PERIOD OF MAY 1, 1961 TO JUNE 30, 1961

CENTRAL RESEARCH LIBRARY
DOCUMENT COLLECTION
LIBRARY LOAN COPY
DO NOT TRANSFER TO ANOTHER PERSON
If you wish someone else to see this document, send in name with document and the library will arrange a loan.

OAK RIDGE NATIONAL LABORATORY
operated by
UNION CARBIDE CORPORATION
for the
U.S. ATOMIC ENERGY COMMISSION

[redacted]

[redacted]

LEGAL NOTICE

This report was prepared as an account of Government sponsored work. Neither the United States, nor the Commission, nor any person acting on behalf of the Commission:

A. Makes any warranty or representation, expressed or implied, with respect to the accuracy, completeness, or usefulness of the information contained in this report, or that the use of any information, apparatus, method, or process disclosed in this report may not infringe privately owned rights; or

B. Assumes any liabilities with respect to the use of, or for damages resulting from the use of any information, apparatus, method, or process disclosed in this report.

As used in the above, "person acting on behalf of the Commission" includes any employee or contractor of the Commission, or employee of such contractor, to the extent that such employee or contractor of the Commission, or employee of such contractor prepares, disseminates, or provides access to, any information pursuant to his employment or contract with the Commission, or his employment with such contractor.

[redacted]

ORNL-3226
C-84 — Reactors—Special Features
of Aircraft Reactors
M-3679 (25th ed.)

This document consists of 112 pages.
Copy 78 of 216 copies. Series A.

Contract No. W-7405-eng-26

AIRCRAFT NUCLEAR PROPULSION PROGRAM
PROGRESS REPORT

for Period of May 1, 1961 to June 30, 1961

A. J. Miller, Program Director

DATE ISSUED
DEC - 8 1961

OAK RIDGE NATIONAL LABORATORY
Oak Ridge, Tennessee
operated by
UNION CARBIDE CORPORATION
for the
U. S. ATOMIC ENERGY COMMISSION

[redacted]

SYSTEMS LIBRARIES
3 4456 0049392 7

[redacted]

FOREWORD

The ORNL-ANP program was discontinued on June 30, 1961, upon the termination of the national ANP program. This progress report covers the two-month period between the last ORNL-ANP semiannual progress report and termination of the program.

For the past three and one-half years the ORNL-ANP program primarily provided research and development support in reactor materials, shielding, and reactor engineering to organizations engaged in the development of air-cooled and liquid-metal-cooled reactors for aircraft propulsion. Most of the work described here was basic to or in direct support of investigations which were carried out at Pratt & Whitney Aircraft Division, United Aircraft Corporation, and General Electric Company, Aircraft Nuclear Propulsion Department.

This report includes a description of the status of each task and information with regard to termination of the task or its continuance in support of some other reactor program. Major portions of the work will be continued under the Space Power Program and the High-Temperature Materials Program.

[redacted]

[redacted]

CONTENTS

PART 1. MATERIALS RESEARCH AND ENGINEERING

1. MATERIALS COMPATIBILITY 3

Oxidation of Columbium and Columbium-Base Alloys 3

Lithium Corrosion Studies 4

Effect of Annealing Temperature on the Corrosion Resistance of Cb–1% Zr Alloy to Lithium 4

Corrosion Resistance of the Cb–1% Zr Alloy in the Aged Condition to Lithium 5

Corrosion Resistance of Oxygen-Contaminated Single Crystals of Columbium to Lithium, Lithium + Li_3N and Lithium + Li_2O 5

Effect of Time on the Corrosion Resistance of Oxygen-Contaminated Columbium Single Crystals to Lithium 6

Corrosion Resistance of Zirconium as a Function of Oxygen Content 6

Potassium Compatibility Studies 6

Purification, Analysis, and Solubility of Oxygen in Potassium 6

Determination of Oxygen in Potassium 7

Boiling-Potassium Compatibility Studies 8

Effect of Oxygen Additions to Cb–1% Zr Alloy on Its Corrosion Resistance to Potassium 9

Oxidation Resistance of Potential Container Materials for Boiling-Potassium Systems 10

Dissimilar-Metal Mass-Transfer Effects in the (Cb–1% Zr)-NaK-Type 316 Stainless Steel System 13

Survey of Columbium-Base Alloys for High-Temperature Service in Liquid-Metal Environments 13

2. AGING STUDIES OF COLUMBIUM-BASE ALLOYS 14

Wrought Material 14

Welded Material 15

Internal-Friction Studies 18

3. MECHANICAL PROPERTIES INVESTIGATIONS 20

4. WELDING AND BRAZING 22

Brazing of Columbium 22

[redacted]

[redacted]

Fabrication of Tube-To-Header Joints of Clad Materials 24

Fabrication of Clad Tubing 25

5. BERYLLIUM OXIDE RESEARCH 28

Phase Relationships in Beryllium Oxide—Metal Oxide Systems 28

The BeO-CaO System 28

The BeO-Eu_2O_3 System 29

The BeO-Y_2O_3 System 29

BeO-MgO-ZrO_2 30

Preparation of Crystalline BeO by Precipitation from Molten Salts 30

Purification of Beryllium Compounds by Solvent Extraction 32

Spectrochemical Analyses of High-Purity Beryllium Oxide 34

6. ENGINEERING AND HEAT-TRANSFER STUDIES 36

Boiling-Potassium Heat-Transfer Experiment 36

Thermophysical Properties 44

7. RADIATION EFFECTS 45

Radiation Effects on Structural Metals 45

Irradiation Damage to BeO 48

Effects of Annealing Irradiated BeO 64

PART 2. SHIELDING RESEARCH

8. APPLIED SHIELDING 69

Tower Shielding Reactor II (TSR-II) 69

Reactor Power Calibration 69

Reactor Linearity 69

Reactor Mechanical System 70

The Pratt & Whitney Divided-Shield Experiment at the Tower Shielding Facility 70

9. DEVELOPMENT OF RADIATION DETECTION EQUIPMENT 73

Gamma-Ray Spectroscopy 73

The Model-IV Gamma-Ray Spectrometer 73

Monte Carlo Calculations of the Pulse-Height Response of NaI(Tl) Scintillation Counters 75

[redacted]

[redacted]

Unscrambling of Scintillation Spectra 75

Neutron Spectroscopy 78

Energy Transmission Functions for Neutron-Chopper Spectrometers 78

Use of Silicon Surface-Barrier Counters in Fast-Neutron Detection and Spectroscopy 79

Experimental Determination of Flux Depression and Other Corrections for Gold Foils Exposed in Water 80

10. BASIC SHIELDING STUDIES 81

Monte Carlo Calculations of Gamma-Ray Penetration Through Shields 81

Grinder — An IBM-704/7090 Monte Carlo Program for Estimating the Scattering of Gamma Rays from a Cylindrical Medium 81

Moments-Method Studies of Neutron Penetration in Be and BeO 82

Spatial and Spectral Details of Neutron Fluxes in Shielding Materials 82

Experiments 82

Calculations 85

Status of the Experiment for Determining the Spectrum of Prompt Gamma Rays from the Fission of U^{235} by Thermal Neutrons 86

Status of the Experiment for Determining the Spectrum of Short-Lived Fission-Product Gamma Radiation 88

Monte Carlo Calculations of Gamma-Ray Heating and Dose-Rate Distributions in Stratified Lead and Water Slabs 89

Experimental Verification of a Geometrical Shielding Transformation 89

11. BIBLIOGRAPHY OF ORNL SHIELDING LITERATURE 91

[redacted]

PART 1. MATERIALS RESEARCH AND ENGINEERING

1. MATERIALS COMPATIBILITY

Oxidation of Columbium and Columbium-Base Alloys

H. Inouye

The effects of oxygen pressure, temperature, gas atmosphere composition, and alloying elements on the oxidation rates of columbium and its alloys have been studied. This information is pertinent to the development of oxidation-resistant alloys for atmospheres containing oxygen in the micron pressure range. Such atmospheres would be encountered in high-temperature liquid-metal heat transfer systems in space or in high-temperature test chambers. The major phases of the research were an oxidation study of unalloyed columbium, a screening study of the effects of alloying elements, and some preliminary studies of oxidation in gas mixtures containing oxygen. A detailed report on the oxidation of unalloyed columbium has been presented,[1] while progress reports can be found elsewhere.[2-5] The principal findings and conclusions are listed below.

The oxidation rates of columbium in oxygen at pressures between 3×10^{-5} to 5×10^{-3} mm Hg and in the temperature range 850 to 1200°C were two or three orders of magnitude lower than at atmospheric pressure. In spite of these reductions in the reaction rates, the metal was severely embrittled after an exposure of 5 to 7 hr. Under these test conditions, columbium oxidized in four distinct stages, which could be correlated with the formation of columbium-oxygen solid solutions, CbO, CbO_2, and Cb_2O_5.

It was deduced from the rate curves and the reaction products that the following events occurred during each stage. Columbium-oxygen solid

---

[1]H. Inouye, The Oxidation of Columbium at Low Oxygen Pressures, Paper presented at the Columbium Metallurgy Symposium, June 1960, Lake George, N. Y.

[2]ANP Semiann. Prog. Rep. April 30, 1960, ORNL-2942, pp. 3–7.

[3]ANP Semiann. Prog. Rep. Oct. 31, 1960, ORNL-3029, pp. 3–6.

[4]ANP Semiann. Prog. Rep. April 30, 1961, ORNL-3144, pp. 3–9.

[5]Met. Div. Ann. Prog. Rep. May 31, 1961, ORNL-3160.

solutions formed when the rate of oxygen diffusion within the metal was high enough to prevent the buildup of a sharp oxygen gradient at the metal surface. Favorable conditions were therefore low oxygen pressures and high temperatures. Initially the weight gain was linear with time, but it became parabolic as the solubility limit of oxygen in columbium was approached.

When the columbium matrix was saturated with oxygen, columbium oxide precipitated internally as fast as oxygen was taken into solution, giving rise again to linear weight gains. The columbium oxide that precipitated from solid solution was nearer the surface as the oxygen pressure was increased, until finally nodules of CbO were nucleated at the metal-gas interface. The observed reaction rates were proportional to the oxygen pressure up to 1×10^{-4} mm Hg and above this pressure varied approximately as the square root of the pressure.

The beginning of the third stage of oxidation was detected by a transition in the weight gain from linear to parabolic and the formation of a continuous oxide surface layer. The time at which the transition begins depends upon the temperature and the oxygen pressure. The new oxide phase associated with the parabolic weight gains is CbO_2, which forms on the CbO. When temperature and pressure conditions are favorable for the formation of CbO_2, the weight gains are parabolic and insensitive to the oxygen pressure, suggesting that the rate-controlling reaction is the diffusion of the reactants through the CbO_2 layer. At pressures between 4×10^{-4} and 2×10^{-3} mm Hg, CbO_2 is the stable oxide at the gas interface for the temperatures studied.

The fourth oxidation stage of columbium commenced when the oxygen reacted with the CbO_2 to form Cb_2O_5. The reaction was characterized by a transition, commonly called the "break-away" phenomenon, from a parabolic to an extremely fast linear weight gain. The reaction products on these specimens consisted of Cb_2O_5 at the gas interface, a uniform sublayer of CbO_2, and an irregular zone of CbO. Prior to this investigation, the presence of CbO and CbO_2 as intermediate oxides between Cb_2O_5 and the metal was postulated but not observed by other investigators.

The third and fourth oxidation stages of columbium observed at low oxygen pressures were concluded to be representative of the initial oxidation stage of the metal at atmospheric pressures. The break-away phenomenon observed here and those observed by several other investigators may be due to a reduction in the thickness of the protective CbO_2 layer as it forms Cb_2O_5.

The constant oxidation rates subsequent to the break-away were concluded to be due to a dynamic equilibrium between the rate of growth in thickness of the CbO_2 layer and the rate of its reduction in thickness as it was converted to the Cb_2O_5. Since the thickness of the CbO_2 layer depends upon the oxygen pressure (this oxide has not been detected when columbium is oxidized at atmospheric pressure), reaction rates associated with Cb_2O_5 formation should be a function of the oxygen pressure. This has been observed experimentally.[6]

The oxidation rates of columbium in low-pressure oxygen were about an order of magnitude greater than in air at equivalent partial pressures of oxygen. This behavior has been interpreted as being due to the competition of both the nitrogen and the oxygen in the air for the available absorption sites. The conclusion was partly based on the experimental evidence that when oxide films were not formed on the metal surface, the reaction rates in pure oxygen were pressure sensitive. This indicates that chemisorption is a preliminary step in the oxidation mechanism. Further support for the hypothesis that the observed reduction in oxidation rate is due to the presence of nitrogen in a chemisorbed layer rather than in a columbium nitride layer is provided by the observation that a nitride layer on columbium is ineffective in reducing the rate of reaction with pure oxygen.

At atmospheric pressure, the oxidation resistance of columbium can be improved by two or three orders of magnitude by alloying. At low oxygen pressures, such improvements in the oxidation resistance were not observed up to temperatures of 1200°C. In fact alloying for low-pressure

---

[6]D. W. Bridges and W. M. Fassel, Jr., J. Electrochem. Soc., 103: 326–30 (1956).

applications was concluded to be detrimental, since reaction rates equal to or greater than those of the unalloyed metal were observed.

Alloying elements that accelerated the oxidation rates were titanium, zirconium, beryllium, aluminum, rhenium, thorium, and the rare earths. Elements having a negligible effect on the reaction rates were molybdenum, tungsten, tin, and palladium. These observations led to the conclusion that when the added element formed oxides more stable than columbium oxides, it acted as an oxygen scavenger and a sink for dissolved oxygen.

Future work in this and related areas will be presented in Space Power Program reports, High Temperature Materials Program reports and Metallurgy Division annual reports.

Lithium Corrosion Studies

J. R. DiStefano E. E. Hoffman

Compatibility studies to determine the mechanism of corrosion in oxygen-contaminated refractory metals when exposed to lithium at elevated temperatures have indicated the importance of variables that influence the form in which oxygen is present. A series of experiments to examine the effect of these and other variables on the corrosion process are discussed below. Future work on this topic will be presented in Space Power Program reports, High Temperature Materials Program reports and Metallurgy Division annual reports.

Effect of Annealing Temperature on the Corrosion Resistance of Cb–1% Zr Alloy to Lithium

Past work[7] has shown that oxygen additions to Cb–1% Zr alloy at 1830°F reduces the corrosion resistance of the alloy to lithium at 1500°F. It has also been demonstrated that a high-temperature annealing treatment (2200–3600°F) restores the corrosion resistance of Cb–1% Zr alloy to lithium.[8,9] In a recent test, 2000 ppm of oxygen was added to a Cb–1%

[7]ANP Semiann. Prog. Rep. Oct. 31, 1960, ORNL-3029, p. 7.

[8]Ibid., p. 8.

[9]ANP Semiann. Prog. Rep. Oct. 31, 1959, ORNL-2840, p. 32.

Zr alloy specimen at 1830°F (1000°C). The specimen was annealed 70 hr at 1830°F prior to exposure to lithium for 100 hr at 1500°F. No attack of the Cb–1% Zr alloy was observed. In the absence of an annealing treatment prior to exposure, complete attack of the 0.040-in.-thick specimen was observed. This result indicates that annealing for longer times at lower temperatures is also a suitable treatment for restoring corrosion resistance.

Corrosion Resistance of the Cb–1% Zr Alloy in the Aged Condition to Lithium

Two tensile specimens of Cb–1% Zr alloy which contained 1000 ppm of oxygen were annealed for 2 hr at 3600°F. One of the specimens was aged for 75 hr at 1700°F, and both specimens were then tensile tested at 1700°F. The aged specimen had an ultimate tensile strength of 37 500 psi compared with 21 000 psi for the annealed specimen. The elongation in the aged condition (2-in.-gage length) was 3% compared with 12% in the annealed condition. Both specimens were then exposed to lithium for 100 hr at 1500°F, and under these conditions both specimens were unattacked. It is, therefore, concluded that the phase responsible for aging is either corrosion resistant to lithium or the lithium does not have access to it.

Corrosion Resistance of Oxygen-Contaminated Single Crystals of Columbium to Lithium, Lithium + Li_3N, and Lithium + Li_2O

Past work[10] had indicated that the corrosion resistance of oxygen-contaminated columbium to lithium plus Li_2O might be better than the corrosion resistance to pure lithium or lithium plus Li_3N. These previous tests were conducted on polycrystalline columbium and the interpretation of these results was complicated by the effect of grain orientation and grain-boundary oxides on the observed attack. Recent tests of specimens from an oxygen-contaminated single crystal, however, seem to indicate that the addition of Li_3N and Li_2O to lithium has no effect on the corrosion susceptibility of columbium to lithium. Further tests are planned to resolve the apparent discrepancies.

---

[10]ANP Semiann. Prog. Rep. April 30, 1961, ORNL-3144, p. 9.

Effect of Time on the Corrosion Resistance of Oxygen-Contaminated Columbium Single Crystals to Lithium

Single crystals of oxygen-contaminated columbium (4500 ppm O_2) were exposed to lithium for 0.1 to 1000 hr at a temperature of 1500°F. Preliminary results from metallographic examination of these specimens indicates that this columbium is attacked to a depth of 15 mils by lithium after only 0.1 hr exposure.

Corrosion Resistance of Zirconium as a Function of Oxygen Content

Zirconium specimens containing from 200 to 3500 ppm O_2 were exposed to lithium at 1500°F for 100 hr. Metallographic examination of the specimens after exposure to the lithium failed to reveal any evidence of corrosion.

Potassium Compatibility Studies

J. R. DiStefano E. E. Hoffman
D. H. Jansen A. P. Litman

Purification, Analysis, and Solubility of Oxygen in Potassium

Potassium is currently being considered as a potential working fluid for Rankine cycle turbine-generator reactor systems. Previous studies[11] on oxygen contamination in sodium have indicated that it can lead to increased corrosion, as well as to plugging of systems with sodium oxide at high oxygen concentrations. In this regard, studies have been initiated to develop detailed information on the potassium-oxygen system. These studies include (1) evaluation of the existing analytical procedures for determing oxygen in potassium, (2) determination of the solubility of oxygen in potassium as a function of temperature, (3) development of purification techniques for removing oxygen from potassium, and (4) determination of the effect of the oxygen concentration in potassium on corrosion.

---

[11]Technical Progress Reviews, Reactor Core Materials, p. 28, Vol. 1, No. 2, Prepared for U. S. Atomic Energy Commission by Battelle Memorial Institute, Columbus, Ohio, 1958.

The n-butyl bromide method[12] for oxygen determination in sodium is being extended to include the determination of oxygen in potassium, rubidium, and cesium. Preliminary data comparing this method with the mercurcy-amalgamation method for the determination of oxygen in potassium are being obtained, and possible sources of error in both methods are being examined.

A recent trial run to prepare K_2O by initial reaction of excess potassium with CO_2 and with H_2O-free air at 135°C, plus final reaction with oxygen at 170°C, produced a beige, homogeneous product. X-ray diffraction analysis indicated the product to be 90% K_2O. The remaining 10% was unidentified. This run was made by the Inorganic Preparation Laboratory (Chemistry Division) in glass equipment.

Initial attempts to prepare the monoxide by reaction of excess potassium with KNO_2 were unsuccessful. Purification of potassium by hot-gettering with titanium sponge has proved to be effective. Oxygen contents have been reduced from 2700 ppm to a level of approximately 200 ppm. These were previously reported[13] as 270 and 20 ppm because of an error in the analytical chemistry calculation manual. Additional purification tests utilizing zirconium, zirconium-titanium alloys, and yttrium are planned. No results are available on the effect of oxygen concentration in potassium on corrosion, since test preparation requires a potassium oxide addition and good analytical chemistry procedures.

Determination of Oxygen in Potassium (H. E. Zittel, G. Goldberg)

The amalgamation[14] and alkyl halide[15] methods for the determination of oxygen in sodium and sodium-potassium alloy are being evaluated for application to the determination of oxygen in potassium. In addition, the problem of sampling techniques is also under investigation. The use of stainless steel containers is indicated to be more conducive to the

[12] J. C. White, W. J. Ross, and R. Rowan, Jr., Anal. Chem., 26: 210 (1954).

[13] ANP Semiann. Prog. Rep. April, 30, 1961, ORNL-3144, p. 24.

[14] L. P. Pepkowitz and W. C. Judd, Anal. Chem., 22: 1283 (1950).

[15] J. C. White, W. J. Ross, and R. Rowan, Jr., Anal. Chem., 26: 210 (1954).

obtaining of representative samples of potassium metal than use of glass or copper containers. With respect to the methods of analysis, studies are in progress to determine the relative accuracy and precision of the amalgamation and butyl bromide methods for determining oxygen in potassium metal. The variables in each method are being studied for determining their effect on accuracy. The effect of CO_2 in both the reaction vessel and the titration vessel is under investigation for both techniques. There is reason to believe that the presence of CO_2 in the reaction vessel of the amalgamation vessel particularly will lead to erroneous results. This work will be continued in the future as part of the High-Temperature Materials Program.

Boiling-Potassium Compatibility Studies

A testing program is being conducted for determining the compatibility of boiling potassium at 1600°F (871°C) with conventional iron-, nickel-, and cobalt-base structural alloys. Previous reports in this series describe both the refluxing capsules[16] and the natural-circulation boiling loops[17] used in this evaluation. The results of this work and allied work to be initiated on refractory metal alloys will appear in future Space Power Program reports, High-Temperature Materials Program reports, and in the Metallurgy Division annual reports.

Refluxing-Potassium Capsule Tests. Type 310 stainless steel, type 316 stainless steel, Haynes Alloy No. 25, and Inconel have been tested at a temperature of 1600°F for a time period of 1000 hr.[18,19] The type 310 stainless steel test capsule and the Inconel test capsule had maximum weight losses in the condenser regions of 9 and 3 mg/in.^{2}, respectively. No attack was observed metallographically in the condenser regions of the type 310 stainless steel capsule, but intergranular attack to a depth of 7 mils was found in the Inconel.

---

[16] ANP Semiann. Prog. Rep. Oct. 31, 1960, ORNL-3029, pp. 14–15.

[17] Ibid., p. 18.

[18] Ibid., pp. 16–17.

[19] ANP Semiann. Prog. Rep. April 30, 1961, ORNL-3144, p. 23.

Boiling-Potassium Loop Tests. A type 316 stainless steel boiling-potassium loop test was conducted for 3000 hr with a boiler temperature of 1600°F. The mass flow rate (170 g/min) and the vapor flow rate (46 ft/sec) were determined by means of a heat balance on the condenser. Metallographic examination of tensile specimens located at various locations around the loop and of the pipe wall revealed a maximum attack of 2 mils at the liquid-vapor interface in the boiler and mass-transfer deposits to a depth of approximately 3 mils in the coldest regions of the loop.[20]

Boiling-potassium loops constructed of Inconel and Haynes Alloy No. 25 are currently in operation at conditions duplicating those that existed in the type 316 stainless steel loop described above. These loops are scheduled to be examined after 3000 hr of operation. A Haynes Alloy No. 25 boiling-potassium loop is being designed to operate at 1800°F (982°C). The design of this loop is such that quantitative data regarding metal losses from the condenser wall can be obtained.

Effect of Oxygen Additions to Cb–1% Zr Alloy on Its Corrosion Resistance to Potassium

Columbium–1% zirconium alloy specimens containing from 100 to 3000 ppm O_2 were exposed to potassium at 1500°F for 100 hr. Metallographically no attack of the Cb–1% Zr alloy was observed after this exposure. The oxygen additions were made at 1000°C, and under these conditions the specimens would have shown increasing attack as a function of oxygen concentration if they had been exposed to lithium. The difference in behavior in potassium and in lithium is believed to occur because the oxides of potassium are thermodynamically less stable than the oxides of columbium, while the oxides of lithium are more stable. Since the oxides of all the alkali metals except lithium are less stable than the columbium oxides, it is tentatively concluded that the corrosion phenomenon observed in the Cb(O)-Li system will not occur with any of the other alkali metals.

---

[20]ANP Semiann. Prog. Rep. Oct. 31, 1960, ORNL-3029, pp. 18–22.

Oxidation Resistance of Potential Container Materials for Boiling-Potassium Systems

In order to utilize simple test equipment to evaluate the compatibility of various conventional alloys with boiling potassium, it is necessary that these alloys possess adequate oxidation resistance in the temperature range from 1800 to 2000°F. Several alloys have been given screening tests to determine their relative oxidation resistance. The results of these short-time tests are given in Table 1.1. Type 318 stainless steel, which contains columbium, displayed surprisingly good oxidation resistance at 2000°F. Although the mechanism for this resistance is not known, other investigators have found similar results with Chromel P alloy containing small amounts of columbium.[21]

Table 1.1. Results of 100-hr Oxidation Tests in Static Air of Potential Container Materials for Boiling Potassium

Material	Nominal Composition (wt %)	Thickness of Surface Layer Affected by Test[a] (mils)	
		1800°F	2000°F
Inconel	78 Ni–14 Cr–7 Fe	0.5	1.0
Haynes alloy No. 25	50 Co–20 Cr–15 W–10 Ni–3 Fe	0.5	2.5
Haynes alloy No. 56	46 Fe–21 Cr–13 Ni–11 Co–5 Mo–2 Fe	2.0	3.0
Type 310 stainless steel	52 Fe–25 Cr–20 Ni–2 Si	2.0	4.0
Type 316 stainless steel	69 Fe–17 Cr–12 Ni–2 Mo	4.5	11.0
Type 318 stainless steel	67 Fe–17 Cr–12 Ni–2 Mo–1 Cb	5.0	2.0
Type 446 stainless steel	75 Fe–25 Cr	0.5	7.0

[a]Includes metal converted to oxide and areas in which subsurface oxidation occurred.

[21]J. F. Potts and D. L. McElroy, Thermocouple Research to 1000°C, Final Report, ORNL-2773, pp. 27–8, Jan. 16, 1961.

Dissimilar-Metal Mass-Transfer Effects in the (Cb–1% Zr)-NaK-Type 316 Stainless Steel System

J. R. DiStefano E. E. Hoffman

In the isothermal static system (Cb–1% Zr)-NaK-type 316 stainless steel, nitrogen has been observed to transfer from the type 316 stainless steel to the Cb–1% Zr alloy. This increase in nitrogen concentration results in an increase in tensile strength and reduction in ductility of the Cb–1% Zr alloy. A report summarizing the results from tests of this system will be issued in the near future.

Survey of Columbium-Base Alloys for High-Temperature Service in Liquid-Metal Environments

D. O. Hobson

An alloy suitable for use in high-temperature (2000 to 2500°F), liquid-metal (Li, Na, K, Rb) environments such as those considered for space power reactors should combine high-temperature strength and creep resistance, corrosion resistance, contamination resistance, and acceptable aging properties. A critical analysis of available literature is being prepared to gain some insight into the effects of alloy additions on these properties of columbium alloys. An important conclusion already reached is that columbium-base alloys which have yield strengths of 25 000 to 45 000 psi in the temperature range 2000 to 2500°F can be developed. Few data are available on the creep properties of these high-strength alloys. Data are available, however, on the corrosion resistance and stability of columbium alloys, and it appears that alloys can be developed that will not be seriously damaged by corrosion or aging in the systems of interest. Additions of a third or fourth element to the columbium-vanadium binary system may give a new alloy with improved properties.

2. AGING STUDIES OF COLUMBIUM-BASE ALLOYS

Wrought Material

D. O. Hobson

It has been shown that the Cb–1% Zr (FS-80) alloy ages under certain conditions of composition and heat treatment. Moreover, it has been observed that a high-temperature solution anneal followed by a lower temperature aging treatment can cause substantial increases in the tensile strength of the alloy, together with a loss in ductility.

Recent experiments[1] have shown that aging did not occur when zirconium was absent or when the major impurity in the alloy was carbon or nitrogen up to 370 ppm. Further experiments indicated that, within the range of heat treatment and composition investigated, the phase or phases responsible for the aging reactions observed at 927°C were compounds of zirconium and oxygen.

The variables investigated were the aging times at 927°C, oxygen levels up to 1000 ppm, and annealing temperatures of 1600, 1800, and 2000°C. The alloys studied included 13 heats of columbium with 1 wt % zirconium (nominal) and alloys with controlled amounts of oxygen. The aging reactions were followed by measuring the changes in the tensile properties and hardness and by metallographic examination.

Variations in the aging response of the alloy have been shown to be a function of the oxygen content and the annealing temperature.[2] When the oxygen content is increased, the annealing temperature also has to be increased to obtain an equivalent aging response. If specimens with various oxygen contents are annealed at a given temperature, the specimens with the highest oxygen contents have the lowest strengths. For a given oxygen content, specimens annealed at the higher temperatures showed

---

[1]D. O. Hobson, Aging Phenomena in Columbium-Base Alloys, Paper Presented at the AIME High-Temperature Materials Conference, Cleveland, Ohio, April 26–27, 1961.

[2]ANP Semiann. Prog. Rep. April 30, 1961, ORNL-3144, pp. 28–31.

greater aging reactions. At very low oxygen levels (approximately 50 ppm O_2), aging reactions were not induced by any of the heat treatments.

In order to fully understand the aging of this alloy, the phase relationships of the columbium-rich corner of the columbium-zirconium-oxygen diagram must be determined. Because of the variations in the aging response induced by the solution-annealing temperature, it is thought that the annealing temperatures place the alloy within a two-phase field and the alloy is not a homogeneous solid solution of columbium-zirconium-oxygen. Efforts are presently under way to obtain more quantitative information on these phase relationships. Lattice parameter measurements are being made on specimens of Cb–1% Zr alloys containing various amounts of oxygen. These measurements are being made on specimens in both the annealed and aged conditions. Future progress will be described in the Space Power Program reports and other reports previously listed.

Welded Material

E. A. Franco-Ferreira

High-temperature aging reactions in welds of Cb–1% Zr alloy have been investigated, including studies of the effectiveness of a postwelding heat treatment on welds of high oxygen-containing Cb–1% Zr alloy. Mechanical property tests have indicated[3] that welds with as much as 4200 ppm O_2 can be made to exhibit good ductility by a 3-hr treatment at 2100°F. Figure 2.1 shows the as-welded microstructure of weld metal having the following composition: O_2, 1700 ppm; N_2, 180 ppm; C, 150 ppm; H_2, 6 ppm; Zr, 0.87%. It may be seen that a considerable amount of precipitated phase is present in the grain and subgrain boundaries. This is to be expected in view of the high oxygen content. As reported before, this weld was quite brittle.

The microstructure of the same weld after heat treatment for 3 hr at 2100°F is shown in Fig. 2.2. The appearance of a heavy network of

[3]Ibid., pp. 31–36.

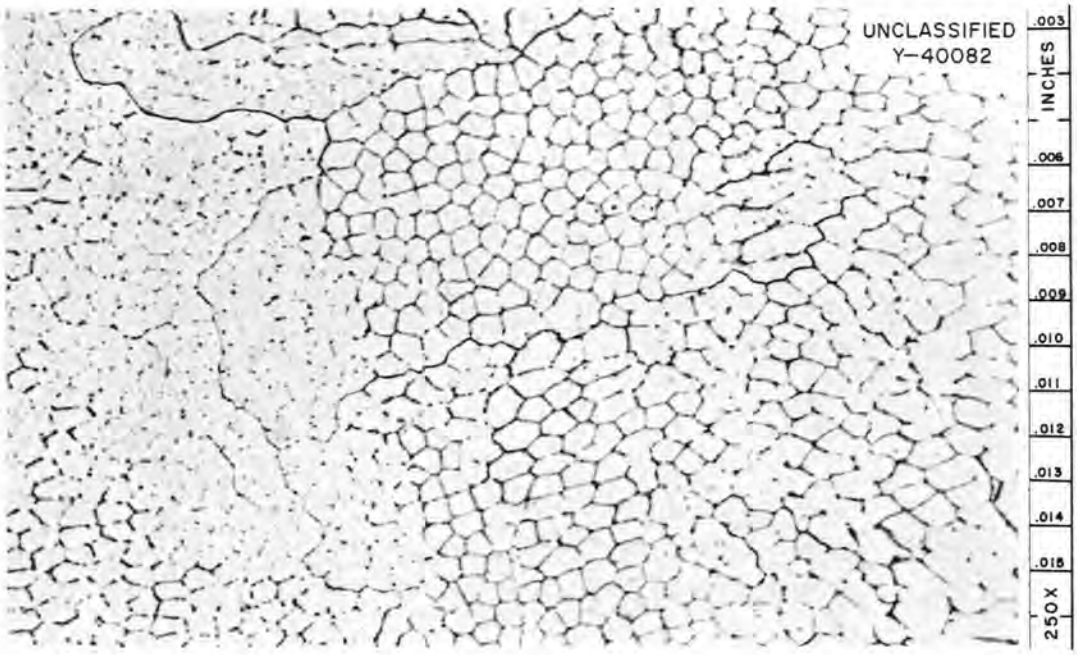

Fig. 2.1. As-Welded Microstructure of High-Oxygen-Containing Cb–1% Zr Alloy. Etchant: 50 parts lactic acid, 30 parts nitric acid, and 4 parts hydrofluoric acid; 1-min swab. 250X

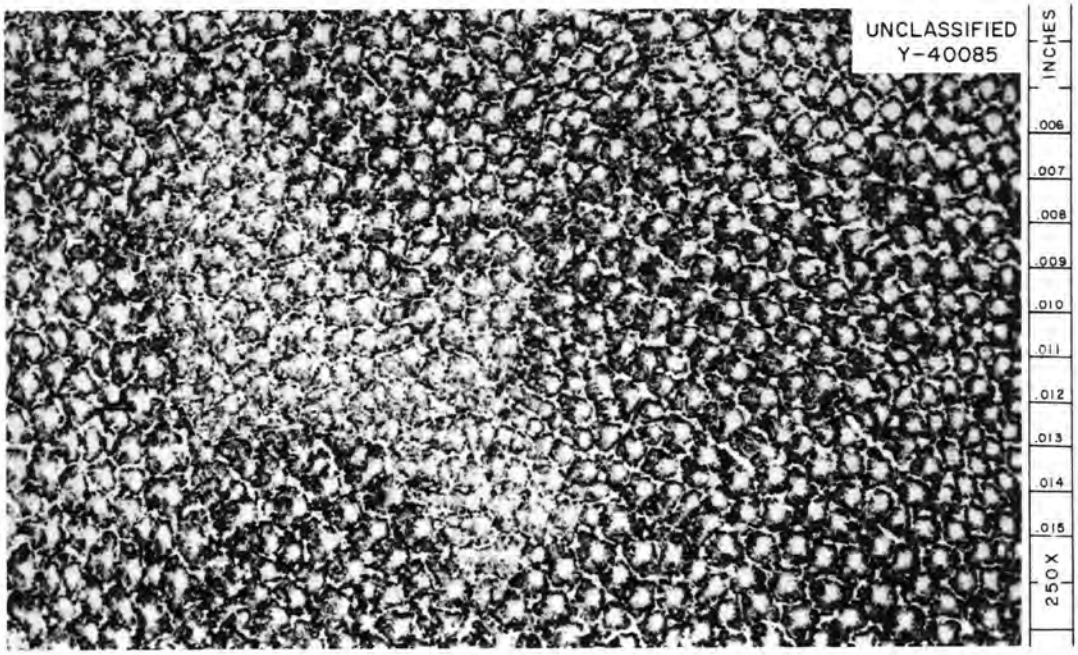

Fig. 2.2. Weld Metal of High-Oxygen-Containing Cb–1% Zr Alloy After Heat Treating and Annealing 3 hr at 2100°F. Etchant: 50 parts lactic acid, 30 parts nitric acid, and 4 parts hydrofluoric acid; 1-min swab. 250X

precipitated phase is similar to that reported in previous studies.[3] The ductility of the weld in this condition was good.

It should be noted that all welds examined were made in material whose oxygen content was high before welding. This study shows that a postwelding heat treatment will result in recovery of the desired mechanical properties even if welds are made in contaminated material. However, it should be observed that extensive microcracks of the type shown in Fig. 2.3 were found in a number of the highly contaminated welds. These cracks developed during welding and were not heated by subsequent thermal treatments.

The work on the welding of columbium and the Cb–1% Zr alloy has been completed and a final report is being prepared. In general, it appears that fabrication of this material by welding is feasible. Proper precautions must be taken, however, to ensure against contamination of the weld by the atmosphere. Welds in Cb–1% Zr alloy are quite subject to

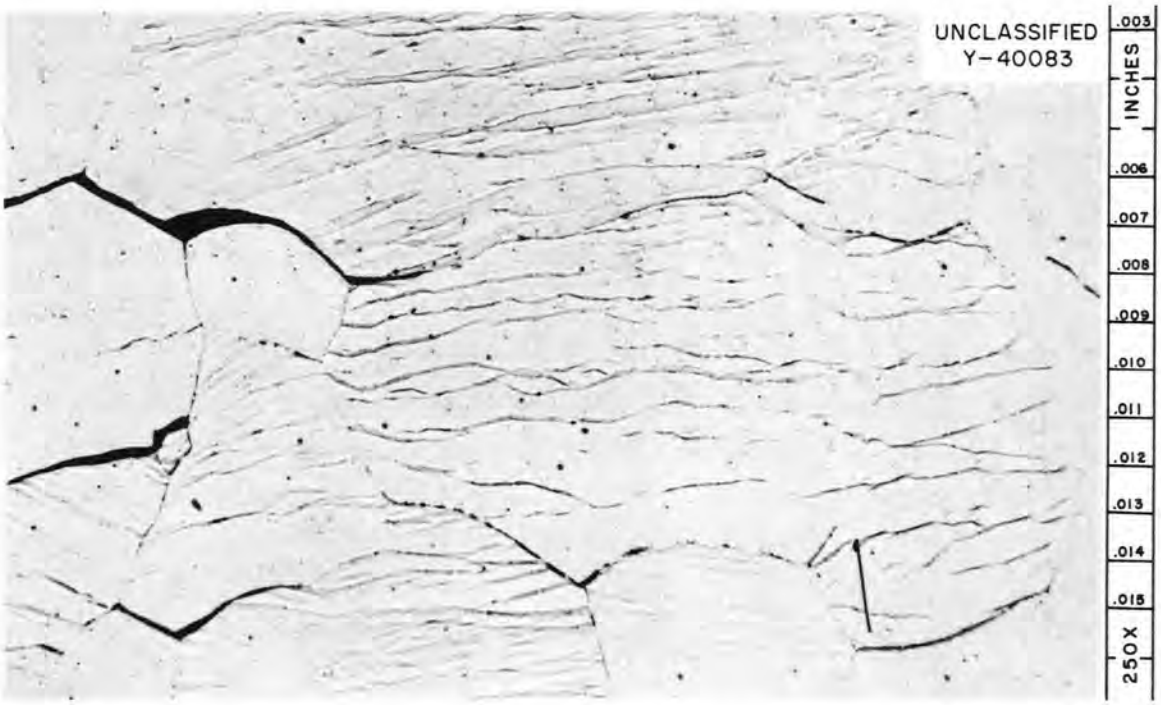

Fig. 2.3. Microcracks in Welds in High-Oxygen-Containing Cb–1% Zr Alloy. Etchant: 50 parts lactic acid, 30 parts nitric acid, and 4 parts hydrofluoric acid; 1-min swab. 250X

embrittlement by aging, but postwelding heat treatment in the temperature range of 2000 to 2200°F restores ductility.

Internal-Friction Studies

R. L. Stephenson

The existence of an aging reaction in Cb–1% Zr has been demonstrated,[4] and this reaction, as mentioned above, is currently thought to involve oxygen. Internal-friction measurements for studying the precipitation of interstitial solutes from supersaturated solid solutions in body-centered cubic metals[5-7] are being used as a means of studying this observed aging. A torsional pendulum has been constructed and a device for automatically sensing and recording the vibrational amplitude as a function of time has been developed. In order to identify the peaks present in the Cb–1% Zr alloy internal-friction spectrum, measurements have been made on pure columbium and on alloys containing 0.66, 0.74, and 1.09% Zr. The 0.66% Zr alloy shows narrow peaks at approximately 155 and 290°C, while a broad peak appears at approximately 440°C. The peak at 440°C declines in height upon aging. The 0.74% Zr alloy shows a peak at approximately 210°C and a complex peak between 300 and 500°C. This peak is apparently composed of at least two superimposed peaks. The heights of all of these peaks decline upon aging. A specimen of the 1.09% Zr alloy containing small amounts of interstitial impurities shows peaks at approximately 270 and 410°C, both of which disappear upon aging.

There are insufficient data at this time to determine with any certainty the elements responsible for peaks in the various alloys or the mechanics responsible for the changes in peak heights with aging time.

---

[4]D. O. Hobson, A Preliminary Study of the Aging Behavior of Wrought Columbium–1% Zirconium Alloys, ORNL-2995, Jan. 6, 1961.

[5]C. Wert, Phenomena Accompanying Precipitation from Solid Solutions of C and N in Alpha-Iron, p. 178 in Thermodynamics in Physical Metallurgy, American Society for Metals, Cleveland, Ohio, 1950.

[6]P. M. Robinson and R. Rowlings, Iron and Steel, 31: 65 (1958).

[7]A. S. Nowick, Progr. in Metal Phys., 4: 37 (1953).

The results of future work in this area will be reported in Space Power Program reports and others previously listed.

3. MECHANICAL PROPERTIES INVESTIGATIONS

R. L. Stephenson

An out-of-pile tube-burst test program is being conducted to provide control data for comparison with in-pile tube-burst data. A tube-burst test apparatus[1] capable of operation at 2200°F and above has been developed and constructed. One furnace has now operated successfully for 1600 hr, and data have been obtained on the tube-burst strength of Cb–1% Zr alloys at 1800 and 2000°F. These data are summarized and compared with the data of other investigators[2,3] in Fig. 3.1. The impurity contents of several specimens are listed in Table 3.1. Specimen 1335 and 1406 were tested

Table 3.1. Contamination Levels of Selected Tube-Burst Specimens

Specimen No.	Test Duration (hr)	Temperature (°F)	Impurity Content (ppm)		
			O_2	N_2	C
851	0	1800	800	850	290
859	0	1800	380	570	190
869	0	1800	340	580	140
913	100.7	1800	120	130	140
870	695.2	1800	1300	1000	
1335	13.1	2000	400	220	
1406	1700.7	2000	1000	1500	

in the tantalum wire furnace. The low oxygen gains indicate that this equipment is fairly successful in minimizing contamination during testing.

[1]ANP Semiann. Prog. Rep. April 30, 1961, ORNL-3144, p. 45.

[2]Discussion of the Structural Alloy Properties Relative to PWAR-11C Reactor Design, CNLM-2487, Aug. 31, 1960.

[3]R. T. Begley et al., WADC-TR-57-344, Part II.

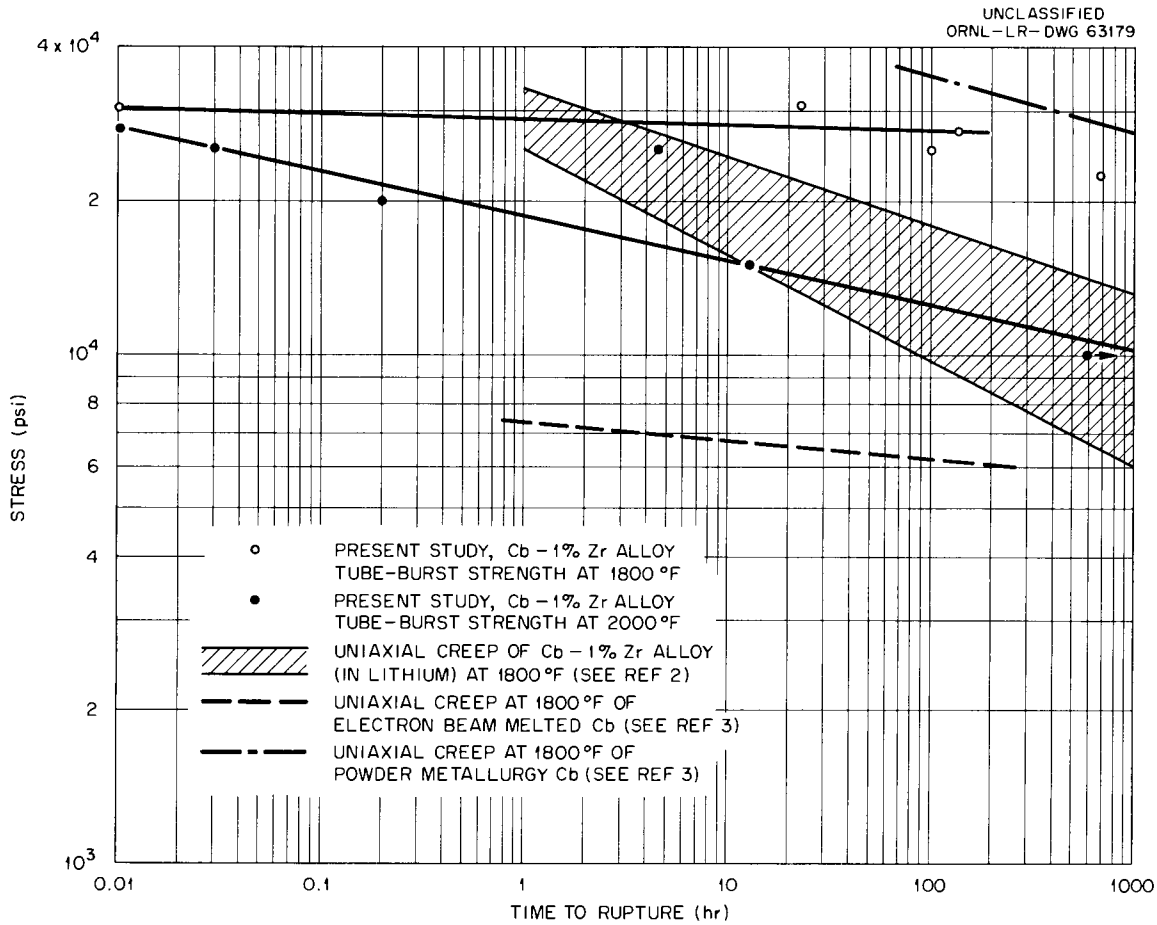

Fig. 3.1. Comparison of Stress Rupture Data on Cb–1% Zr Alloy.

4. WELDING AND BRAZING

Brazing of Columbium

C. W. Fox

The results of the earlier phases of the development of brazing alloys for joining columbium for use in high-temperature liquid-metal service have been reported.[1] After visual examination of brazed specimens, approximately 12 alloys appeared promising. Experimental joints made with these alloys have been thermal cycled 500 times from 1300 to 400°F. Approximately one-half the brazed joints looked satisfactory after this treatment; the remainder had cracks. A thermally cycled joint brazed with one of the most promising alloys, 46 Ti–46 Zr–4 V–4 Be (wt %), is shown in Fig. 4.1a, and the cracking observed after thermally cycling a joint brazed with one of the less satisfactory brazing alloys, 63 Ti–27 Fe–10 V (wt %), may be seen in Fig. 4.1b.

The results of the work conducted to date are summarized in Table 4.1. It is concluded that the brazing of columbium components for high-

[1]ANP Semiann. Prog. Rep. April 30, 1961, ORNL-3144, pp. 51–53.

Table 4.1. Results of Preliminary Studies on Columbium Brazed T-Joints

Brazing Alloy (wt %)	Flow Point (°C)	Metallographic Observations After Thermal Cycling[a]
67 Zr–29 V–4 Fe	1300	Severe cracking
60 Zr–25 V–15 Cb	1280	Severe cracking
48 Zr–48 Ti–4 Be	1050	Slight cracking
63 Ti–27 Fe–10 Mo	1250	Slight cracking
63 Ti–27 Fe–10 V	1280	Severe cracking
68 Ti–28 V–4 Be	1250	Sound joint
45 Ti–40 Zr–15 Fe	1050	Severe cracking
75 Zr–19 Cb–6 Be	1050	Sound joint
80 Zr–17 Fe–3 Be	1000	Severe cracking
46 Ti–46 Zr–4 V–4 Be	1000	Sound joint
95 Zr–5 Be	1000	Slight cracking
62 Ti–26 Fe–8 Mo–4 Zr	1250	Diffusion voids in alloy; no cracking

[a]All brazed specimens showed excellent flow of the brazing alloy and no cracks prior to thermal cycling.

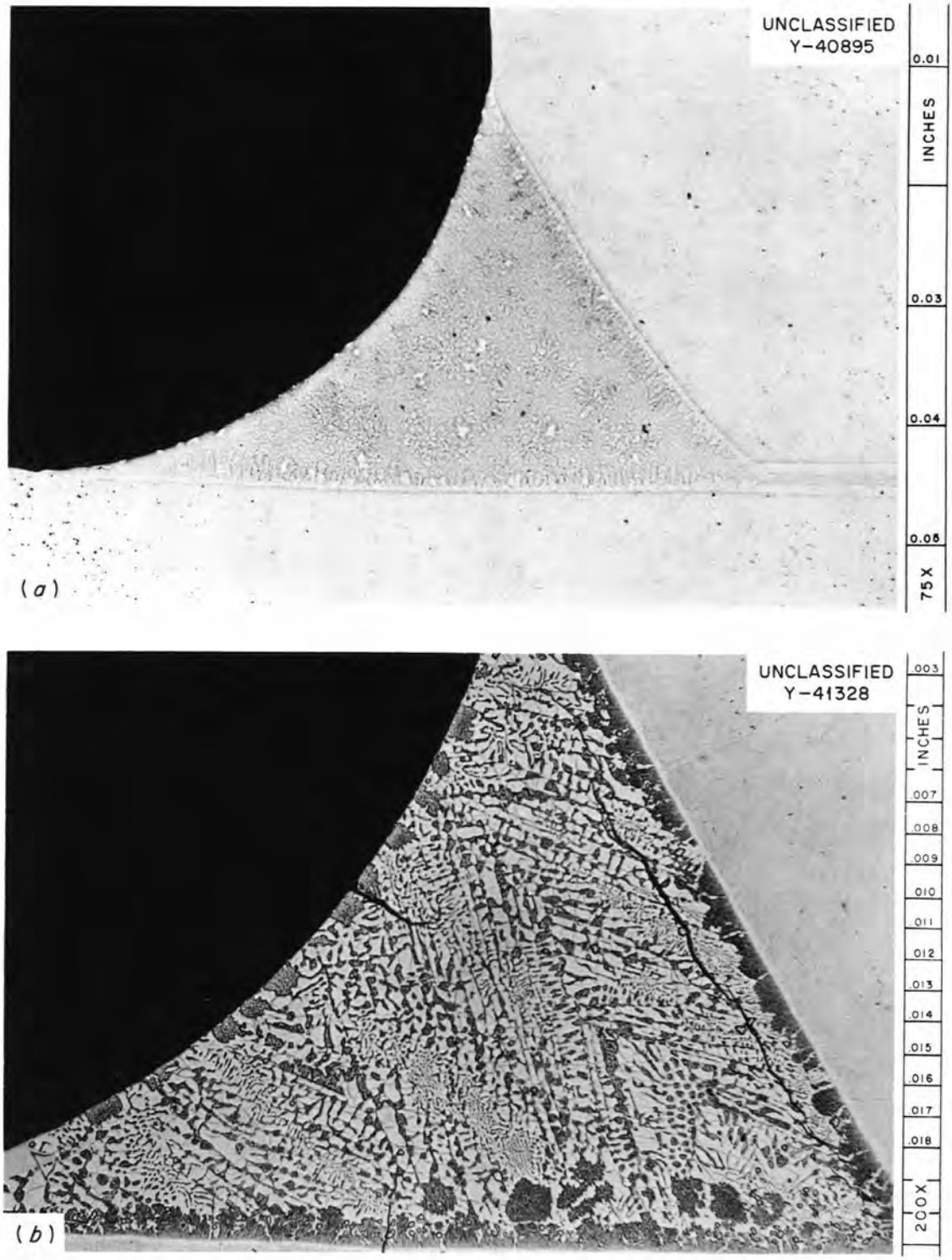

Fig. 4.1. Columbium T-Joints After Thermal Cycling 500 Times Between 1300 and 400°F. (a) Brazed with 46% Ti–46% Zr–4% Be. Etchant: 50 parts lactic acid, 30 parts concentrated nitric acid, and 2 parts hydrofluoric acid. 75X (b) Brazed with 63% Ti–27% Fe–10% V. As polished. 200X

temperature service is feasible. This work is to be continued as part of the High-Temperature Materials Program. Tests are currently under way to determine the mechanical properties of these joints, including their behavior after aging at elevated temperatures. A progress report is being prepared summarizing the results of the studies to date.[2]

Fabrication of Tube-To-Header Joints of Clad Materials

C. W. Fox

The recent acquisition of a quantity of stainless steel-clad columbium tubing has permitted the study of a joint design for heat exchangers of triplex material, such as the heat exchanger proposed several years ago.[3] The triplex tubing was supplied by Superior Tube Company, and the Metal Forming and Casting Group at the Oak Ridge National Laboratory fabricated the triplex header plate. These materials have been used to fabricate typical tube-to-header joints of the type illustrated in Fig. 4.2. Both the tube and the header plate are stainless steel—copper—columbium triplex composites.

The columbium-to-columbium weld was made in an inert-atmosphere chamber, while the stainless steel-to-stainless steel back braze was performed in vacuum using a commercial nickel-boron-silicon brazing alloy. The intermediate layer of copper serves as a diffusion barrier between the columbium and stainless steel and acts as a deterrent to the flow of brazing alloy. The joints have been inspected metallographically, and they appear to be sound. A typical joint is shown in Fig. 4.3.

This work is to be continued as a part of the High-Temperature Materials Program. Among the studies to be conducted are methods of back brazing the columbium-to-columbium weld, thermal-cycling tests, and aging tests at temperatures up to 1800°F. Small prototype heat exchangers will be fabricated.

---

[2]C. W. Fox and R. G. Gilliland, Progress Report on Brazing of Columbium, ORNL CF-61-7-24, Aug. 15, 1961.

[3]ANP Semiann. Prog. Rep. Oct. 31, 1959, ORNL-2840, pp. 42–43.

UNCLASSIFIED
Y-40530

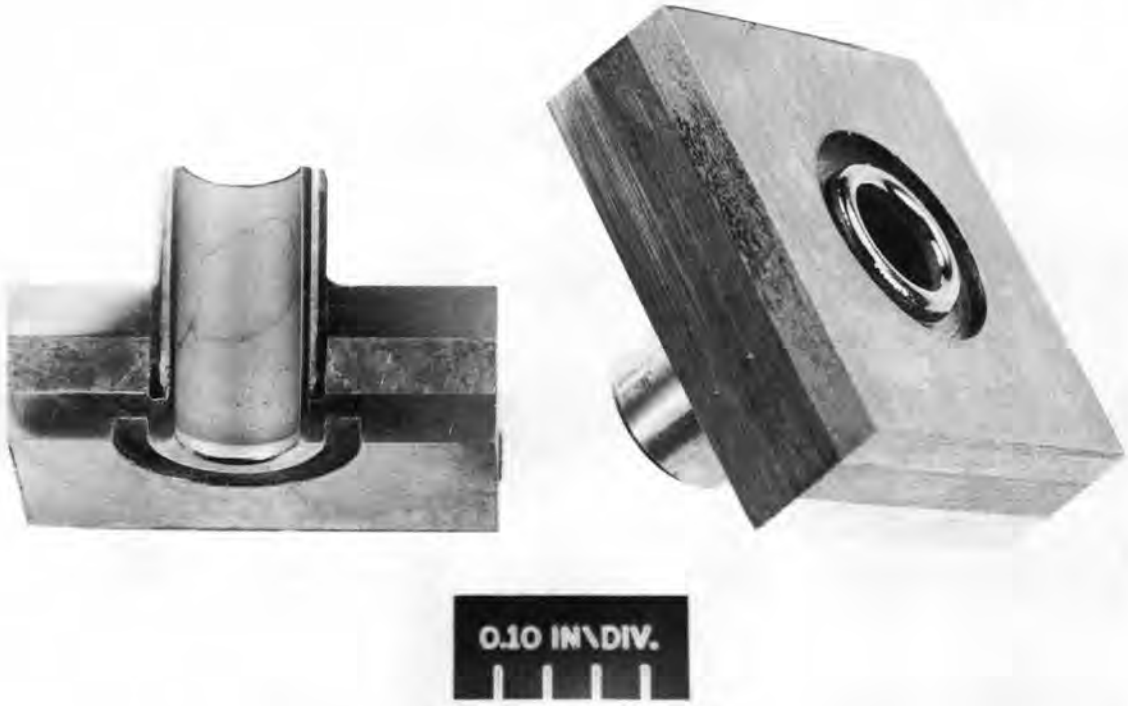

Fig. 4.2. Typical Welded and Back-Brazed Joint Fabricated from Stainless Steel-Copper-Columbium Triplex Material. (Confidential with Caption)

Fabrication of Clad Tubing

T. K. Roche

The feasibility of cladding columbium and columbium-base alloys for protection against oxidation at temperatures in excess of 1600°F is being studied in an effort to develop suitable composite materials for liquid metal-to-air radiators. Emphasis has been placed on the fabrication of small-diameter composite tubing. For purposes of optimum heat transfer, the cladding should be metallurgically bonded to the columbium. Differences in thermal expansion, together with interface reactions that occur between columbium and conventional iron- and nickel-base oxidation-resistant alloys present difficulties in meeting this requirement. It has not been possible by cold-drawing and vacuum-annealing treatments at 1850°F

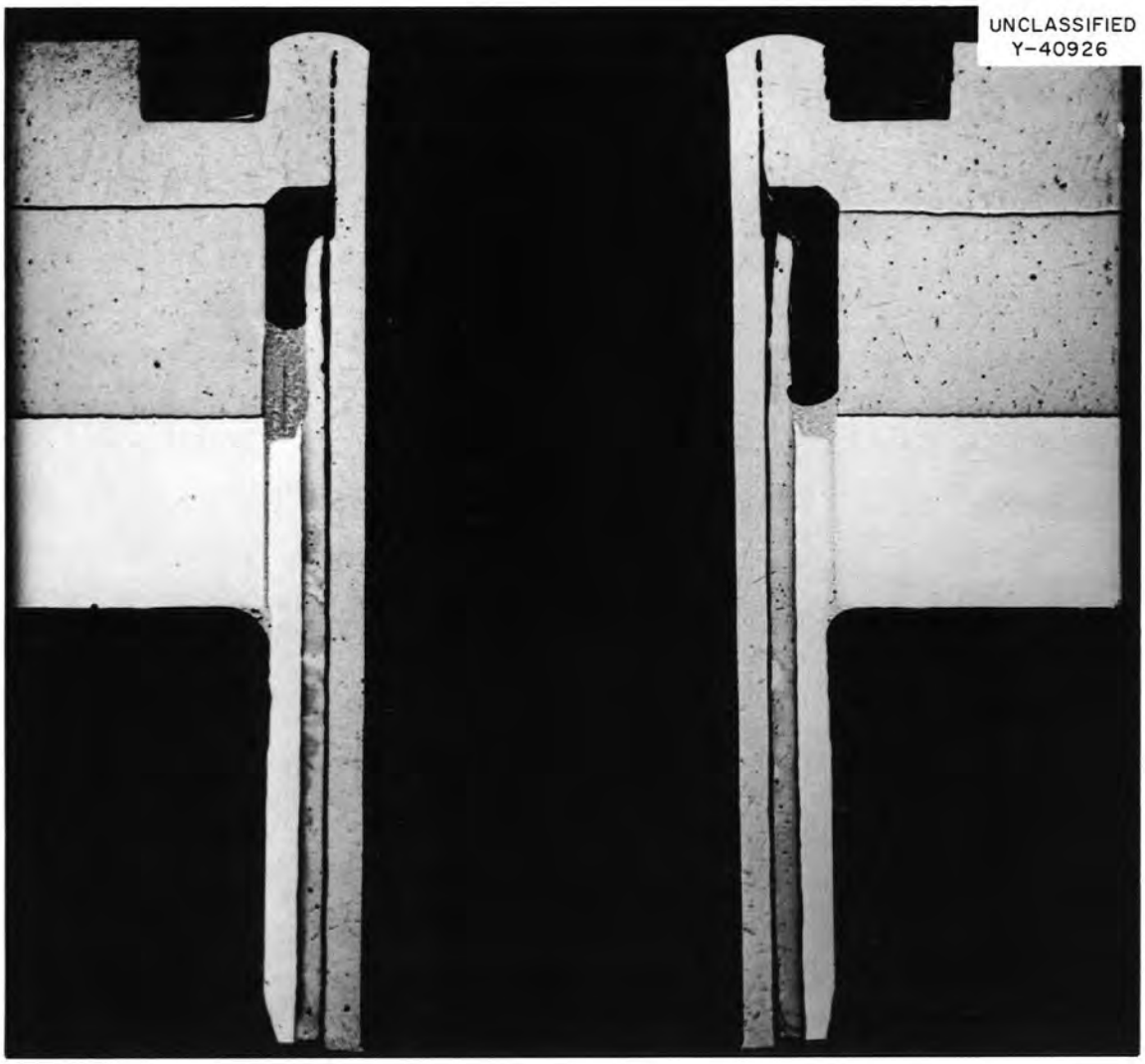

Fig. 4.3. Stainless Steel-Copper-Columbium Triplex Tube-to-Header Joint as Polished. 10X (Confidential with Caption)

to achieve good metallurgical bonding of types 304 and 446 stainless steels over columbium using copper and copper electroplates as intermediate layers.[4]

Aluminum bronze (8 wt % Al–92 wt % Cu) has excellent oxidation resistance up to its melting point of approximately 1900°F. A recent experiment has been concerned with the cladding of columbium with aluminum bronze by hot rolling at 1750°F using the picture-frame technique. Preliminary evaluation of the hot-rolled composite showed bonding of the

[4]ANP Semiann. Prog. Rep. April 30, 1961, ORNL-3144, pp. 54–55.

components, but subsequent cold rolling resulted in bond failure. Interface reaction with the formation of a brittle layer was undoubtedly responsible for this behavior. Confirmation of the presence of such a layer is presently being attempted by x-ray and metallographic studies. This experiment points out that difficulties could be expected in fabricating duplex-radiator tubes of these materials by hot extrusion and cold-drawing operations.

Future work on this problem will be reported in High-Temperature Materials Program reports, Space Power Program reports, and in the Metallurgy Division annual reports.

5. BERYLLIUM OXIDE RESEARCH

Phase Relationships in Beryllium Oxide—Metal Oxide Systems

A. T. Chapman R. A. Potter

Two papers, "Preliminary Observations of Mixed Oxide Compounds Containing BeO" by L. A. Harris, R. A. Potter, and H. L. Yakel, and "Phase Relationships and Kinetic Studies in the BeO-CaO System" by R. A. Potter and L. A. Harris, which summarize recent work, have been prepared for publication in the open literature. A report describing the porous-collector technique for investigation of BeO—metal oxide systems and experimental results will also be published upon completion of the current experimental program.

It is anticipated that some work in BeO—metal oxide systems will continue and that future results will appear in quarterly Gas-Cooled Reactor Program progress reports and the Metallurgy Division annual reports.

The BeO-CaO System

Investigations were continued to determine the effects of heat treatment and cooling rates in dry argon on the formation and decomposition of the intermediate phase $Ca_2Be_3O_5$. To determine whether the phase can be formed at temperatures less than the eutectic temperature of approximately 1360°C, mixtures containing 60 mole % BeO were melted and cooled at a rate of 8°C/min from 1500°C in separate experiments to 1270, 1290, 1300, 1325, and 1330°C. Samples were held at temperature for 1 hr and air quenched. In each instance, two-phase structures containing BeO and CaO resulted. It appears, therefore, that under conditions of slow cooling, followed by isothermal treatment at temperatures just below the solidus temperature, the more stable configuration of two phases develops.

Samples of $Ca_2Be_3O_5$ were subjected to extensive heat treatments at temperatures in the range 900 to 1355°C. The significant data obtained in these heat treatments are summarized in Table 5.1.

Table 5.1. Results Obtained by Heat Treatment of $Ca_2Be_3O_5$

Sample No.	Soak Temperature (±5°C)	Accumulated Time at Temperature (hr)	Phases Present[a]
1	900	65	$Ca_2Be_3O_5$
2	1000	165	$Ca_2Be_3O_5$
3	1100	165	$Ca_2Be_3O_5$[b]
4	1250	65	CaO, BeO, $Ca_2Be_3O_5$
5	1325	118	CaO, BeO, $Ca_2Be_3O_5$
6	1345	25	CaO, BeO, $Ca_2Be_3O_5$
7	1355	39	CaO, BeO, $Ca_2Be_3O_5$

[a]Analyses by x-ray diffraction.

[b]Splits observed in several diffraction peaks for $Ca_2Be_3O_5$.

Evidence of x-ray diffraction line splitting in the specimen heated for 165 hr at 1100°C makes it possible to state that the compound is not stable above 1100°C. The actual decomposition temperature of the compound, if in fact it is thermodynamically stable in any temperature range, has not been established.

The BeO-Eu_2O_3 System

Mixtures of BeO-Eu_2O_3 containing 5 to 75 wt % BeO were heated to approximately 1600°C on a platinum strip and air quenched. No evidence of an intermediate phase in the system was detected. Liquid formation was visually observed in the Eu_2O_3-rich mixtures (5 to 20 wt % BeO).

Cooling curves obtained from mixtures of 5, 12, and 20 wt % BeO cooled from 1550°C in a tube furnace showed a thermal arrest occurring at approximately 1425°C in each of the compositions. The longest thermal arrest occurred in the specimen containing 12 wt % BeO.

The BeO-Y_2O_3 System

An intermediate compound in the BeO-Y_2O_3 system[1] was produced by quenching melted mixtures of the oxides. The composition of this phase

[1]Met. Div. Ann. Prog. Rep. May 31, 1961, ORNL-3160.

was tentatively established as $2BeO \cdot Y_2O_3$. Single crystals of the compound were successfully grown from melts of $BeO-Y_2O_3$ and were submitted to the x-ray diffraction group for crystal structure analysis.

BeO-MgO-ZrO_2

A technique of investigating high-melting BeO binary systems by draining the eutectic liquid from wafer-shaped specimens has been used to study both the BeO-MgO and BeO-ZrO_2 systems.[2] As a continuation of this work, the ternary system BeO-MgO-ZrO_2 was investigated.

Specimens containing 86 mole % BeO and 7 mole % each of MgO and ZrO_2 were heated in air between 1700 and 1800°C. An appreciable loss of liquid was evident at temperatures above 1720°C. Wafers containing 86 mole % MgO and 7 mole % each of BeO and ZrO_2 indicated that the first liquid formation occurred at 1730°C. These data support the existence of a ternary eutectic at 1730 ± 10°C. However, when specimens containing 80 mole % ZrO_2 and 10 mole % each of BeO and MgO were heated under similar conditions, there was no indication of liquid formation, even at 2100°C. These data suggest that BeO is soluble in MgO-stabilized ZrO_2. Additional investigations are planned in the ZrO_2-rich portion of the BeO-MgO-ZrO_2 ternary system.

The compositions of the liquid lost from wafer-shaped specimens containing 86 mole % MgO and 7 mole % each of BeO and ZrO_2 are presented in Table 5.2. Attempts to establish the composition of the liquid drained from specimens containing 86 mole % BeO and 7 mole % each of MgO and ZrO_2 were unsuccessful. At present, it may be concluded that the first melting in the BeO-MgO-ZrO_2 system occurs at 1730 ± 10°C and that a ternary eutectic probably exists near the composition 50% MgO–20% ZrO_2–30% BeO.

Preparation of Crystalline BeO by Precipitation from Molten Salts

R. E. Moore J. H. Shaffer

The direct crystallization of BeO (and UO_2 coated with BeO) from molten salts upon the addition of sources of oxide ion (e.g., CaO and H_2O)

[2] ANP Semiann. Prog. Rep. April 30, 1961, ORNL-3144, pp. 61–66.

Table 5.2. Composition of Liquid Drained from Wafer-Shaped Specimens Containing $MgO-BeO-ZrO_2$ (86-7-7 mole %)

Maximum Firing Temperature (°C)	Composition of Lost Liquid (mole %)		
	MgO	ZrO_2	BeO
1755	52	18	30
1775	50	20	30
1740	57	17	26

has been under study as a possible technique for furnishing high-temperature fuel or moderator material. Samples of BeO crystallized from molten $LiF-BeF_2$ at 800°C upon the exposure of the melt to a helium-water vapor stream have been submitted to GE-ANP for evaluation. Because of the presence of container corrosion products in this BeO, it was desirable to attempt to produce material of higher purity.

In two experiments which have recently been completed, hydrogen has been compared with helium as a carrier gas for the water vapor. Thermodynamic considerations suggest that a high H_2-to-H_2O ratio should inhibit the corrosion of the container during the hydrolytic precipitation. Both experiments were performed at 800°C, with a high-purity starting mixture of $LiF-BeF_2$ (75-25 mole %). The results of spectrographic analyses of the two BeO products are presented in Table 5.3. The improvement in quality, with respect to container corrosion, which can be attributed to the use of hydrogen carrier gas, is substantial. Both samples had been washed with aluminum nitrate solution and extracted with hot water in pyrex apparatus; this is believed to be responsible for the large quantities of aluminum, boron, and silicon observed. Such a washing procedure could be avoided in a larger scale study. The further development of this method for preparing single-crystal refractory oxides will be a part of the Pure Materials Research and Development Program.

Table 5.3. Spectrographic Analyses of BeO Samples Prepared by Precipitation from Molten Salts by Two Methods

Impurities	Impurity Concentration (ppm)	
	Helium Carrier Gas Method	Hydrogen Carrier Gas Method
Cr	150	60
Fe	300	50
Ni	150	70
Cu	20	<10
Mn	20	20
Al	1500	5000
B	150	300
Li	5	200
Mg	20	10
Si	1000	2000
Ti	20	40

Purification of Beryllium Compounds by Solvent Extraction

R. E. Moore J. H. Shaffer

A process for purifying beryllium hydroxide by a solvent extraction technique has been successfully demonstrated by small-scale laboratory preparations. The process consists of extracting beryllium from an aqueous phase containing nitric acid and ethylenediaminetetraacetic acid (EDTA) into an organic phase containing acetylacetone in carbon tetrachloride. The EDTA in the aqueous phase complexes impurity ions, while beryllium is extracted into the organic phase as beryllium acetylacetonate. Beryllium is back-extracted into a strong acidic solution and recovered as $Be(OH)_2$ upon neutralization with ammonia.

The distribution coefficients of beryllium and the more common impurity ions that were determined during this investigation are shown in Fig. 5.1. Aluminum, the impurity most difficult to remove from beryllium, can be efficiently separated at about pH 4.5. Most cations such as Na^+, K^+, Ca^{++}, Ba^{++}, Sr^{++}, Zn^{++}, Cu^{++}, Ni^{++}, Ce^{3+}, ZrO^{++}, and anionic impurities have favorable distribution coefficients that are considerably greater

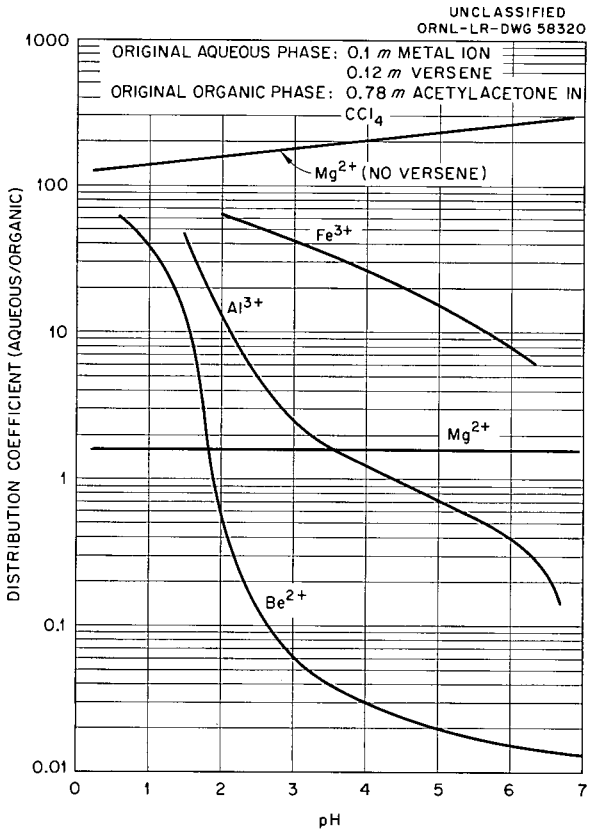

Fig. 5.1. Distribution Coefficients for Beryllium and Impurities as a Function of pH.

than 100 at this pH level. Typical spectrographic analyses of the impurities in purified beryllium hydroxide, expressed as ppm in BeO, are as follows:

<20 ppm Ti
<10 ppm Al, Ba, Ca, Cr, Fe, K, Na, Ni
<5 ppm Co, Cu, Li, Mg, Mn, Mo, Pb, Sn
<1 ppm B

Anions P and F were not detected. These results are representative for 10 to 400 g batches of prepared beryllium hydroxide. The pure materials obtained during the development of this extraction process will be used in preparing spectrographic standard mixtures.

Current efforts are being directed toward investigations of the various extraction characteristics of this process. The phase diagram of the ternary organic system (Fig. 5.2) was determined at 27°C from measurements

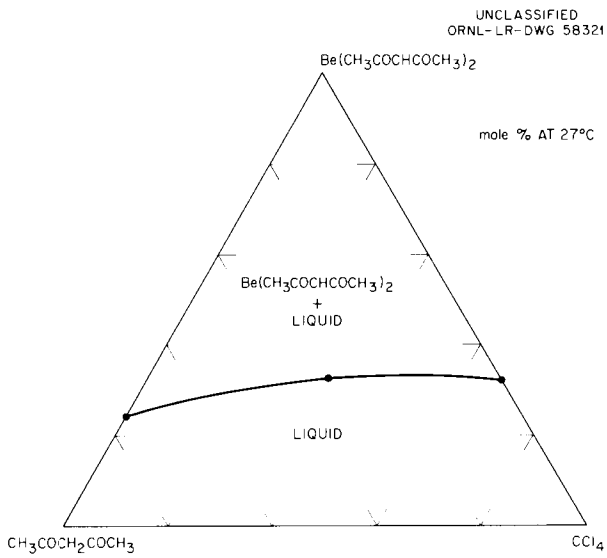

Fig. 5.2. Phase Diagram of Organic System.

of the solubilities of beryllium acetylacetonate in carbon tetrachloride, acetylacetone, and a solution containing 49 mole % acetylacetone in carbon tetrachloride. The solubilities are 32, 24, and 32.5 mole %, respectively. These values, together with the density values of the three solutions (1.355, 1.011, and 1.17 g/ml), permit calculations of the maximum beryllium concentrations in various mixtures of acetylacetone and carbon tetrachloride. Similar studies are in progress to determine the solubilities of acetylacetone and beryllium acetylacetonate in the aqueous phase.

Preliminary experiments have indicated that the extraction rates for this process are quite rapid. For example, a dilute nitric acid solution (pH 0.5), when vigorously shaken with an equivolume mixture of carbon tetrachloride and 10 mole % beryllium acetylacetonate, attained an equilibrium pH of 2.5 in less than 15 sec. While the extraction of impurities may possibly be less rapid, reactions of metallic ions with EDTA occur almost instantaneously. Further development of this extraction process will be continued as a part of the Pure Materials Research and Development Program.

Spectrochemical Analyses of High-Purity Beryllium Oxide

J. A. Norris Zell Combs

Spectrochemical methods of analysis of high-purity beryllium oxide are currently under evaluation. The impurities in beryllium oxide are presently being analyzed to the limits listed below:

Element	Limit of Detection (ppm)	Element	Limit of Detection (ppm)
Al	5	Na	10
Ba	5	Ni	10
Ca	5	Pb	2
Co	1	Si	5
Cr	10	Sn	5
Cu	5	Sr	20
Fe	5	Ti	20
K	5	V	5
Li	5	Zn	20
Mg	5	B	1
Mn	5		
Mo	2		

Two general methods are used for analysis: (1) direct burning utilizing a 10-mg sample to determine Al, Ca, Cu, Fe, K, Li, Mg, Mn, Na, Ni, Si, Ti, and Sr and (2) pyroelectric burning (AgCl-AgF) utilizing a 20-mg sample to determine Ba, Co, Cr, Mo, Pb, Sn, V, Zn, and B. Material for Mg, Ca, and Si standards has been prepared by the Reactor Chemistry Division and has been found to contain less than 5 ppm each of Mg, Ca, and Si. In the cooperative testing program with GE-ANP for the analysis of beryllium oxide, large disagreements still remain in the reported values for Al, Ca, Mg, and Si.

New standards for Mg, Si, and Ca will be prepared as purer base materials become available. A practical limit to this approach will soon be reached because of general laboratory contamination by unclean air from the ventilating system. New methods for specific elements will be developed as requested. This program will be continued in the future as part of the Pure Materials Research and Development Program.

6. ENGINEERING AND HEAT-TRANSFER STUDIES

Boiling-Potassium Heat-Transfer Experiment

H. W. Hoffman A. I. Krakoviak

The investigation of the boiling characteristics of potassium was undertaken to define the limits of feasible operation of a directly coupled reactor-turbine system for electric power generation in a space power plant utilizing boiling potassium as the coolant in the reactor and potassium vapor as the thermodynamic medium in the turbine portion of the cycle. One of the major points of uncertainty in designing such a system resides in the lack of knowledge of the peak (burnout) heat flux associated with the saturation (bulk) boiling of potassium. Attempts at estimating this quantity,[1] using correlations developed for water and for organic fluids have yielded widely disparate results (see Table 6.1) and have increased the importance of the experimental program. In addition to defining the burnout heat flux (under saturation conditions) in terms of the fluid flow rate and the exit vapor quality, this study will provide information on (1) boiling heat-transfer coefficients at heat fluxes less than the burnout value, (2) subcooled boiling with potassium, (3) pressure losses associated with bulk boiling, (4) condensing heat-transfer coefficients, (5) stability criteria for boiling in a single tube as characterized by the nature of the two-phase flow and the tube attitude, and (6) the effect of swirl flow on all of these parameters.

The experimental system for accomplishing these measurements has been described in previous reports in this series.[2-4] A temporary boiler section (shown in Fig. 6.1) was used for initial experiments, since fabrication of a high-flux boiler ($\phi = 5 \times 10^5$ Btu/hr·ft^2) has not yet been

---

[1]W. R. Gambill and H. W. Hoffman, Boiling Liquid-Metal Heat Transfer, American Rocket Society Paper No. 1737–61 (May 1961).

[2]ANP Semiann. Prog. Rep. April 30, 1960, ORNL-2942, pp. 64–71.

[3]ANP Semiann. Prog. Rep. Oct. 31, 1960, ORNL-3029, pp. 62–64.

[4]ANP Semiann. Prog. Rep. March 31, 1961, ORNL-3144, pp. 67–72.

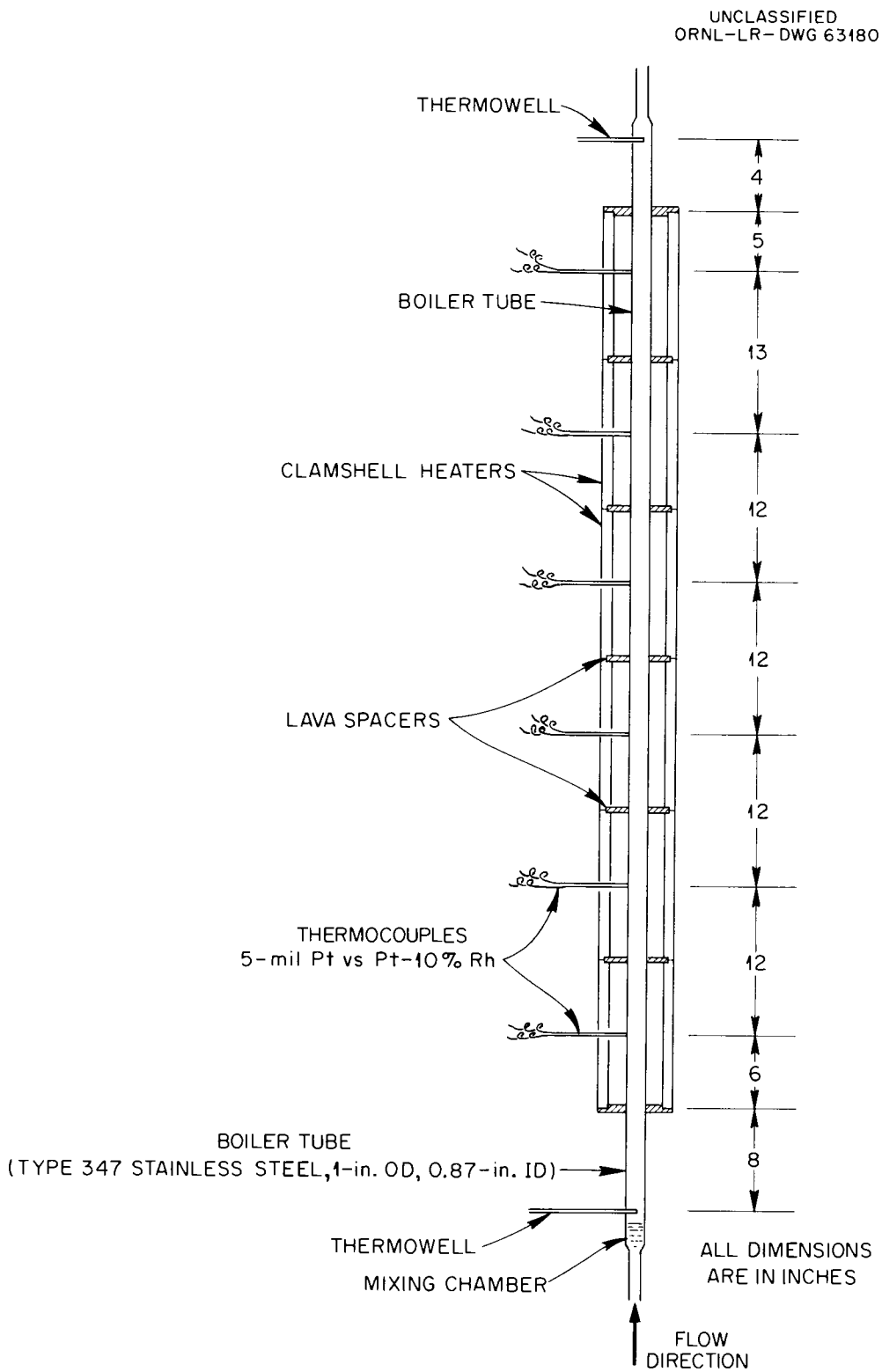

Fig. 6.1. Test Section I, Boiling-Potassium Experiment.

Table 6.1. Estimated Burnout Heat Fluxes for Water and Potassium Under Forced-Convection Bulk-Boiling Conditions[a]

Fluid	Exit Quality[b]	ϕ_{bo}, Burnout Heat Flux (Btu/hr·ft^2)		
		Griffith[c]	Additive[d]	Lowdermilk et al.[e]
		$\times 10^6$	$\times 10^6$	$\times 10^6$
H_2O	0.10	2.52	0.76	
	0.30	5.07	0.89	1.25
K	0.10	89.1	0.66	
	0.30	184	0.85	
	0.50	214	0.96	

[a]Calculated for P = 1 atm abs, D_i = 3/8 in., $t_{in} = t_{sat}$, V_{in} = 2.5 ft/sec.

[b]Exit qualities at which the vapor velocity equals the acoustic velocity in the medium are 0.35 for H_2O and 0.52 for K.

[c]Generalized expression of P. Griffith, The Correlations of Nucleate Boiling Burnout Data, ASME Paper No. 57-HT-21 (Aug. 1957).

[d]Presupposes the independence of the boiling and convective modes of heat transfer and sums the individual contributions to effect the estimate of burnout (see ref. 1).

[e]Experimental data of Lowdermilk, Lanzo, and Siegel (see ref. 6).

completed. This unit consisted of a 1-in.-o.d., 0.87-in.-i.d., 6-ft-long, type 347 stainless steel tube heated by six 3-in.-i.d. clamshell heaters rated at 4 kw/ft and instrumented with six 0.005-in.-diam Pt vs Pt–10% Rh thermocouples resistance-welded to the tube wall at the approximate midpoint of each heater. The temperatures of the inlet and exit fluid were obtained about 2 in. upstream and downstream, respectively, of the boiler section by thermocouples inserted in wells extending to the tube centerline.

In the course of shakedown operation of the loop (including calibration of pressure and flow-measuring devices), data were obtained on heat transfer with potassium under nonboiling conditions. The results are shown in Fig. 6.2, in comparison with the data of Johnson, Hartnett, and Clabaugh,[5]

[5]H. A. Johnson, J. P. Hartnett, and W. J. Clabaugh, Heat Transfer to Lead-Bismuth and Mercury in Laminar and Transition Pipe Flow, Inst. Eng. Res., University of California, August 1953.

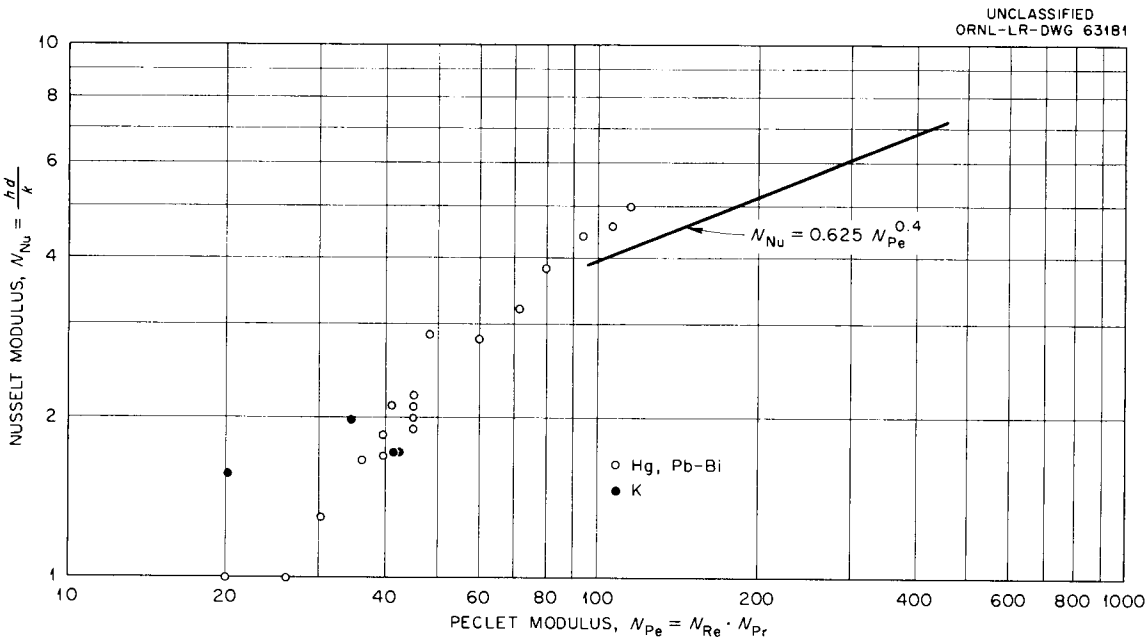

Fig. 6.2. Forced-Convection Nonboiling Heat Transfer with Potassium.

for the laminar and transition flow of mercury and lead-bismuth in round tubes; excellent agreement of the potassium data with these results is noted.

The results of measurements to date on the forced-convection boiling of potassium are summarized in Table 6.2. In the initial experiments (runs 1 through 4), inlet liquid temperatures were held to relatively low values (1125 to 1160°F) corresponding to approximately 250°F subcooling at the boiler inlet. Large-scale fluctuations in the boiler tube-wall temperatures, the boiler inlet and exit pressures, and the boiler inlet flow rate were observed; the fluctuation frequency was of the order of 3 cycles/min. A typical tube-wall temperature trace obtained near the boiler exit is given in Fig. 6.3. The data are for run 6.1 in which the subcooling was ~45°F; the fluctuation frequency was 3 to 4 cycles/min with an amplitude of ±85 to ±90°F. As the inlet liquid temperature approached the saturation temperature, the amplitude of these oscillations was reduced. This is shown graphically in Fig. 6.4 in which the subcooling is measured in relation to the saturation temperature at the boiler exit. The data indicate that stable flow (presuming the wall temperature fluctuation to be

Table 6.2. Summary of Results on Boiling Potassium

Run No.	Flow Rate (lb/hr)	Potassium Temperature (°F)		Heat Flux (Btu/hr.ft^2)	Heat Balance	Quality (%)	Exit Vapor Velocity (ft/sec)
		Inlet	Exit				
1	76.9	1128	1376	28 755	0.77	53	107
2	87.4	1125	1377	33 100	0.88	53	122
3	87.4	1157	1390	34 830	0.93	57	130
4	98.4	1134	1383	34 540	0.92	49	127
5.1	114.7	1321	1392	32 076	0.82	41	110
5.2	104.6	1336	1396	32 357	0.81	45	108
5.3[a]	90.9	1328	1386	30 749	0.79	49	108
6.1	145.5	1358	1395	30 677	0.79	33	105
6.2	147.2	1402	1405	31 887	0.82	33	107
6.3	147.2	1404	1393	32 967	0.84	34	119
6.4	90.9	1384	1361	33 065	0.85	61	136
6.5	64.6	1361	1364	32 368	0.83	81	132
6.6[a]	55.5			32 368		92	124
7.1	116.2	1373	1365	37 634	0.85	49	147
7.2	116.3	1367	1349	37 632	0.84	50	166
7.3	117.3	1395	1370	37 973	0.85	51	156

[a]Indicates burnout run.

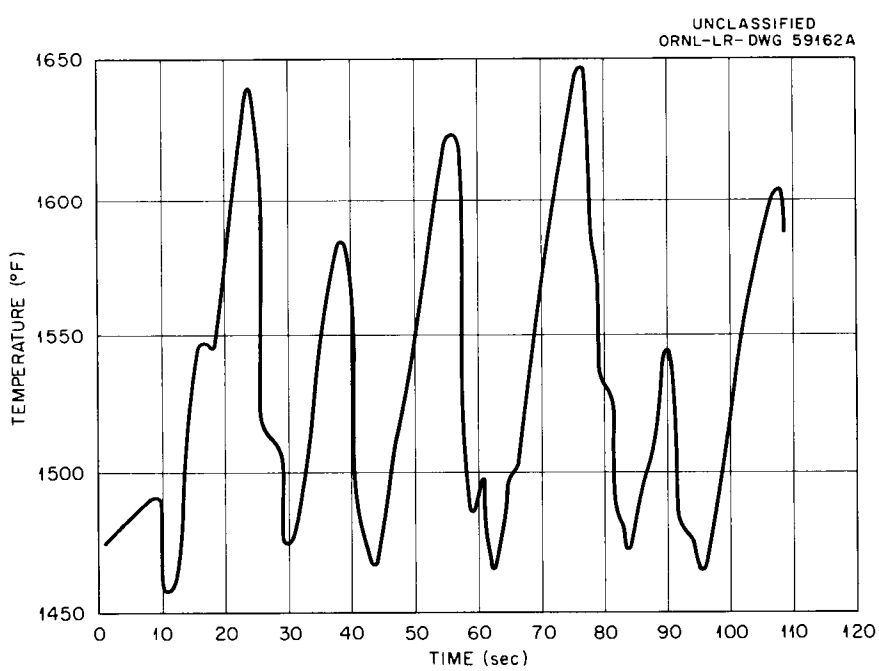

Fig. 6.3. Tube-Wall Temperature Near Boiler Exit for Run No. 6.1.

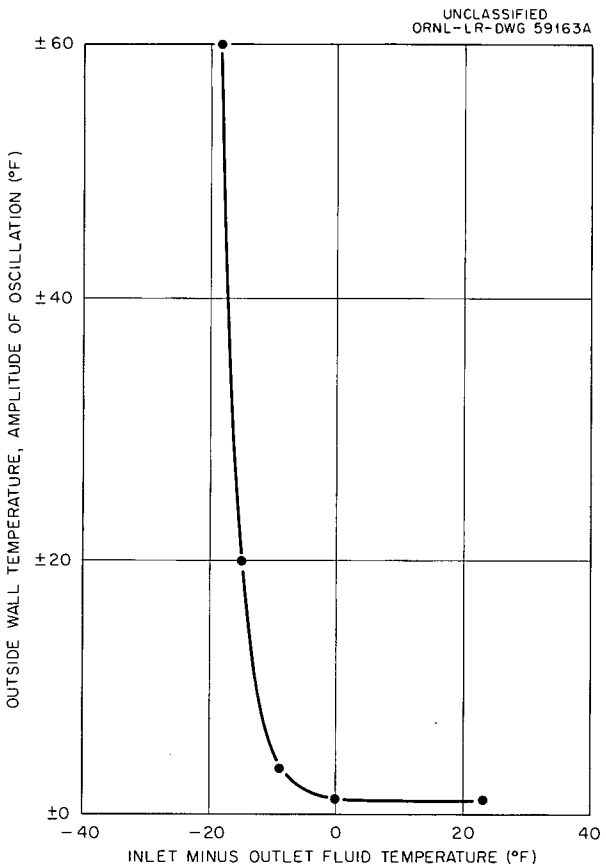

Fig. 6.4. Stability Curve as Developed from Preliminary Data on Potassium Boiling.

a measure of the flow situation in the tube) exists only when the temperature of the liquid entering the boiler is close to the saturation temperature.

A measure of the peak heat flux was obtained by systematically decreasing the inlet flow rate for runs 6.2–6.6 while maintaining a constant heat flux and saturated inlet conditions. Typical temperature patterns observed in following this procedure are shown in Fig. 6.5, in which the temporal variation of the tube-wall temperature near the boiler exit is related to the potassium flow rate and the exit quality. Burnout was indicated by the automatic interruption of the heater power at a tube wall temperature of 1700°F. (In some of the earlier runs with large instabilities, the controller was set at 1900°F.) The starred items in Table 6.2 indicate the conditions at which the peak flux was achieved. The vapor quality may be overestimated in that the pressure loss between the boiler exit and the liquid-vapor separator results in additional vaporization.

Preliminary data for the peak heat flux are shown in Fig. 6.6 and compared with a correlation based on the results of Lowdermilk, Lanzo, and Siegel[6] for water. (Included is an unstable-flow burnout point obtained in run 8.3; this run is not listed in Table 6.2, since data reduction for the series 8 runs has not been completed.) These investigators

[6]W. H. Lowdermilk, C. D. Lanzo, and B. L. Siegel, Investigation of Boiling Burnout and Flow Stability for Water Flowing in Tubes, NACA-TN-4382, Sept. 1958.

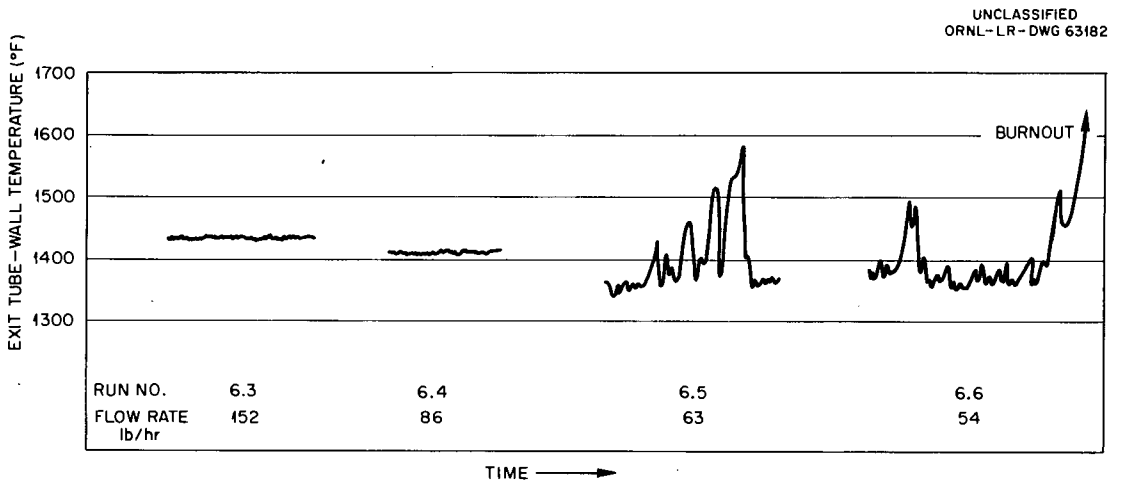

Fig. 6.5. Sequence of Tube-Wall Temperatures Preceding Burnout; Runs 6.3–6.6.

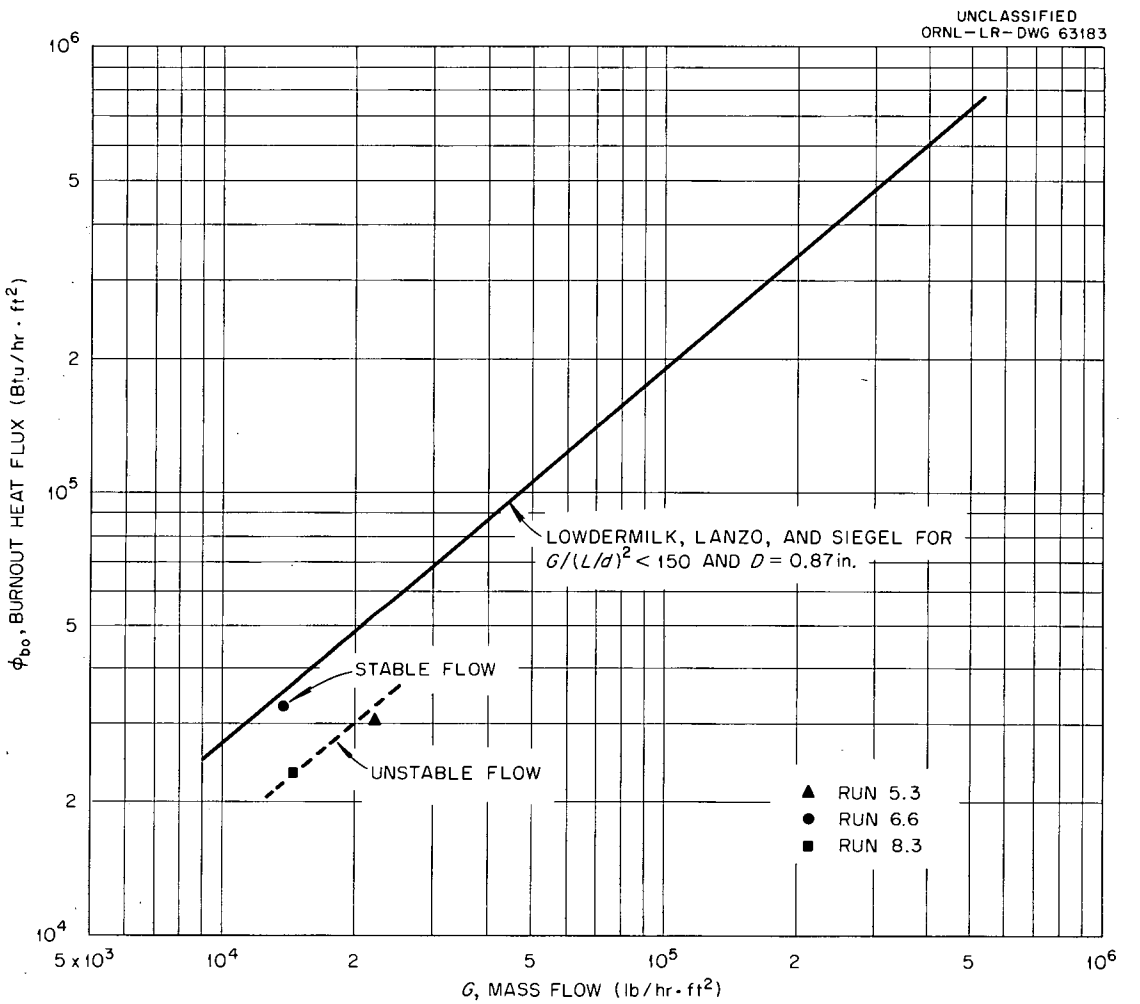

Fig. 6.6. Preliminary Results on Boiling-Potassium Burnout.

found that their stable flow data could be resolved into two boiling regimes (low-velocity high-exit-quality and high-velocity low-exit-quality) with the distinction between these depending on whether the parameter $G/(L/d)^2$ was less than or greater than 150, respectively. For the high-quality region with stable flow, their data were correlated by the relation:

$$\phi_{bo}\ d^{0.2}\ (L/d)^{0.85} = 270\ G^{0.85} \quad , \tag{1}$$

where ϕ_{bo} is the peak heat flux (Btu/hr·ft^2); d, the tube inside diameter (ft); L/d, the tube length-to-diameter ratio; and G, and the mass flow rate (lb/hr·ft^2). For the conditions of the boiling-potassium experiment (d = 0.87 in. and L/d = 82.8), Eq. (1) reduces to:

$$\phi_{bo} = 10.681\ G^{0.85} \quad . \tag{2}$$

The comparison curve in Fig. 6.6 is based on Eq. (2). It maybe seen that the burnout flux for run 6.6 agrees closely with that which would be predicted by the water correlation. There is not yet sufficient data to justify a correlation of the unstable flow burnout heat fluxes. However, there is an indication that, for the same mass flow, the peak heat flux with unsteady flow will be only about 60% of the value which could be attained when stable flow exists.

Brazing of the high-flux boiler (capable of thermal fluxes up to 5×10^5 Btu/hr·ft^2) has been completed, and the unit is undergoing nondestructive examination to establish the adequacy of the brazes. A number of other modifications to the experimental system are planned; these include substituting an electrodynamic pump for the present pair of electromagnetic pumps, the inclusion of additional pressure taps, and replacement of the cold trap with a hot-gettering system.

This program is being continued; future progress will be reported as part of the Space Power Program.

Thermophysical Properties

J. W. Cooke H. W. Hoffman

The development of high-temperature, high-specific-power reactors for aircraft nuclear propulsion created a need for information on the thermophysical properties of new and unusual fluids and solids to function as fuels, coolants, moderators, and containment materials. Recent measurements of thermophysical properties have included the thermal conductivity of lithium[7,8] and a lithium-silver alloy,[7] the enthalpy of lithium hydride,[9] and the thermal conductivity of a columbium-zirconium (99-1 wt %) alloy.[9,10]

The future program will include an extension of the thermal conductivity measurements of lithium and the columbium-zirconium alloy to temperatures up to 2000°F, the measurement of the thermal conductivity of liquid LiH, and a study of the properties of liquid and gaseous potassium and rubidium. The results of these measurements will be covered in the progress reports for the Space Power Program.

---

[7]ANP Semiann. Prog. Rep. Oct. 31, 1960, ORNL-3029, pp. 64–69.

[8]ANP Semiann. Prog. Rep. March 31, 1961, ORNL-3144, pp. 72–76.

[9]ANP Semiann. Prog. Rep. April 30, 1960, ORNL-2942, pp. 60–63.

[10]ANP Semiann. Prog. Rep. Oct. 31, 1959, ORNL-2840, pp. 59–62.

7. RADIATION EFFECTS

Radiation Effects on Structural Metals

N. E. Hinkle J. W. Woods
J. C. Zukas

The effects of neutron bombardment on the creep and stress-rupture properties of structural metals of interest to the aircraft reactor program have been studied. The materials investigated have included Inconel, type 304 stainless steel, and a Cb–1% Zr alloy. The specimens were irradiated in the poolside facility of the ORR at fast-neutron fluxes (>1 Mev) of 0.5×10^{13} to 1×10^{13} neutrons/cm^2·sec and thermal-neutron fluxes of 5×10^{13} to 8×10^{13} neutrons/cm^2·sec. Except as noted in Tables 7.1 and 7.2, all the rupture times listed correspond to the periods of irradiation.

The studies of Inconel tubing processed from two different heats revealed that the time to rupture under stress at 1500°F in an air environment, as measured in a tube-burst test, was decreased by a factor of 3 to 5 by neutron exposure. Postirradiation measurements of the change in diameter of the tubing (Table 7.1) have indicated that the ductility at rupture is decreased by a factor of 2 to 5 and that the ductility decreases as the time to rupture increases (stress decreases). It has been suggested that natural boron (20 to 100 ppm, containing 20% B^{10}) impurity may have a deleterious effect on the in-pile rupture time because of the formation of pockets of helium gas during thermal-neutron bombardment. These pockets of helium gas might exert an internal stress on the material or merely create a weakness in the grain boundaries. Studies for determining the validity of this postulate are presently being conducted. The limited data available at this time do not permit a conclusive statement.

In-pile tests have been conducted on type 304 stainless steel in an air environment at 1300, 1500, and 1600°F. The results available at this time indicated a factor of 3 reduction in time to rupture at 1500°F but no appreciable irradiation effect on time to rupture at 1300 and 1600°F. Postirradiation diameter measurements (Table 7.2) indicate, however, a

Table 7.1. Results of Stress-Rupture and Tangential-Strain Measurements of In-Pile and Control Tube-Burst Specimens of Inconel[a] Tested at 1500°F

Specimen No.	Stress (psi)	Time to Rupture (hr)	Average Tangential Strain (%)	Maximum Tangential Strain (%)
11-5	5000	173[b]	0.45	0.6
11-6	5000	73	2.7	5
11-7	5000	140[b]	2.5	4.4
11-8	5000	91	1	1.6
9-4	5000	117[c]	0.55	0.8
4-5	5000	109[d]	1.5	2.3
4-6	5000	110[e]	4.7	5.6
35 control	5000	473		11.2
41 control	5000	487		8.4
28 control	5000	410		5.7
43 control	4000	801		13.8
44 control	4000	797		10.7
4-10	3000	774	0.65	0.8
37-2-71	3000	784		0.8
37-2-73	3000	>870		1.25
48 control	3000	>2850		9.6

[a]INCO Heat No. NX 8962.

[b]Stressed 48 hr prior to start of irradiation.

[c]Irradiated more than 1000 hr at 1500°F prior to stressing out-of-pile.

[d]Irradiated 100 hr at 1500°F prior to stressing.

[e]Irradiated 550 hr at 1500°F prior to stressing.

reduction in ductility at rupture by a factor or 2 to 5 at all test temperatures. The ductility at 1300°F appears to be limited to about 1%, while the ductility at 1500 and 1600°F is somewhat higher than at 1300°F. There appears to be a decrease in the ductility with increasing time to rupture. The strain in tests of 1500 hr is as low as 2% at the higher temperatures.

Irradiation-effect studies on a Cb–1% Zr alloy have been conducted at 1800°F in a helium environment. The results indicate no greater than a 10% reduction in rupture strength for short-time tests. Tests of longer duration at 2000°F will begin soon.

Table 7.2. Results of Stress-Rupture and Tangential-Strain Measurements of In-Pile and Control Tube-Burst Specimens of Type 304 Stainless Steel[a]

Test Temperature (°F)	Specimen No.	Stress (psi)	Time to Rupture (hr)	Average Tangential Strain (%)	Maximum Tangential Strain (%)
1300	15-2	13 000	127	1	1.4
	15-3	13 000	217[b]	0.4	0.6
	15-6	13 000	141	1.1	2.1
	15-8	13 000	116	0.85	1.15
	126 control	13 000	144	1.57	2.33
	127 control	13 000	144	2.72	3.49
	15-4	11 000	502	0.9	1
	15-7	11 000	470	1.1	1.9
	15-10	11 000	452	0.8	1.1
	124 control	11 000	470	3.57	4.12
	128 control	11 000	550	2.86	4.21
	15-1	9 000	1642	1	1.1
	15-5	9 000	>1860	0.85	1.1
	15-9	9 000	>1860	0.8	1
1500	9-7	5 000	337	3.3	3.8
	9-8	5 000	518	3.2	3.8
	73 control	~5 250	1130	8.1	9.3
	239 control	~5 250	1025	12.5	15
	9-6	4 000	673	3.8	5.3
	17-3	4 000[c]	851	1.3	3.6
	72 control	~4 200	1670	9.6	11.5
	240 control	~4 200	2450	9.2	12.4
	17-1	3 000	>1600	0.5	0.6
	17-9	3 000	>1600	0.7	0.85
	310 control	~6 300	520	10	15
	537 control	~6 300	184	7	9
1600	17-8	5 000	50	1.1	1.5
	1066 control	~4 600	82	7.5	9.8
	control	~4 300	175		
	1112 control	~4 200	63	11	17
	control	~3 800	180		
	control	~4 100	142		
	360 control	~3 700	265	10.2	13.5
	718 control	~3 200	243	18.5	24.2
	1068 control	~3 200	197		
	17-5	3 000	414	3.3	6.8
	17-6	2 600	870	3.2	5.6
	17-4	2 200	1430	2.2	3.8
	17-7	2 200	>1500	1.5	1.8

[a]Superior Tube Co., Heat No. 23999x.

[b]Irradiated more than 500 hr at 1300°F and 16 Mw prior to stressing.

[c]Irradiated more than 500 hr at 1500°F and 30 Mw prior to stressing.

Future information concerning these radiation damage studies will be reported in the Solid State Division annual progress reports. In addition, the results of tests on Inconel and stainless steel will be reported in the Gas-Cooled Reactor Program progress reports and the columbium alloy (and other high-temperature materials) data will be presented in the High-Temperature Materials Program and Space Power Program reports.

Irradiation Damage to BeO

R. P. Shields J. E. Lee, Jr.
W. E. Browning, Jr.

Beryllium oxide has for some time been of interest as a possible moderator material in reactors of advanced design because of its inherently favorable nuclear properties, its high-temperature strength, and its relatively high thermal conductivity. Information has been somewhat limited, however, on the ability of this material to maintain its integrity after prolonged exposure to reactor environment and neutron reactions. During recent months it has been possible for the first time in American reactor technology to examine a number of BeO specimens which have been irradiated to the point of serious deterioration. The observations presented here result from a program of irradiation experiments performed in the Engineering Test Reactor at Idaho.

The experiments were conducted with multiple-capsule assemblies in which the basic sample units were cylindrical BeO specimens in an argon or helium atmosphere encapsulated in groups of three in stainless steel. The stainless steel capsule was installed in a gas annulus thermal barrier. There have been some variations from this type of assembly; for example, some water-cooled capsules have been irradiated, one capsule contained 12 pellets, and the currently operating assembly includes both unclad and encapsulated monolithic specimens. The samples or pellets have been 1 in. in length and, nominally, 400, 600, or 800 mils in diameter. Larger specimens, 3 in. long and 1100 mils in diameter, were installed in the latest assembly.

Emphasis has been placed on irradiation of BeO at elevated temperatures, namely 900 to 1000°C, but data have been accumulated for a range of temperatures from 110 to 1100°C. The integrated dosages for these experiments have varied from about 1.4×10^{20} neutrons/cm^2 for the first test to exposures in excess of 10^{21} fast neutrons/cm^2. Neutron dosages are correlated with fast-neutron flux because the predominant reactions involved and the atom displacements are attributed to neutrons of energies greater than 1 Mev.

A typical capsule is shown in Fig. 7.1 prior to assembly. The penetration of the end cap for an internal thermocouple may be seen. The components are press-fitted together, welded, and finish-machined. A diagram of an assembled capsule is shown in Fig. 7.2. Five of these experimental assemblies have been irradiated and then disassembled in the hot cells at ORNL and at Battelle Memorial Institute. Extensive damage was found in the fourth and fifth units. The conditions of irradiation and results of the experiments are summarized in Fig. 7.3, which indicates the vertical position of the specimen, the irradiation temperature, and the approximate degree of damage found after irradiation. An approximation of the flux profile appears at the right and the megawatt days of irradiation time are given for each experiment. The integrated exposure for each capsule is given in Table 7.3.

The beryllium oxide specimens in all the capsules of experimental assemblies 1 and 2, the No. 1, 3, and 7 capsules of experimental assembly 3, and the first capsule of experimental assembly 5 survived the specified dosages without visible failure at the temperatures listed and under conditions normal to an operating test reactor, including a certain amount of thermal cycling incident to startup operations.

The first evidence of failure was found in capsule 5 of experimental assembly 3. Here each pellet sustained a single longitudinal fracture and a dimensional increase of 0.7% at the indicated fast-neutron exposure of 4.5×10^{20} neutrons/cm^2. Similar pellets, which in this case were hot-pressed BeO of 2.75 g/cm^3 density, irradiated at reactor water temperature to a similar dose remained sound, although a 0.5% increase in gross

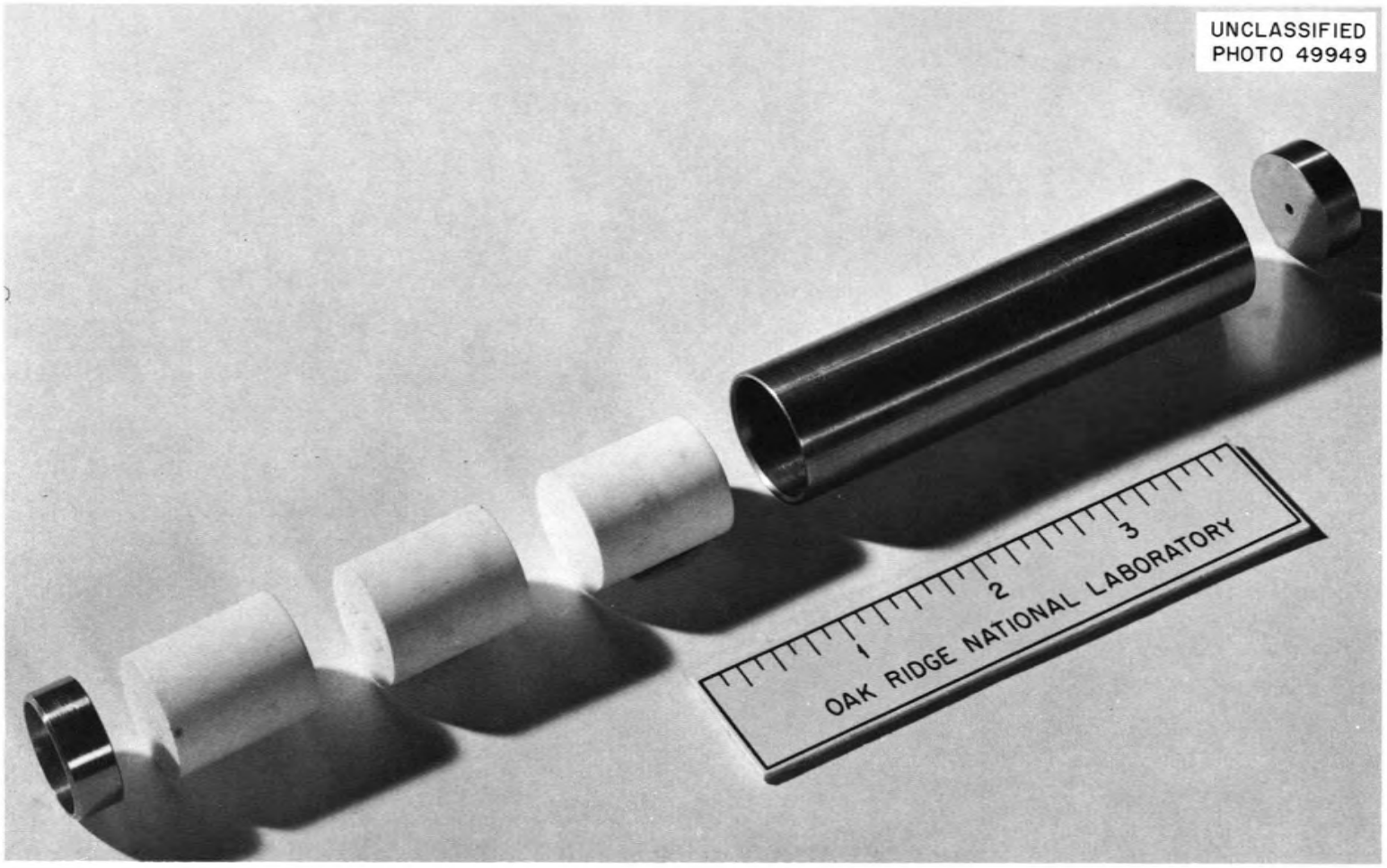

Fig. 7.1. Components of Capsule for Irradiation of BeO Specimen.

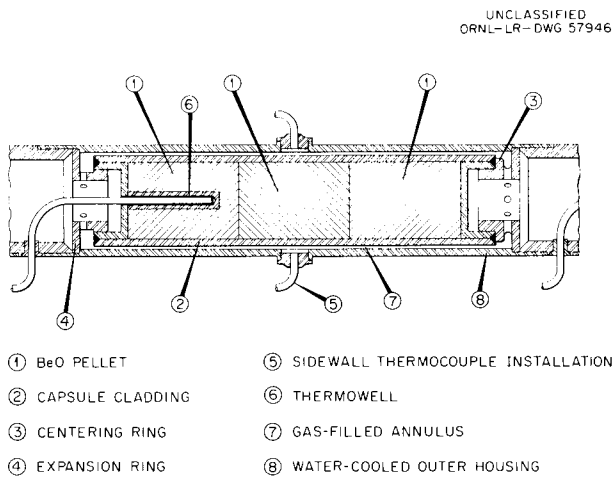

Fig. 7.2. Diagram of Assembled BeO-Irradiation Capsule.

dimensions occurred. Identical BeO specimens of smaller diameter, irradiated at 850°C to a slightly lower dose, also remained visibly sound.

A single longitudinal fracture was found again in the second capsule of experimental assembly 5. This BeO specimen was of slightly lower density (2.68 g/cm^3) and was prepared by isostatic pressing and sintering. It

Table 7.3. Integrated Fast Neutron Dosages of ORNL-41 Experiments

Experiment No.[a]	Capsule No.	Average Density (g/cm^3)	Specimen Diameter (in.)	Fast Neutron (>1 Mev) Dose (neutrons/cm^2)	Irradiation Temperature (°C)	Relative Damage[b]
1	1	2.87	0.636	1.4×10^{20}	722	0
2	1	2.75	0.636	1.1×10^{20}	219	0
	2		0.636	2.3×10^{20}	388	0
	3		0.636	3.5×10^{20}	500	0
3	1	2.75	0.428	1.1×10^{20}	458	0
	3		0.636	3.1×10^{20}	858	0
	5		0.800	4.5×10^{20}	1025	1
	7		0.800	4.4×10^{20}	120	0
4	1	2.68	0.800	$1.8–2.8 \times 10^{21}$	120	(1–3)
5	1	2.68	0.800	1.1×10^{21}	444	0
	2		0.800	1.6×10^{21}	737	0
	3		0.800	2.1×10^{21}	827	1
	4		0.800	2.6×10^{21}	900	2
	5		0.800	2.3×10^{21}	944	2
	6		0.800	2.1×10^{21}	950	2
	7		0.800	1.5×10^{21}	110	3

[a]Specimens for experiments 1–3 were machined from hot-pressed blocks fabricated by the Norton Company for the Aircraft Reactor Experiment. Specimens for experiments 4 and 5 were manufactured from Brush Beryllium UOX grade powder by isostatic cold-pressing at 22 000 psi followed by sintering at 1570°C for 1 hr in nitrogen in a carbon-tube induction furnace. After machining, the specimens were annealed for 24 hr in air. The annealing temperature for experiment 4 was 1400°C and for experiment 5 was 1000°C.

[b]Relative damage: (0) sound specimens; (1) first cracks; (2) general fractures; (3) powder present.

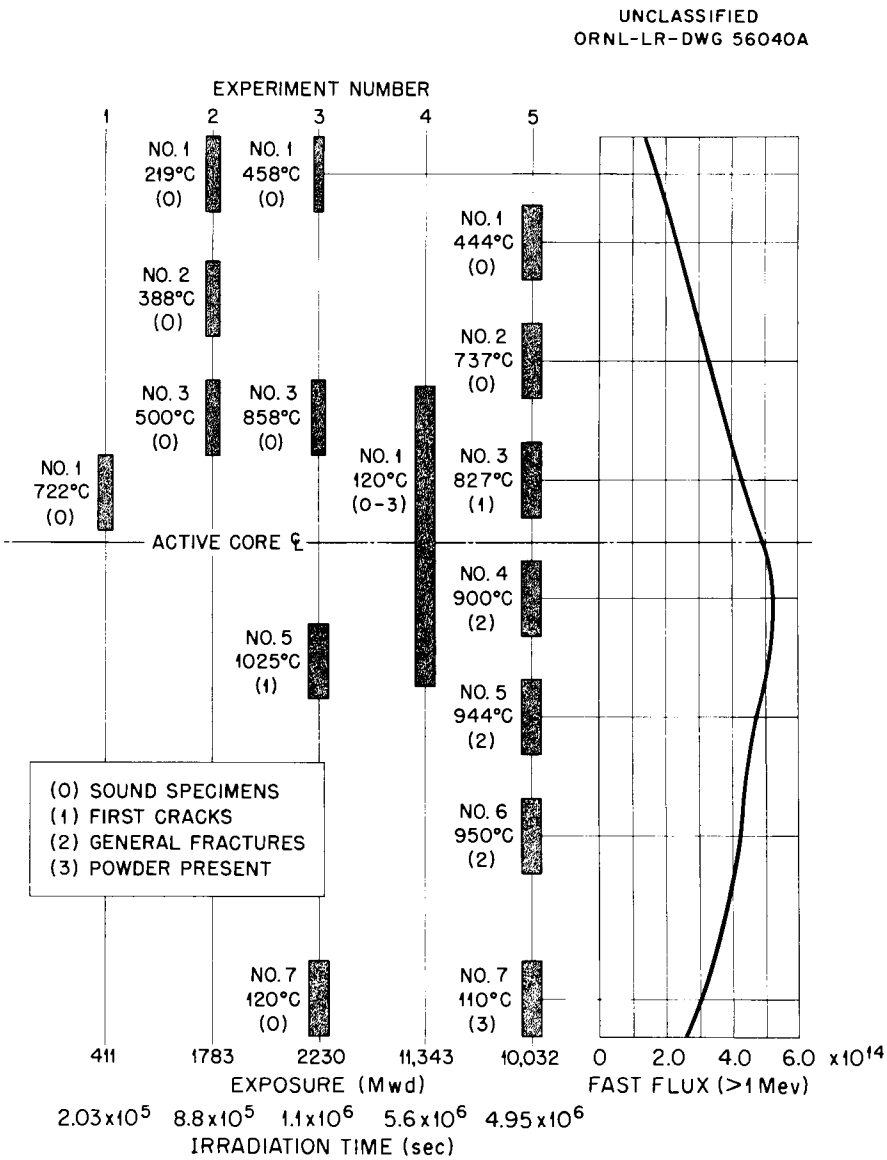

Fig. 7.3. Irradiation Conditions and Results of ORNL-41 Experiments.

sustained a fracture similar to that in capsule 5 of experimental assembly 3 after a fast-neutron dosage of approximately 2×10^{21} neutrons/cm^2. The lower density and intermediate irradiation temperature may have contributed to the apparent ability to survive an increase in total dosage.

Every BeO specimen of capsules 3 through 6 of experimental assembly 5, which was irradiated at higher temperatures and to the progressively greater exposures of more active positions in the core lattice, fractured

completely. The fracturing occurred in both vented and sealed capsules and there was corresponding dimensional growth of 1.5 to 3%.

An example of apparently sound material which was irradiated to a high fast-neutron dose of 1.1×10^{21} neutrons/cm^2 at 440°C without failure is shown in Fig. 7.4. This is typical of some 25 of the irradiated samples described in Fig. 7.3. An example of the initial failure is visible in Fig. 7.5 as a single straight crack across the end of the pellet. Some peripheral separation is also visible in this specimen, which received an exposure of 1.6×10^{21} neutrons/cm^2 at 737°C. The severe radial separation that had begun after an exposure of 2.1×10^{21} neutrons/cm^2 at 827°C may be seen in Fig. 7.6. Note the 90-deg symmetry of the crack dividing the pellet into four groups of radial sections. The three BeO pellets that were exposed at 900°C to a dose of 2.6×10^{21} neutrons/cm^2 are shown in Fig. 7.7. These pellets are typical of the pellets in the three lower capsules of experimental assembly No. 5.

In marked contrast to the higher temperature irradiations mentioned above, the irradiations carried to similarly high exposures at low temperatures, 110 to 120°C internally, yielded BeO material which disintegrated to powder. The capsules containing this material showed a 2.5 to 3.0% increase in diameter of the cladding. A composite photograph of the low-temperature experimental assembly 4, which contained 12 one-inch pellets in a single capsule, is presented in Fig. 7.8. Extensive deterioration may be seen, and the flux variation of 1.8 to 2.8×10^{21} neutrons/cm^2 is evident by comparison of the pellets from one end of the capsule with the pellets from the other. The total length is divided into two sections here in order to display as much detail as possible. It is obvious from the photograph that much of the material disintegrated to powder. The larger fragments were easily ground in a hand mortar.

The BeO in another water-cooled capsule containing three pellets completely burst the cladding after an irradiation dose of 1.5×10^{21} neutrons/cm^2. A portion of the ruptured steel is shown in Fig. 7.9. This view is typical of several fissures extending the full length of the capsule and of the circumferential cladding rupture completely encircling

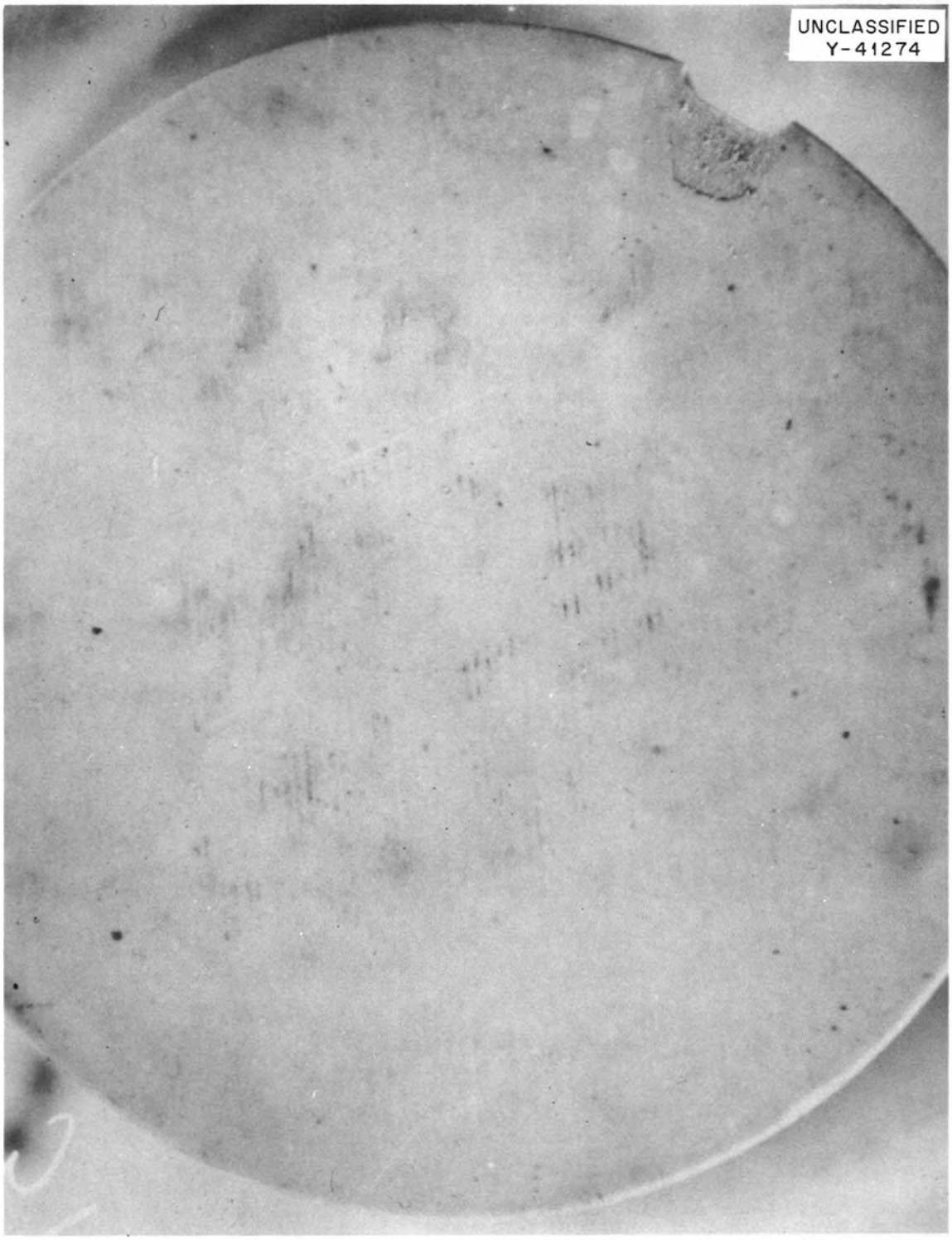

Fig. 7.4. BeO Pellet 5-11B After Irradiation at 444°C to a Fast-Neutron (>1 Mev) Dose of 1.1×10^{21} Neutrons/cm^2. (BMI Print)

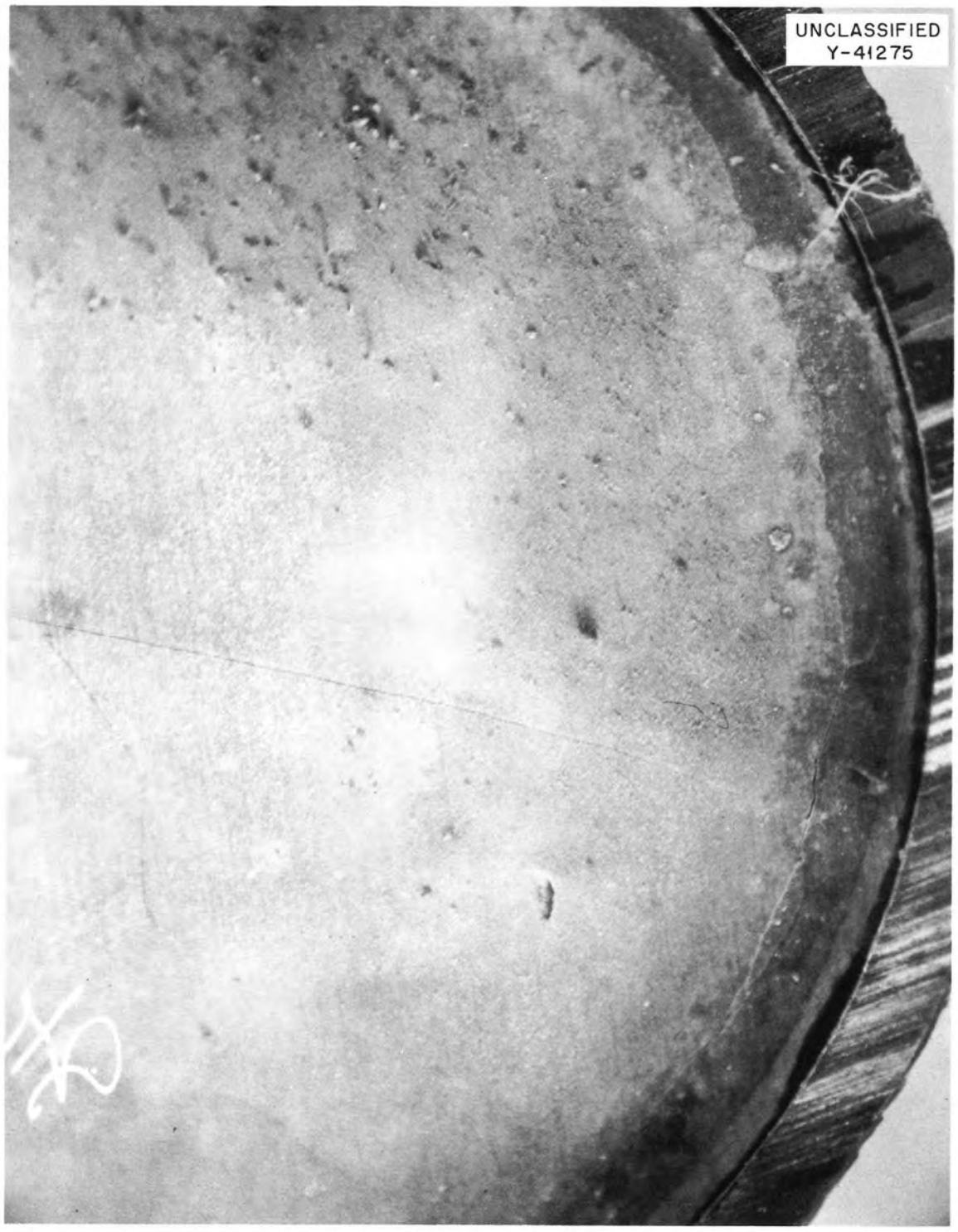

Fig. 7.5. BeO Pellet 5-21A After Irradiation at 737°C to a Fast-Neutron (>1 Mev) Dose of 1.6×10^{21} Neutrons/cm^2. (BMI Print)

Fig. 7.6. BeO Pellet 5-31A After Irradiation at 827°C to a Fast-Neutron (>1 Mev) Dose of 2.1×10^{21} Neutrons/cm^2. (BMI Print)

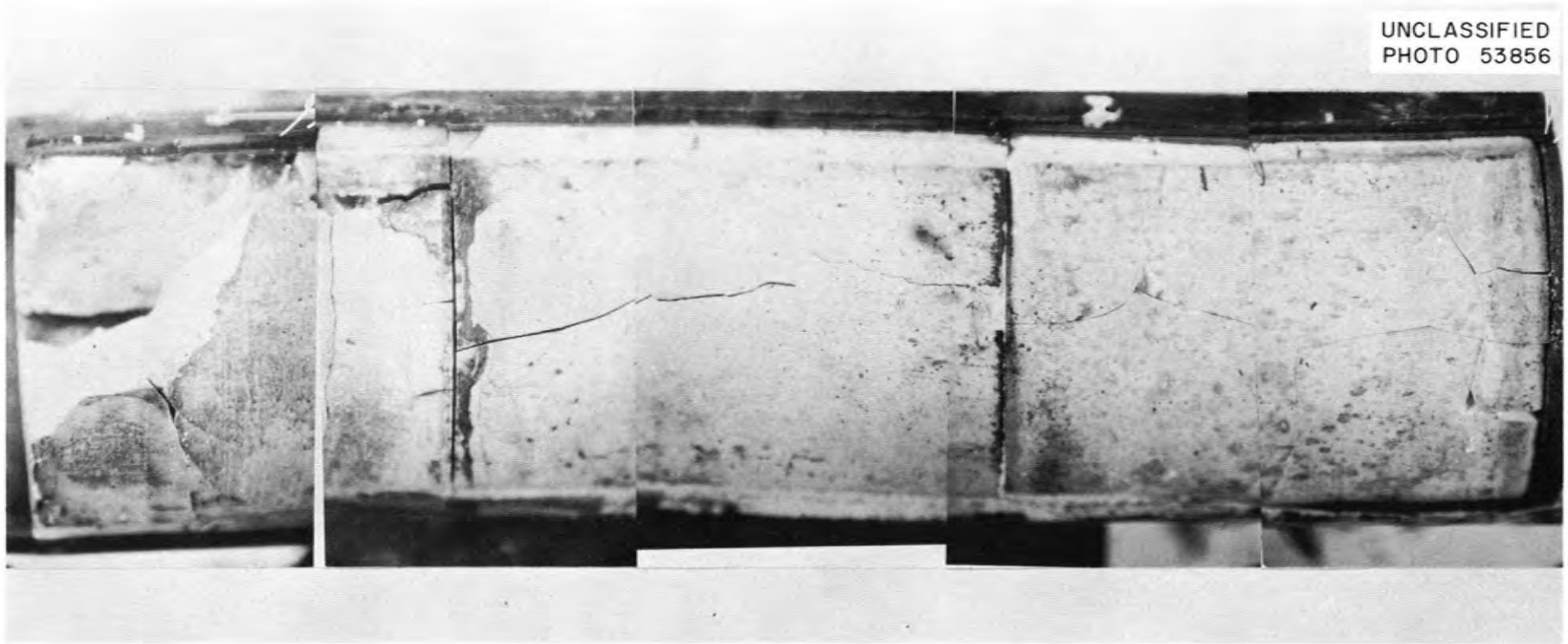

Fig. 7.7. BeO Experimental Assembly 5, Capsule 5, Which Was Irradiated at 900°C to a Fast-Neutron (>1 Mev) Dose of 2.6×10^{21} Neutrons/cm^2.

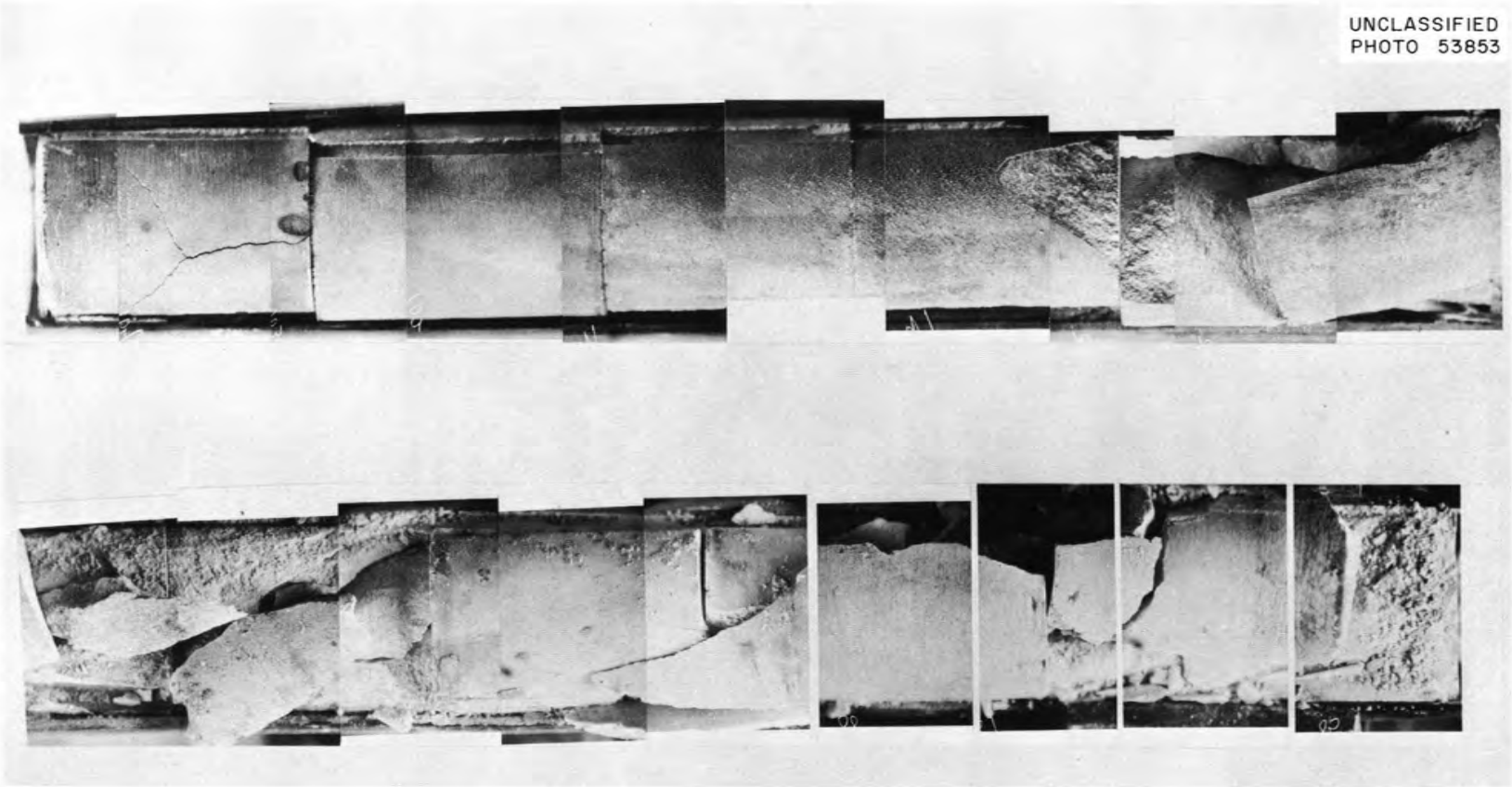

Fig. 7.8. BeO Experimental Assembly 4 with 12 Pellets After Irradiation at 110 to 120°C to a Fast-Neutron Dose of 1.8 to 2.8 × 10^{21} Neutrons/cm^2.

Fig. 7.9. Typical Rupture of Stainless Steel Cladding of Capsule 5-7 Irradiated at 110 to 120°C to a Fast-Neutron (>1 Mev) Dose of 1.5×10^{21} Neutrons/cm^2. (BMI Print)

both ends. A stress of some 7000 psi would be required to effect a rupture of 35-mil cladding in this manner. Thus evidence is available of the internal forces which must be considered. A close-up view of the disintegrated BeO recovered from this capsule is shown in Fig. 7.10.

Metallographic examination of the BeO specimens suggested grain growth at both high and low temperatures in the material irradiated at the intermediate and higher neutron dosages in these experiments. The observed growth may not be firmly defined, since it is random in nature, and irradiated samples can be compared only to representative control samples instead of the same samples before irradiation. The lower density material, 2.68 g/cm^3, of the later tests has been the most difficult to polish satisfactorily because extensive intergranular fracture is apparently present, as evidenced by excessive pullout. Porosity sites and void structures are apparently unchanged in the irradiated material.

X-ray diffraction has been a most effective and informative method in assessing the nature of the damage observed. Beryllium oxide irradiated to a high dose at a low temperature produces diffraction patterns with an unusual asymmetric line broadening. The average hexagonal c_0 parameter is expanded by approximately 0.7% relative to that of the unirradiated oxide, in contrast to the a_0 parameter, which is expanded by only about 0.1%. This is interpreted to indicate a preferred accumulation of defects between oxygen layers in the C-axis direction. Beryllium oxide irradiated at higher temperatures shows only symmetrical line broadening indicating lattice strain of the order of half that measured for low-temperature irradiations at comparable dosage. The diffraction patterns of BeO irradiated to high dosage at low temperature and subsequently annealed at 1100 to 1200°C shows some residual expansion of the C parameters, but the asymmetric line-broadening is no longer present. This condition then is similar to that of the high-temperature irradiated material annealed at several temperatures. The progressive recovery of line broadening at the 0,0,2 peak may be seen in Fig. 7.11.

A lowering of the refractive index occurred in the BeO of capsule 1, pellet 9, in experimental assembly 4, which was irradiated at low temperature and to a high dose. The apparent crystalline expansion detected

Fig. 7.10. BeO from Capsule 5-7 Irradiated at 100 to 120°C to a Fast-Neutron Dose of 1.5×10^{21} Neutrons/cm^2. (BMI Print)

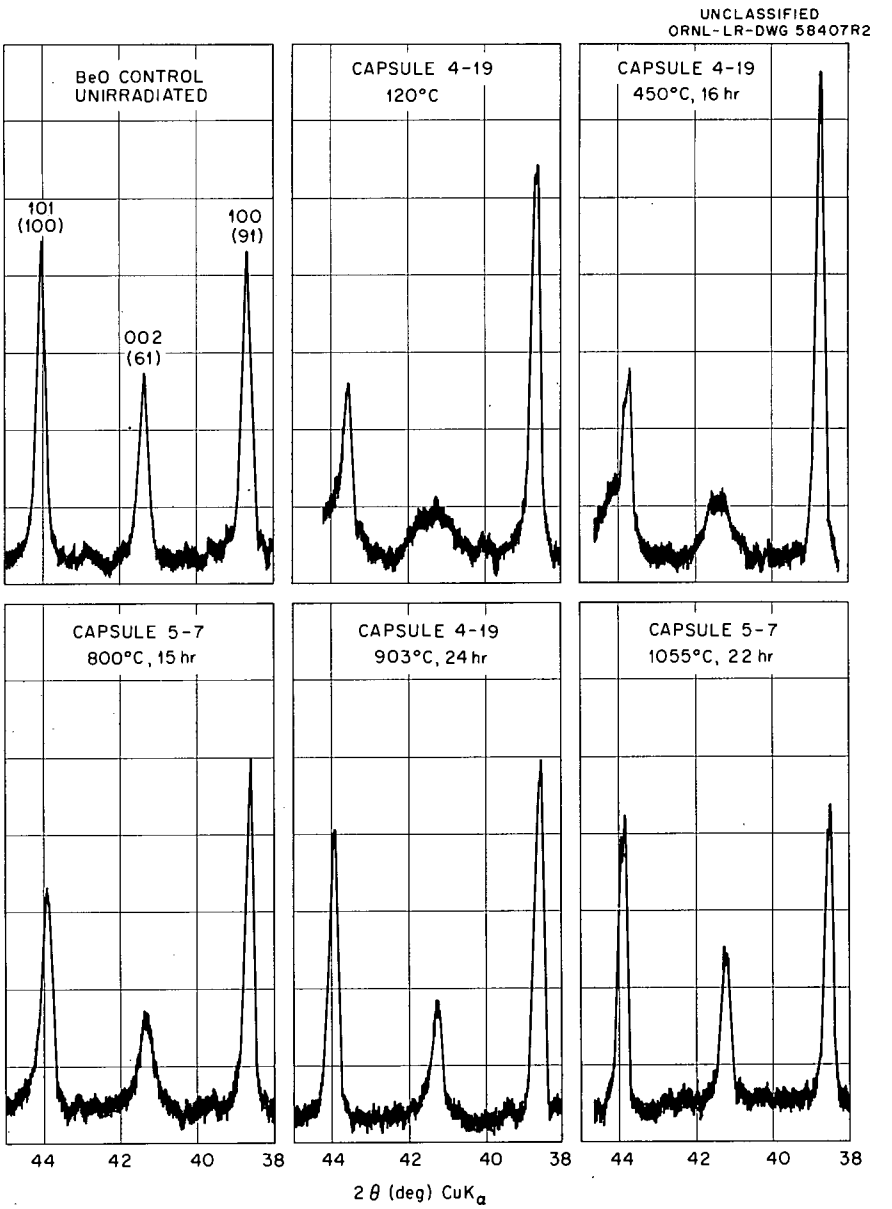

Fig. 7.11. Diffraction Patterns of BeO Specimens Irradiated at 110 to 120°C to an Approximate Dose of 1.5×10^{21} Neutrons/cm^2.

with the polarized-light petrographic microscope may be annealed out by heating to 1055°C, as shown in Fig. 7.12. The effect begins at 770°C, and the refractive index is restored to that of the control material after 22 hr at the peak temperature. This method has been proposed by McVay, Thoma, and Weaver as a simple and inexpensive procedure for evaluating the extent of damage or its repair by annealing; it has not been applied as yet to the material irradiated at higher temperatures.

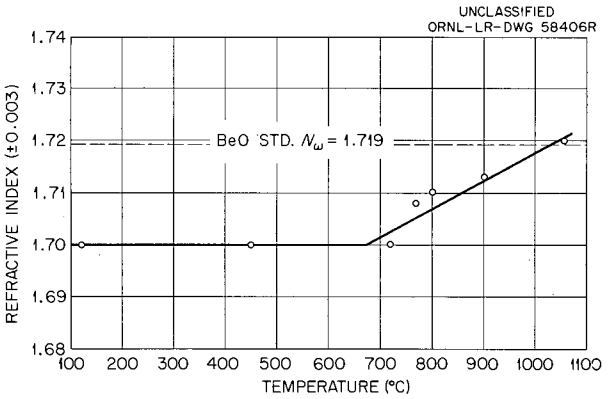

Fig. 7.12. Refractive Index of Irradiated BeO Samples (Series ORNL X-41) as a Function of Annealing Temperature. Same sample as used for Fig. 7.11.

A statistical analysis of data obtained from this series of experiments was performed in an effort to determine whether the changes observed in the material could be correlated with the conditions of irradiation. Information from this kind of analysis is useful for testing hypotheses as to the mechanism of damage. The change in dimension upon irradiation was found to depend more upon integrated exposure than on any other single factor. The changes in dimensions are proportional to the integrated fast flux to a power greater than 1 and less than 2 and inversely proportional to irradiation temperature. The dimensions of BeO specimens could not be correlated with thermal stress. The x-ray diffraction data reveal changes in the c lattice parameter up to 7×10^{-3} $\Delta c/c_0$ for material irradiated at 110°C but only 1 to 2×10^{-3} $\Delta c/c_0$ at 444 to 1025°C. The $\Delta c/c_0$ value appears to saturate by a dose of 3×10^{20} neutrons/cm^2 in the latter temperature range. All temperatures above 444°C were equally effective in suppressing the $\Delta c/c_0$ values.

Beryllium oxide specimens were analyzed for retained helium by dissolving the BeO in fused salt. The helium content was found to vary linearly with fast neutron dose up to 1.6×10^{21} neutrons/cm^2 with a slope of 205 standard microliters per gram of BeO per 10^{21} neutrons/cm^2. This is much lower than the value of 1.32 ml/g per 10^{21} neutrons/cm^2 which would be expected based on data in the present literature. Helium was retained even at irradiation temperatures up to 1025°C. The tritium content of BeO irradiated at 110°C followed a (neutrons/cm^2)^2 curve up to 6.4 ppm at 2.1×10^{21} neutrons/cm^2 in agreement with theoretical expectation, since two neutrons are required to produce tritium. Specimens irradiated above 444°C contained much less tritium, which was lost to an increasing degree at higher temperatures. The apparent activation energy for diffusion of

tritium was calculated to be 6 kcal/mole and the diffusion rate at 950°C is 7×10^{-7} sec^{-1}.

Thermal conductivity changes in irradiated BeO are important to complete evaluation of this material. No such measurements have been completed, but changes in barrier gas composition required to maintain constant temperature during irradiation indicate qualitatively that the conductivity does decrease. The temperature gradient has also been found to increase by as much as 100% after an irradiation of 3 to 4×10^{20} at 1000 to 1100°C.

The current experiment which was designed to test larger sized specimens at correspondingly greater thermal stresses and to permit more accurate thermal gradient measurements has apparently functioned normally in the ETR. A preliminary review of the critical first hours of operation at full reactor power indicates that there was no failure detectable by abnormalities in the temperature records or the barrier gas flow and pressure data. A detailed report giving information on this experiment and the entire test series is being prepared. Additional studies will be reported in future Reactor Chemistry Division progress reports.

Effects of Annealing Irradiated BeO

T. N. McVay C. F. Weaver
H. Insley H. A. Friedman
R. E. Thoma

Simple techniques for quantitative petrographic measurements of the changes in the crystallinity of BeO upon irradiation are being used to show the effects of annealing at various temperatures. The results have been correlated with x-ray diffraction information which indicated, semi-quantitatively, changes attributable to radiation damage and subsequent thermal annealing.

Petrographic examination of series ORNL-41 samples of BeO, irradiated to a fast-neutron (>1 Mev) dosage of 1.5×10^{21} neutrons/cm^2 at 120°C revealed that the indices of refraction were substantially lower than those of normal unirradiated control specimens, suggesting that an expansion of

the crystal lattice had occurred. A similar and even more disordering effect of radiation on crocidolite and amosite has been reported in the literature.

Heating the irradiated material overnight at 800°C raised the refractive indices from N_O = 1.700 and N_E = 1.712 to N_O = 1.710 and N_E = 1.722, suggesting that the annealing treatment had removed a substantial fraction of the radiation damage. Subsequent annealing tests at temperatures of 450 to 1055°C for periods from 16 to 143 hr showed that the return of the refractive indices to their normal values, N_O = 1.719 and N_E = 1.733, appeared to be complete at 1055°C (see Fig. 7.12). The values for the index of refraction given in Fig. 7.12 are those reached by annealing at the indicated temperatures. Different effects might be obtained if the annealing were continued for times very large relative to 100 hr.

In connection with the annealing studies discussed above, routine x-ray diffraction patterns were obtained as indicated by Fig. 7.11. In these diffraction patterns the 002 line is associated with the c-axis; the effects of irradiation and subsequent annealing were quite striking. It should be noted that both the position of the 101 line and its relative intensity were affected by the irradiation and that these changes were reversed by the annealing. Although the interpretation of the x-ray diffraction patterns is not so simple or so amenable to quantitative treatment as are the measurements of refractive index, the correlation between the two types of results is believed to provide considerable support for the usefulness of each in determining the effects of radiation on the crystallinity of BeO.

The results of continuing investigations of the crystal characteristics of irradiated and annealed BeO will be included in reports of the Pure Materials Research and Development Program.

PART 2. SHIELDING RESEARCH

8. APPLIED SHIELDING

Tower Shielding Reactor II (TSR-II)

L. B. Holland

Reactor Power Calibration

During the experiments with the Pratt & Whitney-designed lithium hydride–uranium reactor shield,[1] an absolute calibration of the power of the Tower Shielding Reactor II (TSR-II) was made by coupling a 40-kw electric water heater to the reactor and circulating water through both the reactor and heater. The first part of the procedure was to gradually heat the system with all pumps running until an equilibrium was reached between the heat input from the pumps and the losses from the system. The system was then cooled to below ambient temperature, and the temperature rise of the system was measured as a function of time, first with the system heated by a heater and then by operation of the reactor. Instruments from the reactor controls standards room were used to measure the electrical power input. The reactor power was changed until the slopes versus time of the temperature rise of the system due to the heater and to the reactor taken at ambient temperature agreed. Without changing settings the runs were repeated under different ambient conditions and the slopes agreed within 0.6%. A complete error analysis has not been made, but the errors should be small because both the reactor fuel elements and the heating elements were submerged in water and the 200-gpm flow rate should minimize losses in the short section of piping between the electric heaters and the fuel elements.

Reactor Linearity

Since preliminary measurements showed a variation of 10% in the linearity of the reactor power,[2] a technique was developed to measure the

---

[1]V. R. Cain, ANP Semiann. Prog. Rep. April 30, 1961, ORNL-3144, pp. 148–59.

[2]L. B. Holland, ANP Semiann. Prog. Rep. April 30, 1961, ORNL-3144, pp. 93–98.

values of the resistors in the micromicroammeter which controls the reactor power. The resistors were found to be nonlinear in a manner which reflected the reactor power nonlinearity. New resistors were selected and the micromicroammeter was rebuilt. The reactor power is now linear to within 1%.

Reactor Mechanical System

Upon completion of the experiments with the lithium hydride—uranium reactor shield, the reactor was dismantled for repairs. A new 6-in. inlet hose was installed to replace hose that had previously failed.[2] At a later date the 6-in. outlet hose from the reactor will be replaced.

The three chamber wells in the ionization chamber guide assembly which had collapsed under high pressure were replaced with heavier walled wells which can be removed for repairs if necessary.

The Pratt & Whitney Divided-Shield Experiment at the Tower Shielding Facility

V. R. Cain S. K. Penny

The Pratt & Whitney divided-shield mockup experiment at the Tower Shielding Facility has been completed. As reported previously,[1] the mockup consists of a reactor shield constructed to a design that was optimized insofar as possible with the available data and the cylindrical compartmentalized crew compartment used in earlier experiments at the TSF. The reactor shield consists of a lithium hydride neutron shield and a uranium gamma-ray shield, both largely concentrated on the side facing the crew compartment. The crew shield material consists of an inner liner of lead surrounded by compartments filled with water, transformer oil, or borated transformer oil. In addition, a water-filled "patch" tank was constructed so that it could be moved around the shield in the horizontal plane to check the shape optimization of the reactor shield.

The completed measurements include the previously planned dose-rate and flux mappings in air around the reactor shield and in the crew compartment. Complete crew-shield parameter studies were made for side and rear

variations of both neutron (water) and gamma-ray (lead) shielding, and some additional measurements were made with the borated and unborated transformer oil. Unfortunately, it was not possible to perform the desired neutron and gamma-ray spectral measurements.

In general, the neutron dose rates measured in the experiment agreed with those calculated in an ORNL preanalysis,[3] as well as with those calculated in a Convair preanalysis;[4] however, the predictions from a third preanalysis, by Pratt & Whitney,[5] disagreed at some points. Specifically, the neutron dose in the crew compartment calculated by ORNL was in exact agreement with the measurements, the Convair prediction was only about a factor of 1.6 too high, and the Pratt & Whitney prediction was practically in agreement, although slightly low. For the neutron dose rates in air, the ORNL and Convair preanalyses agreed with the experiment within 20% for most points, although some ORNL points disagreed by as much as 50%. The Pratt & Whitney calculations included only two in-air points (50 ft from the front and rear of the reactor shield, respectively), and both points were a factor of 2.7 low.

In the case of the gamma-ray dose rates, the Pratt & Whitney prediction for a point in air 50 ft from the rear of the reactor shield was only very slightly low, whereas the ORNL calculation was approximately a factor of 2 high and the Convair prediction a factor of 2 low. The discrepancy between the ORNL prediction and the measured value at the rear can be attributed to the method used for calculating the attenuation of the direct radiation through large thicknesses. At a point 50 ft from the front of the reactor shield, the ORNL prediction agreed with the measured value, while the Pratt & Whitney and Convair values were a factor of 3.7 and 9.8 too low, respectively.

---

[3]S. K. Penny and D. K. Trubey, ANP Semiann. Prog. Rep. April 30, 1961, ORNL-3144, pp. 129–48.

[4]J. B. Eggen and E. E. Jones, Preanalysis of Pratt and Whitney Experiment at the Tower Shielding Facility, Convair, NARF-61-2R (MR-N-277), Feb. 1, 1961.

[5]Calculations of the Expected Dose Rates for the P & WA Divided Shield Mockup at ORNL, Pratt & Whitney Aircraft, CNLM-3596, March 13, 1961.

All the gamma-ray dose-rate predictions for the crew compartment disagreed with the experimental results, the ORNL calculation being a factor of 3.5 too low, the Convair calculation a factor of 7.8 low, and the Pratt & Whitney prediction a factor of 2.9 low. These disagreements are confused by the fact that the Convair calculation, which disagreed the most, included air-capture and crew-shield secondary gamma-ray effects, whereas the Pratt & Whitney calculation neglected the secondary effects and the ORNL calculation neglected both the air-capture and the secondary effects.

No postanalyses will be performed by ORNL; however, it appears that an analysis will be made by Convair. This will be facilitated by a forthcoming ORNL topical report which will include all the TSF measurements and a discussion of the ORNL preanalysis.[6]

---

[6]V. R. Cain, S. K. Penny, and D. K. Trubey, The Pratt and Whitney Divided Shield Mockup Experiment at the TSF: Comparison of Experiment and Preanalysis (to be published as an ORNL report).

9. DEVELOPMENT OF RADIATION DETECTION EQUIPMENT

Gamma-Ray Spectroscopy

The Model-IV Gamma-Ray Spectrometer (G. T. Chapman)

A series of experiments intended to assist in the development of an optimum collimator system for the Model-IV Gamma-Ray Spectrometer has been completed, and data analysis is being carried out. The collimator system, including the port through the shield and the 5-ft-long air cone previously added, will be acceptably optimized when the contribution to a measured spectrum due to scattering from the collimator walls is reduced to a minimum. The cone has decreased the number of capture gamma rays born in the spectrometer shield by introducing a greater thickness of water for neutron shielding between the source and spectrometer housing.

A thorough study of the background associated with the spectrometer has suggested that a major contribution is due to cosmic-ray interactions with the components of the spectrometer shield. As shown in Fig. 9.1, there exist peaks in the distribution up to 116 Mev. (Engeries for peaks below 3.26 Mev were assigned by comparison with known source energies; above 3.26 Mev they were estimated by extrapolations based on the linearity of the system as determined by a standard pulser). A 19-ft water thickness above the spectrometer reduced the background about 30% in amplitude in the high-energy region. The possibility that the peaks shown are due to neutron capture reactions within the spectrometer shield was minimized when a comparison of data obtained with the spectrometer approximately 6 ft from a reactor operating at a power of 2 watts with data obtained at the same distance from the shutdown reactor showed no observable change. A measurement taken 72 hr after the spectrometer was last exposed to reactor neutrons failed to show any decay of the peaks with time, indicating that the peaks cannot logically be associated with any expected neutron-activated isotope in the spectrometer.

The Model-IV spectrometer, now ready for use, will initially be employed in a measurement of the energy distribution of the gamma rays from

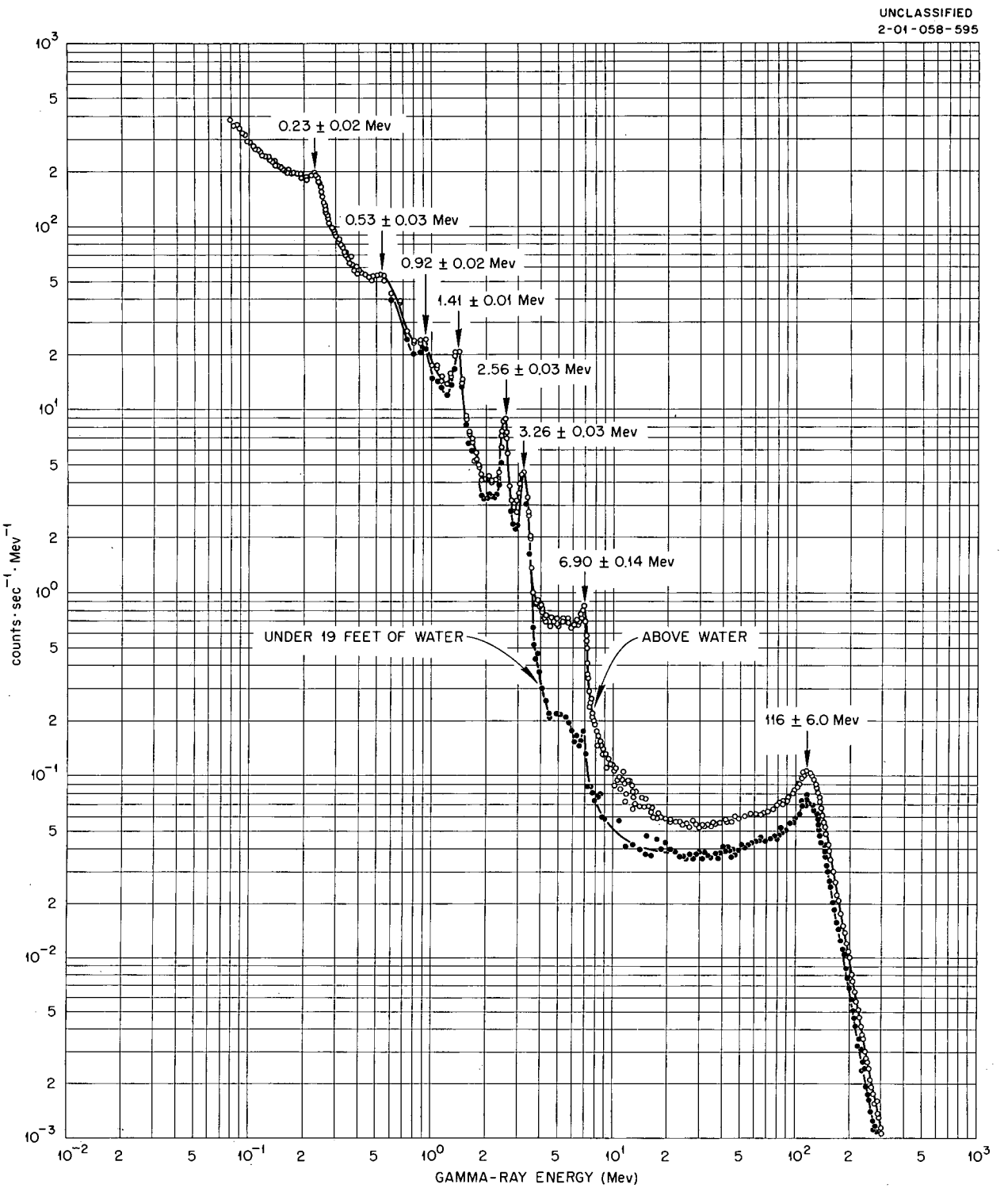

Fig. 9.1. Model-IV Gamma-Ray Spectrometer Background.

the stainless steel BSR-II. These data will be reported in future Neutron Physics Division publications.

Monte Carlo Calculations of the Pulse-Height Response of NaI(Tl) Scintillation Counters (C. D. Zerby, H. S. Moran)

An extensive series of calculations of the pulse-height response of a 3-in.-diam by 3-in.-high NaI(Tl) crystal have been performed using a Monte Carlo code that was previously reported.[1] In these calculations the source was taken as a point isotropic source of gamma rays located on the centerline of the crystal 10 cm from one end. The energy of the gamma rays ranged from 0.1 to 6.0 Mev.

The pulse-height response spectra from these calculations will be reported in detail in a later publication;[2] however, the peak-to-total ratios and the intrinsic efficiencies are given here (Table 9.1). The peak-to-total ratio is the ratio of the number of counts in the total absorption peak to the total number of counts, and the intrinsic efficiency is the probability that an incident proton will have at least one collision in the crystal. The error indicated on the peak-to-total ratio is plus or minus one standard deviation and was estimated in the course of the calculation.

Unscrambling of Scintillation Spectra

W. R. Burrus

In scintillation spectroscopy, the aim is to estimate the spectrum of a source of radiation or to estimate some function of the spectrum (such as tissue dose). Instead of measuring the spectrum, a set of numbers is observed which represent the accumulated number of counts in the "bins" of a multichannel pulse-height analyzer. The "unscrambling" problem is that of estimating the desired spectrum or quantities from the observed count data.

---

[1]ANP Semiann. Prog. Rep. Oct. 31, 1960, ORNL-3029, p. 96.

[2]C. D. Zerby and H. S. Moran, Calculation of the Pulse-Height Response of NaI(Tl) Scintillation Counters, ORNL-3169, July 7, 1961.

Table 9.1. Intrinsic Efficiency and Peak-to-Total Ratio for a 3-in.-diam by 3-in.-High NaI(Tl) Scintillation Counter

Source Energy (Mev)	Intrinsic Efficiency	Peak-to-Total Ratio
0.1	0.972	0.9919 ± 0.0004
0.15	0.927	0.9779 ± 0.0009
0.2	0.874	0.9520 ± 0.0016
0.25	0.825	0.9080 ± 0.0025
0.279	0.798	0.8845 ± 0.0030
0.3	0.781	0.8546 ± 0.0034
0.35	0.745	0.8102 ± 0.0041
0.4	0.714	0.7622 ± 0.0049
0.45	0.688	0.7078 ± 0.0054
0.5	0.666	0.6683 ± 0.0060
0.6	0.632	0.6014 ± 0.0068
0.661	0.615	0.5693 ± 0.0058
0.7	0.605	0.5538 ± 0.0073
0.8	0.583	0.5036 ± 0.0079
0.9	0.563	0.4692 ± 0.0083
1.114	0.530	0.3842 ± 0.0091
1.275	0.510	0.3413 ± 0.0095
1.38	0.498	0.3262 ± 0.0079
1.6	0.478	0.3016 ± 0.0099
1.78	0.465	0.2862 ± 0.0101
2.14	0.445	0.2441 ± 0.0102
2.4	0.435	0.2143 ± 0.0104
2.76	0.424	0.1962 ± 0.0085
3.13	0.417	0.1650 ± 0.0088
3.57	0.411	0.1548 ± 0.0107
4.0	0.408	0.1345 ± 0.0109
5.0	0.405	0.1035 ± 0.0112
6.0	0.405	0.0918 ± 0.0113

Two previous progress reports[3,4] have discussed the use of the non-negativity property of the spectrum in improving estimates and the nature of the restrictions imposed on the resulting estimates by this property. This report summarizes a newly developed technique of unscrambling. Further details will appear in ORNL reports.[5,6]

[3]ANP Semiann. Prog. Rep. Oct. 31, 1960, ORNL-3029, pp. 121–8.

[4]ANP Semiann. Prog. Rep. April 30, 1961, ORNL-3144, pp. 100–12.

[5]Walter R. Burrus, The Theory of Corrections for Instrumental Scrambling of Spectra (preliminary copy of dissertation), to be published.

[6]Walter R. Burrus, Unscrambling of Scintillation Spectra, to be published as an ORNL Report.

Unfortunately, as will be seen later, no method of estimation can determine the incident spectrum from a finite number of observed counts. If additional information about the form or shape of the spectrum is available, then it may be possible to determine the spectrum. But in this study, an estimation method is described which makes no prior assumptions about the spectrum. As an alternative to the spectrum itself, it is possible to estimate a smoothed spectrum, $\phi^*(e')$, such that for a discrete source at energy e, $\phi^*(e') = S(e,e')$. It is also possible to estimate macroscopic quantities, such as tissue dose, which are related to the incident spectrum by a cross section.

In principle, the method considers that each pulse-height channel of the spectrometer is an independent detector with a certain energy-dependent sensitivity $K_i(e)$ such that $K_i(e)$ is the average number of counts obtained in the ith channel for a unit source of energy e. Then an effort is made to find a combination of these independent pseudo-detectors that gives a combined response similar to the desired response. By combining the observed counts obtained in the different channels (or pseudo-detectors), an estimate of the desired quantity is obtained. Thus if an estimate of the tissue dose were desired, an effort would be made to match the dose cross section of the tissue, and if an estimate of a smoothed spectrum were desired, an effort would be made to match the function $S(e,e')$ for various values of e', each corresponding to one point of the smoothed spectrum.

The problem of finding the combination of pseudo-detectors which results in the best estimate for each quantity, in the sense of the narrowest confidence interval, has been formulated as a problem in mathematical programming. Most previous unscrambling methods displayed a tendency to give surreptitious results if the desired response could not be matched exactly by the available pseudo-detectors. This tendency is avoided by finding two combinations of pseudo-detectors: one which has a greater response than the desired one at all energies and another which has a smaller response at all energies. Then, even though the desired response cannot be matched exactly, it can be bracketed between two limits. Then,

because of the nonnegative property of the spectrum, the upper and lower bounds for the desired quantity can be estimated.

By the use of this technique, an interval can be obtained with a specified degree of confidence. The formulation considers the expected statistical variations in the counting rates and also estimated uncertainties in the response of the individual pseudo-detectors, which is to say, in the response of the spectrometer. The reason the spectrum itself cannot be estimated is that it would be necessary to match a delta function in order to obtain one point of the spectrum, and the delta function can only be crudely approximated with a finite number of pseudo-detectors.

Neutron Spectroscopy

Energy Transmission Functions for Neutron-Chopper Spectrometers
(V. V. Verbinski)

As part of the design effort on a neutron-chopper spectrometer for the Bulk Shielding Facility,[7,8] an IBM program was developed for calculating the energy dependence of neutron transmission through the slits of the chopper rotor. This "transmission function" is by far the most important unknown in converting observed time-of-flight spectra to energy spectra. Also, computation of the transmission function for a few basic slit geometries is important in obtaining a good slit design. Several techniques were developed that make the computation both efficient and accurate, and although the chopper project has been terminated, the techniques will be described in a forthcoming report, since they will be applicable to other chopper designs and can be used with many modern computers.

The calculated transmission function has been compared with that deduced from experiments with the fast chopper facility at the Oak Ridge Research Reactor. Curves of the calculated and experimental transmission functions have the same general shape but do not overlap. The mismatch is in a direction expected when the chopper rotor oscillates laterally

---

[7]ANP Semiann. Prog. Rep. Oct. 31, 1960, ORNL-3029, p. 142.

[8]ANP Semiann. Prog. Rep. April 30, 1961, ORNL-3144, p. 123.

with respect to the entrance and exit collimator. These oscillations are in evidence from the pattern of light pulses through the chopper slits. Such oscillations decrease the effective average slit width and strongly suggest that a rotor designed for obtaining neutron spectra over several orders of magnitude in neutron energy either have a fixed-bearing rotor with bearing play small compared with slit width or that the fine entrance and exit collimators be replaced with coarse collimators. The latter expedient would change the chopper to a beam sweeper for which no accurate alignment of rotor and collimator is needed, although burst width and background tend to be larger.

Further discussion of the transmission functions and a reference to the topical report will appear in the forthcoming annual progress report of the Neutron Physics Division.

Use of Silicon Surface-Barrier Counters in Fast-Neutron Detection and Spectroscopy (T. A. Love, R. B. Murray, K. M. Henry)

It was reported previously[9] that the newly developed semiconductor neutron detector, which consists of a thin layer of Li^6F between two silicon-gold surface-barrier counters, would be used to measure the neutron spectrum at the surface of the Tower Shielding Reactor II. When the attempt was made, however, it was discovered that the method used for obtaining the background which compared diodes with and without the Li^6F coating was inadequate. As a result, the measurement was discontinued. A method has now been developed for obtaining the background, which involves the adjustment of the barrier depth of the uncoated diode to be equal to that of the coated diode. A series of measurements showed that the normalization was good to within 1%.

Other developments have included the construction and testing of a large-area diode (1.69 cm in diameter). The efficiency of this diode was determined by comparing it with gold foils, and the agreement was to within 10% for thermal neutrons.

---

[9]T. A. Love, R. B. Murray, H. A. Todd, and J. J. Manning, ANP Semi-ann. Prog. Rep. April 30, 1961, ORNL-3144, pp. 113–21.

Thus far attempts to substitute Li^6 metal for Li^6F have been unsuccessful. Also, the magnitude of the count loss at 14 Mev is still undetermined; however, this will be investigated further with measurements of 14.7-Mev neutrons from the T(d,n) reaction in the Cockcroft-Walton generator.

It is planned to later measure the spectrum of a loading of the new stainless-steel-clad Bulk Shielding Reactor II. The results of these measurements will be reported in Neutron Physics Division annual progress reports.

Experimental Determination of Flux Depression and Other Corrections for Gold Foils Exposed in Water

W. Zobel

No additional experimental data have been obtained in the continuing investigation aimed at determining a correction factor for thermal-neutron flux measurements made with gold foils in water;[10] however, the analysis of the data for 40-$\mu g/cm^2$ to 493-mg/cm^2 foils is still incomplete. The attempts to obtain a correction factor ϕ_0/ϕ, where ϕ_0 is proportional to the unperturbed flux and ϕ is proportional to the flux calculated from measurements with a foil of a given thickness, by fitting the data with polynomials proved not to be very satisfactory. It appears that a better fit may be obtainable with exponential functions, and calculations along this line are currently in progress. The results will be reported in future Neutron Physics Division annual progress reports.

[10]ANP Semiann. Prog. Rep. Oct. 31, 1960, ORNL-3029, p. 151.

10. BASIC SHIELDING STUDIES

Monte Carlo Calculations of Gamma-Ray Penetration Through Shields

S. K. Penny

Success in using the "conditional" Monte Carlo method to predict gamma-ray energy buildup factors[1] in water to approximately 20 mfp and in lead to approximately 10 mfp led to plans for continued research on the method for deep penetration of gamma rays in infinite slabs or finite spherical geometries. Further, a careful analysis of the angular and energy distributions of the penetrating gamma rays, whether in infinite or finite media, was to have been carried out. As of June 30, 1961, however, the study was suspended, at least temporarily. If additional support should be obtained for this work, it will be extended to include studies of buildup factors and differential energy spectra of gamma rays penetrating various types of concrete. It will also include general research on Monte Carlo methods, a phase of which could be carried out with a fairly general gamma-ray history generating code which is now being developed and which is similar to the 05R Code for neutrons.[2]

Grinder – An IBM-704/7090 Monte Carlo Program for Estimating the Scattering of Gamma Rays from a Cylindrical Medium

D. K. Trubey

The Monte Carlo program[3] written for IBM-704/7090 computations of energy spectra and dose rates of gamma rays scattered from within a homogeneous right-circular cylinder (such as a crew shield) to various positions outside the cylinder was never actually applied to ANP calculations; however, it could be applicable to other projects. For example, small

---

[1] ANP Semiann. Prog. Rep. Oct. 31, 1960, ORNL-3029, p. 166.

[2] R. R. Coveyou, J. G. Sullivan, and H. P. Carter, Neutron Phys. Ann. Prog. Rep. Sept. 1, 1958, ORNL-2609, p. 87.

[3] ANP Semiann. Prog. Rep. Oct. 31, 1960, ORNL-3029, p. 177.

modifications will probably be done in connection with duct and collimator studies in basic shielding research. Another modification could make it useful for computing the dose rate in civil defense shelters. The need for cylinder calculations, as opposed to slab calculations, was expressed by Spencer.[4]

Moments-Method Studies of Neutron Penetration in Be and BeO

H. Goldstein, NDA Subcontract 1468

A comprehensive moments-method study of neutron penetration in beryllium and BeO has been carried out by Nuclear Development Corporation of America. Both a fission source and monoenergetic sources from 0.5 to 8 Mev have been covered, and the calculations have yielded information on ages, fast effects, flux spectra, and neutron dose. The effects of changing cross sections were observed during the calculations.

The best value that has been computed for the indium resonance age of neutrons from a fission source in beryllium is 69 cm^2, which is definitely in disagreement with the experimental value of 80 ± 2 cm^2 obtained by Nobles and Wallace.[5] The calculated value for the age in BeO is 89 cm^2, which is in reasonable agreement with the experimental value of 93.5 ± 5 cm^2 obtained by Goodjohn and Young.[6]

This work will be discontinued and the results reported in a topical report.

Spatial and Spectral Details of Neutron Fluxes in Shielding Materials

V. V. Verbinski

Experiments

The series of measurements at the Linear Accelerator Facility of General Atomic, San Diego, to determine the energy spectra of neutrons

---

[4]L. V. Spencer, Shielding Symposium Proceedings 31 October – 1 November 1960, NRDL-OCDM R and L No. 110, p. 481, U. S. Naval Radiological Defense Laboratory.

through lithium hydride slabs has been completed, and analysis of the data is under way. As was discussed previously,[7] use of the GA facility was decided upon when construction of the neutron-chopper facility planned for the BSF was cancelled. The GA facility provides a pulsed-neutron source that approximates a fission source. Five-microsecond bursts of 18-Mev electrons strike a lead target. Bremsstrahlung radiation from the electrons excite the lead nuclei and give rise to a boil-off of neutrons that resembles a fission-neutron spectrum. The LiH slabs were positioned about 10 cm from the 5-μsec bursts of neutrons. Some of the neutrons that penetrated the shield passed through a pre-collimator and down a 16-m drift tube where they were counted by a stack of $B^{10}F_3$-filled proportional counters. Pulses from the counters were sent to a time-of-flight analyzer. The resultant time-of-flight spectra were converted to energy spectra with the aid of computer codes developed at GA. The codes subtracted background, corrected for the burst width and counter response, and grouped the time-of-flight data into 10% energy intervals.

Spectra of leakage neutrons emitted normal to the slab face of the LiH were measured for slab thicknesses of 2.5, 5, and 10 cm, and the maximum energy range covered was 400 ev down to about 0.003 ev. A preliminary examination of the data shows this low-energy leakage spectrum to be nearly constant with thickness between 5 and 10 cm. A 10-cm slab was used to obtain leakage spectra for neutrons emerging at angles of 30 and 60 deg from the normal. For these measurements, the slab-source configuration was rotated bodily with respect to the drift tube. At these angles the beam flash that had previously incapacitated the $B^{10}F_3$ counters for over 100 μsec was greatly reduced and enabled spectral measurements to be made to several hundred electron volts.

---

[5]R. Nobles and J. Wallace, The Diffusion Length and Age in Beryllium, ANL-4076, 1947.

[6]A. J. Goodjohn and J. C. Young, The Slowing Down of Fission Neutrons in Beryllium Oxide, Paper 29-6, Transactions of the American Nuclear Society, Winter Meeting, December 12-15 1960, p. 488.

[7]V. V. Verbinski, ANP Semiann. Prog. Rep. April 30, 1961, ORNL-3144, p. 123.

Neutron spectra were also obtained within slabs of LiH, at several distances from the neutron source. Two methods were used. In the first method a 4-in.-thick LiH slab through which a 1 1/4-cm-diam hole was cut was always placed at the outer surface of the shield. Between this slab and the source were positioned other slabs of LiH varying in thickness from 2.5 to 10 cm. The spectrum of neutron current leaking from the hole (the precollimator occludes the walls) in the outer slab was thus obtained, and it is presumably related to the internal total-flux spectrum through an expression derived by Purohit.[8] This presumption will be checked by applying Purohit's corrections to the neutron-current spectrum and comparing this spectrum with that of the scalar flux spectrum obtained by the second method. In this second method an 8-in.-thick LiH slab with a 1 1/4-cm-diam hole all the way through it was placed adjacent to the source, and the spectrum was obtained with a zirconium-scatterer positioned at various distances from the source corresponding to the thickness of LiH between the source and the bottom of the hole in the first method. Zirconium is used because it has a flat scattering cross section and low absorption. A $B_4^{10}C$ block at the bottom of the hole intercepts the direct beam. This method, which has been carefully investigated by GA, yields the total-flux spectrum inside the medium at the depth of the zirconium scatterer. These spectral measurements are now being processed and will be reported in the forthcoming Neutron Physics Division annual report (ORNL-3193).

In addition to the energy spectral measurements, the data from the earlier BSF measurements[7] of the angular distribution of leakage neutrons from a 4-in.-thick LiH slab have been re-examined. The low-energy angular distribution, $\phi(\mu)$, is linear with μ and varies as $1 + A\mu$, where A increases with neutron energy. The measured values of A for epithermal neutrons are A = 2.3 and 1.9 for 5-ev and 1.5-ev neutrons, respectively, which are to be compared with calculated values (NIOBE Code calculations, see below) of A = 2.45 and 2.1. The calculated and measured values do

[8]S. N. Purohit, Neutron Phys. Div. Ann. Prog. Rep. Sept. 1, 1960, ORNL-3016, p. 191.

not compare for sub-cadmium neutrons because free atom cross sections were used in the calculations. The scattering law for LiH is not known in this energy region.

Current plans are to continue this investigation with a determination of high-energy leakage spectra and angular distributions, the results of which will be included in the Neutron Physics annual reports.

Calculations

An intercomparison of the spectra of neutrons in LiH calculated by three different techniques is under way. (The spectra will also be compared with the measured spectra discussed above.) Early this year NDA,* under subcontract with ORNL, completed some moments-method calculations of neutron spectra at three distances from four-point monoenergetic sources in an infinite LiH medium, the source energy varying from 10 kev to 16 Mev. More recently, the NDA NIOBE code (Direct Numerical Integration of the Boltzmann Equation) was used to compute internal energy spectra, leakage spectra as a function of escape angle, and leakage angular distributions as a function of energy for spherical LiH shells of several thicknesses around a fission source of neutrons.

The third calculational technique used the ORNL 05R code, a weighted Monte Carlo code. It was applied to the penetration of fission neutrons through flat slabs of LiH. Both the leakage spectra as a function of angle, $\phi(E,\mu_0)$, and the leakage angular distribution, $\phi(\mu,E_0)$, where μ is the cosine of the escape angle measured from the normal of the LiH slab, have been obtained with the code. The spectrum at several points within a reasonably thick slab of LiH is to be furnished soon.

All these calculations have recently been completed, with the exception of the last one, the 05R internal spectra in LiH. To date, close checks have been made in a small number of cases. There are minor disagreements, but none has yet been observed that may be considered important. Leakage angular distributions, both measured and calculated, are quite similar in the epicadmium region (above 0.5 ev), where the free-atom

*Now United Nuclear Corporation.

assumptions in the calculations are valid. Measured spectra, both leakage and internal, show a sharp rise with decrease in energy below 0.01 ev. This rise may be due to some systematic source of error as yet not ascertained. However, the data below 0.1 ev cannot be used for comparison with calculations because the calculations employed free-atom cross sections. The data below 0.1 ev may be useful as an aid in obtaining the scattering law for LiH in this energy region.

In general, the Monte Carlo codes are most easily adapted to realistic geometries. However, brute-force codes are inefficient and cannot calculate neutron penetration in a high-performance shield beyond a few inches without great expenditures of computer time. Weighting schemes have been developed to select the more penetrating neutrons, but each weighting scheme must be critically evaluated: it must be compared with experiment or with a less versatile but better established calculational technique for some equivalent geometric configuration. The moments-method calculations are applicable only to a configuration of a point source in an infinite medium. The NIOBE code is quite efficient, being semianlytical, and it has produced outputs for very deep neutron penetration. Unfortunately, however, the NIOBE code has not as yet been adapted to handle other than spherical geometry.

The progress of future calculations and comparisons will be reported in Neutron Physics Division annual progress reports.

Status of the Experiment for Determining the Spectrum of Prompt Gamma Rays from the Fission of U^{235} by Thermal Neutrons

R. W. Peelle F. C. Maienschein

Experimental pulse-height spectra of gamma rays emitted in coincidence with the thermal fission of U^{235} in a fission chamber were obtained some time ago with three types of scintillation spectrometers in the appropriate energy ranges. A small single crystal was used for energies below 800 kev, together with time-of-flight methods to eliminate fast-neutron effects. A Compton scintillation spectrometer was used for the range 400 to 2200 kev, and a pair scintillation spectrometer was utilized

for energies from about 1.6 Mev to the highest energy gamma rays observed at about 7.5 Mev. Preliminary analyses of these data have been published.[9]

In order to interpret accurately the observed pulse-height spectra, it is necessary to know the response of the spectrometers to gamma rays of all relevant energies. About 150 test pulse-height spectra were observed to provide this information, using radioactive sources and reaction gamma rays. At the time of the last progress report, all the experimental data had been accumulated, and efforts to ascertain the disintegration rates of the sources used for the test spectra had virtually been completed.[10] It remained to interpolate between the test spectra to find the responses of all the spectrometers for a gamma ray of arbitrary energy and to apply this information to the observed pulse-height spectra to obtain the "unscrambled" gamma-ray spectrum.

The calibration of the radioactive sources has now been completed, including results based on direct measurement and on the calibration of the high-pressure ionization chambers used.[11] Progress on the interpolation problem is described below.

In order to enable the fitting of a fairly simple formula to the pulse-height response functions for every gamma-ray energy, the method of nonlinear least-squares fitting was adopted, and an IBM-7090 program was prepared to handle the large mass of data. The program will also yield the output information needed to provide an error analysis of the results. (Previous workers have not produced plausible error analyses for unscrambled continuous gamma-ray spectra.) Quite adequate fitting of the response

---

[9]F. C. Maienschein et al., Proceedings of Second United Nations Internal Conference on the Peaceful Uses of Atomic Energy, Geneva, 1958, Vol. 15, pp. 366–72; see also R. W. Peelle, F. C. Maienschein, and T. A. Love, Neutron Physics Ann. Prog. Rep. Sept. 1, 1958, ORNL-2609, pp. 45–46; see also T. A. Love, F. C. Maienschein, and R. W. Peelle, Neutron Physics Ann. Prog. Rep. Sept. 1, 1959, ORNL-2842, pp. 93–97.

[10]F. C. Maienschein and R. W. Peelle, Neutron Physics Ann. Prog. Rep. Sept. 1, 1960, ORNL-3016, pp. 82–95.

[11]R. W. Peelle, Use of 4π High-Pressure Ionization Chambers as Secondary Standards for Calibration of Gamma-Ray Sources, ORNL CF-61-4-32, April 17, 1961.

functions for the Compton spectrometer has been demonstrated for nearly every test spectrum, and it is anticipated that by the end of this fiscal period the final parametric representation of the response of this spectrometer will have been completed.

In addition, all the test spectral data have been converted to the appropriate form for fitting (counts/kev vs kev) using the experimental gain relations, and by the end of fiscal year 1961 the experimental data for the pair spectrometer had been largely parameterized. The remaining problem of data unscrambling, a serious one both conceptually and numerically, will not have been completed. Descriptions of the methods used and the final resulting gamma-ray spectrum will be found in the future progress reports of the Neutron Physics Division.

Status of the Experiment for Determining the Spectrum of Short-Lived Fission-Product Gamma Radiation

W. Zobel

Upon completion of the experiment for determining the spectra of short-lived fission-product gamma radiation several years ago, it was decided to divide the analyses of the data into two phases: (1) the energy spectra at certain times after fission, and (2) the time spectra of several energy groups. Efforts were first directed toward the determination of the energy spectra, and a method of data reduction was developed which bypassed the usual difficulty caused by the so-called "nonuniqueness" effect inherent in any spectrometer. The application of the method resulted in the publication of energy spectra at times after fission varying from 1.7 to 1550 sec.[12,13]

Efforts have since been concentrated on the problem of analyzing the data taken for six energy groups as a function of time after fission. Thus

---

[12]W. Zobel, T. A. Love, G. M. Estabrook, and R. W. Peele, Neutron Physics Division Ann. Prog. Rep. Sept. 1, 1958.

[13]F. C. Maienschein et al., Proceedings of Second United Nations International Conference on the Peaceful Uses of Atomic Energy, Geneva, 1958, Vol. 15, pp. 366–72.

far the determination of the source term used in a preliminary analysis has been refined, and work is in progress to remove the influence of the instrument response on the data. For the latter, the energy spectra deduced from phase (1) are being used to estimate the correction required for each group owing to the "tails" from gamma rays with energies lying above or within the group. It is presently contemplated that a thorough error analysis will be performed for the final data.

Further work in this analysis will be reported in Neutron Physics Division annual progress reports.

Monte Carlo Calculations of Gamma-Ray Heating and Dose-Rate Distributions in Stratified Lead and Water Slabs

D. K. Trubey

In spite of the fact that considerable effort has been expended on the analysis of the Monte Carlo calculations of gamma-ray heating and dose rates in stratified lead and water slabs,[14,15] a large amount of analysis remains to be done. Specifically, a complete analysis of dose rates as a function of the angle of incidence is incomplete, as is the cataloging of reflected and transmitted energy and angular distributions. Since the original calculations were performed, however, great advances in computing machinery have been made, and it appears that further work should be directed toward recalculating many of the problems using the old data as a guide. The future of this work is at present undetermined.

Experimental Verification of a Geometrical Shielding Transformation

L. Jung
F. J. Muckenthaler
J. M. Miller
J. K. Grant

Data taking has been completed in the Lid Tank Shielding Facility experiment for testing the validity of the transformation

[14] L. A. Bowman and D. K. Trubey, ANP Semiann. Prog. Rep. Sept. 30, 1958, ORNL-2599, p. 123.

[15] L. A. Bowman and D. K. Trubey, ANP Semiann. Prog. Rep. Sept. 30, 1957, ORNL-2387, p. 320.

$$D(z,a) = \sum_{n=1}^{m} D\left[\sqrt{z^2 + \frac{(n-1)\,a^2}{m}}\ ,\ \frac{a}{\sqrt{m}}\right],$$

where

a = radius of the LTSF source plate (14 in.),

$\frac{a}{\sqrt{m}}$ = radius of a smaller source disk,

m = integer,

z = axial distance from source plate.

The m values used in the experiment were somewhat arbitrarily chosen to be 16, 9, 4, and 2, giving source-plate diameters of 7, 9.33, 14, and 19.80 in. These choices permitted study of a reasonable range of source-plate sizes and allowed a cross check between the 7- and 14-in.-diam source plates.

The data are now undergoing final analysis and evaluation. Preliminary computations tend to support the correctness of the transformation.

11. BIBLIOGRAPHY OF ORNL SHIELDING LITERATURE*

Author(s)	Title	Report Number	Publication Date
J. L. Meem E. B. Johnson	Determination of the Power of the Shield Testing Reactor. Part I. Neutron Flux Measurements in the Water-Reflected Reactor	ORNL-1027	8-13-51
A. Simon C. E. Clifford	The Attenuation of Neutrons in Air Ducts in Shields	ORNL-1217	11-11-52
B. R. Gossick	General Principles of a Proton Recoil Fast-Neutron Spectrometer	ORNL-1283	4-1-53
J. L. Meem E. B. Johnson	Determination of the Power of the Bulk Shielding Reactor – Part II	ORNL-1438	4-21-53
J. L. Meem L. B. Holland G. M. McCammon	Determination of the Power of the Bulk Shielding Reactor. Part III. Measurement of the Energy Released per Fission	ORNL-1537	Rev. 11-30-53
	Report of the 1953 Summer Shielding Session	ORNL-1575	6-11-54
H. E. Hungerford	The Skyshine Experiments at the Bulk Shielding Facility	ORNL-1611	7-2-54
F. N. Watson et al.	Lid Tank Shielding Tests for the Reflector-Moderated Reactor	ORNL-1616	10-5-54
R. G. Cochran J. L. Meem T. E. Cole E. B. Johnson	Reactivity Measurements with the Bulk Shielding Reactor	ORNL-1682	11-9-54
F. C. Maienschein	Gamma Radiation in a Divided Aircraft Shield	ORNL-1714	8-20-54
J. R. Bohannon	Cost Study of a Power Increase of the Bulk Shielding Reactor	ORNL-1790	5-19-55
F. C. Maienschein	A Hazards Summary for Routine Operation of the Bulk Shielding Facility Reactor at One Megawatt	ORNL-1823	12-14-54
G. T. Chapman C. L. Storrs	Effective Neutron Removal Cross Sections for Shielding	ORNL-1843	8-31-55
E. B. Johnson F. C. Maienschein R. G. Cochran K. M. Henry J. D. Flynn	Reactivity Measurements with the Bulk Shielding Reactor: Control Rod Calibration; Beam Hole Coefficients; Partial Reflector Coefficients	ORNL-1871	9-6-55
F. C. Maienschein	Attenuation by Water of Radiations from a Swimming-Pool Type Reactor	ORNL-1891	9-7-55

*Includes only those documents issued as ORNL reports or CF memoranda since 1953. (Exception: ORNL-1027 and ORNL-1217.)

Author(s)	Title	Report Number	Publication Date
T. A. Love R. W. Peelle F. C. Maienschein	Electronic Instrumentation for a Multiple Crystal Gamma-Ray Scintillation Spectrometer	ORNL-1929	10-3-55
F. C. Maienschein K. M. Henry	Operating Procedures for the Bulk Shielding Facility, Third Edition	ORNL-2018	11-28-55
F. C. Maienschein E. B. Johnson	A Bibliography of ORNL-BSF Reports Pertinent to Swimming-Pool Type Reactor Design	ORNL-2036 (Rev. from CF-55-5-45)	
C. D. Zerby	Radiation Flux Transformation as a Function of Density of an Infinite Medium with Anisotropic Point Sources	ORNL-2100	10-9-56
C. D. Zerby	A Monte Carlo Method of Calculating the Response of a Point Detector at an Arbitrary Position Inside a Cylindrical Shield	ORNL 2105	6-12-56
C. D. Zerby	Radiation Fluxes in a Cylindrical Cavity Resulting from an Idealized Entering Current	ORNL-2177	2-12-57
S. Auslender	A Monte Carlo Study of the Gamma-Ray Energy Flux, Dose Rate and Buildup Factors in a Lead-Water Slab Shield of Finite Thickness	ORNL-2194	1-10-57
R. W. Peelle F. C. Maienschein T. A. Love	The Energy and Angular Distribution of Gamma Radiation from a Co^{60} Source After Diffusion Through Many Mean-Free Paths of Water	ORNL-2196	8-12-57
D. K. Trubey G. T. Chapman	The Effective Neutron Removal Cross Sections of Carbon and Oxygen in Continuous Mediums	ORNL-2197	9-3-58
D. K. Trubey	An Estimation of Photoneutrons from C^{13} in an Oil Shield	ORNL-2200	5-13-58
C. D. Zerby	Transmission of Obliquely Incident Gamma Radiation Through Stratified Slab Barrier's (Master's Thesis) — Part I	ORNL-2224	11-29-56
C. D. Zerby	Transmission of Obliquely Incident Gamma Radiation Through Stratified Slab Barriers — Part II	ORNL-2224 Vol. II	1-8-57
C. D. Zerby	A Monte Carlo Calculation of Air-Scattered Neutrons	ORNL-2277	4-1-57
C. D. Zerby R. E. Lynch J. W. Benoit W. P. Johnson	A Monte Carlo Calculation of Air-Scattered Gamma Rays	ORNL-2292	9-10-58
D. R. Otis	The Lid Tank Shielding Facility of the ORNL — Part II. Determination of the Fission Rate of the Source Plate	ORNL-2350	7-7-59

Author(s)	Title	Report Number	Publication Date
J. Hilgeman F. L. Keller C. D. Zerby	Monte Carlo Calculations of Fluxes and Dose Rates Resulting from Neutrons Multiply Scattered in Air	ORNL-2375	12-15-58
C. D. Zerby H. S. Moran	Bremsstrahlung Spectra in NaI and Air	ORNL-2454	2-25-58
W. W. Dunn F. L. Keller C. D. Zerby	Gamma-Ray Dose Rate Resulting from Neutron Capture in Air	ORNL-2462	12-15-58
E. G. Silver J. Lewin	Safeguard Report for a Stainless Steel Research Reactor for the BSF (BSR-II)	ORNL-2470	7-16-58
W. R. Burrus	Radiation Transmission Through Boral and Similar Heterogeneous Materials Consisting of Randomly Distributed Absorbing Chunks	ORNL-2528	1-5-60
G. deSaussure	Calculation of the Photoneutron Flux in the Water Near the Bulk Shielding Reactor	ORNL-2545	7-9-58
C. D. Zerby H. S. Moran	Bremsstrahlung Spectra in an Infinite Sodium Iodide Medium	ORNL-2754	8-3-59
R. W. Peelle T. A. Love	Observation of Nonproportionality of Response for a NaI(Tl) Scintillation Crystal	ORNL-2801	10-20-59
E. Troubetskey H. Goldstein	A Compilation of Information on Gamma-Ray Spectra Resulting from Thermal-Neutron Captures	ORNL-2904	5-17-60
D. K. Trubey	The Single-Scattering Approximation to the Gamma-Ray Air-Scattering Problem	ORNL-2998	1-20-61
E. P. Blizard	The Shielding of Nuclear Powered Aircraft	CF-53-2-250	2-27-53
M. K. Hullings	Gamma-Ray Total Mass Absorption Coefficients	CF-53-2-266	2-12-53
J. L. Meem E. B. Johnson H. E. Hungerford	Energy per Fission and Power of the BSR	CF-53-5-21	5-12-53
R. G. Cochran K. M. Henry	Fast-Neutron Spectrum of the Bulk Shielding Reactor	CF-53-5-105	5-23-53
F. C. Maienschein F. Bly	A Calculation of the Gamma Radiation Reaching the ANP-53 Crew Shield	CF-53-5-117	8-24-53
M. K. Hullings T. V. Blosser	After-Shutdown Gamma Measurements at the BSF	CF-53-6-1	6-22-53
J. D. Flynn G. T. Chapman	Attenuation by Lead of Fast Neutrons from a Fission Source	CF-53-6-166	3-10-53
J. D. Flynn G. T. Chapman	The Effect of Iron Behind Beryllium in the ORNL Lid Tank (Expt. 38)	CF-53-6-185	6-30-53

Author(s)	Title	Report Number	Publication Date
E. P. Blizard G. T. Chapman J. D. Flynn	A Comparison of the Streaming of Thermal Neutrons Through Iron and Stainless Steel in the ORNL Lid Tank (Expt. 37)	CF-53-6-186	6-30-53
G. T. Chapman J. D. Flynn	A Comparison of the Shielding Properties of Iron and Stainless Steel in the ORNL Lid Tank (Expt. 38)	CF-53-6-187	6-30-53
E. P. Blizard H. E. Stern M. K. Hullings	Effective Fission Product Decay Rates for Various Reactor Operation and Shutdown Times	CF-53-8-47	8-14-53
M. P. Haydon E. B. Johnson J. L. Meem	Measurement of the Fast-Neutron Spectrum of the Bulk Shielding Reactor Using Nuclear Plates	CF-53-8-146	8-31-53
E. P. Blizard	Minimum Shield Weight Penalty for Air Ducts	CF-53-9-16	9-2-53
J. M. Miller C. L. Storrs	Shielding Properties of Uranium	CF-53-9-96	9-30-54
H. E. Stern	An Estimate of the Neutron Reflection Coefficient Using the Concept of Removal Cross Sections	CF-53-9-161	9-29-53
F. C. Maienschein T. A. Love	Spectrum of Gamma Rays Emitted by the BSR	CF-53-10-16	10-31-53
E. P. Blizard	The Shielding of Nuclear Radiations. Lecture 1: Introductory Survey	CF-53-11-2	10-1-54
M. K. Hullings	The Effect of Some Liquid-Metal Ducts on Reactor Shields	CF-53-11-53	2-12-54
F. H. Murray	Notes on the Calculation of the Attenuation of Neutrons Through Thick Shields	CF-53-11-64	11-30-53
J. E. Faulkner	Critique of LiH as a Neutron Shield	CF-53-12-13	12-2-53
C. E. Clifford	Estimate of Neutron and Gamma Doses Expected at Tower Shielding Facility	CF-53-12-23	12-11-53
F. H. Murray	Some Estimates of Removal Cross Sections Based on the Continuum Theory of the Scattering of Neutrons from Nuclei	CF-53-12-60	12-11-53
H. E. Stern	Calculations of Shielding for Burned-Out Reactor Fuel Elements	CF-53-12-111	12-23-53
C. L. Storrs	Statistical Fluctuation in the Fast-Neutron Dosimeter	CF-53-12-120	12-30-53
J. E. Faulkner	Analysis of the Response Characteristics of Fast-Neutron Dosimeter Integrating Circuit	CF-54-4-17	4-30-54
C. L. Storrs	Operation of the Glass-Hurst Pulse Integrator	CF-54-4-59	4-8-54

Author(s)	Title	Report Number	Publication Date
E. P. Blizard	Procedure for Obtaining Effective Removal Cross Sections from Lid Tank Data	CF-54-6-164	6-22-54
E. B. Johnson	Fuel Activation Methods for Power Determination of the ARE	CF-54-7-11	7-31-54
C. E. Clifford et al.	Effectiveness of Lead Gamma Shielding in the Fuel Elements of the Tower Shielding Reactor	CF-54-7-14	7-27-54
R. G. Cochran et al.	Reactor Radiations Through Slabs of Graphite	CF-54-7-105	8-31-54
H. E. Hungerford	Bulk Shielding Facility Tests of the GE-ANP R1 Divided Shield Mockup	CF-54-8-94	2-17-55
C. E. Clifford T. V. Blosser D. L. Gilliland J. Van Hoomissen F. N. Watson	A Preliminary Study of Fast-Neutron Ground and Air Scattering at the Tower Shielding Facility	CF-54-8-95	8-23-54
J. E. Faulkner	Single Isotropic Air Scattering of Neutrons in the Presence of the Ground (Unshielded Detector)	CF-54-8-96	8-31-54
J. E. Faulkner	Calculation of Fission Neutron Age in $NaZrF_5$	CF-54-8-97	8-31-54
J. E. Faulkner	Age Measurements in LiF	CF-54-8-98	8-31-54
J. E. Faulkner	Visible Light Produced in Air Around Reactors	CF-54-8-99	8-30-54
J. E. Faulkner	Neutron Leakage Spectrum of the BSR	CF-54-8-101	8-31-54
R. G. Cochran K. M. Henry J. D. Flynn	Oak Ridge Research Reactor Shadow Shield Experiment	CF-54-8-102	8-31-54
F. H. Murray	Single Anisotropic Air Scattering of Neutrons in the Presence of the Ground (Shielded Detector)	CF-54-8-104	8-18-54
E. P. Blizard	The Time Variation of Injury from Radiation	CF-54-9-119	9-30-54
C. D. Zerby	Preliminary Report on the Penetration Composite Slabs by Slant Incident Radiation	CF-54-9-120	9-21-54
G. T. Chapman et al.	Measurement of an Effective Neutron Removal Cross Section for Lithium at the Lid Tank Shielding Facility	CF-54-11-3	11-2-54
F. H. Murray	Anisotropic Scattering of Neutrons in a Uniform Medium with Beam Sources	CF-54-11-83	11-18-54
F. C. Maienschein K. M. Henry	Standard Operating Procedure for the Bulk Shielding Reactor	CF-55-1-131	1-25-55

Author(s)	Title	Report Number	Publication Date
D. L. Gilliland	Calibration of the Revalet, A Remotely Variable Lead-Transmission Gamma-Ray Dosimeter	CF-55-2-111	2-55
K. M. Henry M. P. Haydon	The Fission Neutron Spectrum of U^{233}	CF-55-4-22	(undated)
J. M. Miller	Effect of GE-ANP Helical Air Ducts in a Gamma Shield	CF-55-5-1	5-25-55
F. H. Murray	Analysis of the Constant Velocity Transport Equation with the Aid of Eigenfunctions of the Various Media	CF-55-5-2	5-5-55
F. C. Maienschein E. B. Johnson	A Bibliography of ORNL-BSF Reports Pertinent to Swimming-Pool Type Reactor Design	CF-55-5-45 (Rev. as ORNL-2036)	6-29-55
J. Van Hoomissen H. E. Stern	Comparison of Hydrogenous Materials for Use in Aircraft Shields	CF-55-6-40	6-9-55
J. B. Dee C. A. Goetz J. R. Smolen	Sources of Radiation in a 300-Mw Circulating Fuel Reactor	CF-55-7-35	7-12-55
K. M. Henry J. N. Anno	Element After-Heating	CF-55-11-94	11-17-55
C. E. Clifford	Proposal for a Design Study for the Shield Mockup Reactor	CF-55-11-81	11-17-55
E. P. Blizard	Gamma-Ray Shielding	CF-56-1-48	1-12-56
J. R. Smolen	Physical Properties of Boral Used in Lid Tank Mockups	CF-56-1-94	1-23-56
J. B. Dee C. A. Goetz D. K. Trubey	Gamma-Ray Dose Rate from the ART	CF-56-1-181	1-9-56
W. J. McCool	Method of Mixing Borated Water at the Lid Tank Shielding Facility	CF-56-2-79	2-20-56
R. B. Murray	Fast-Neutron Spectrometer Development	CF-56-11-5	11-5-56
C. D. Zerby	Transformation of TSF Data to Apply at Various Altitudes	CF-56-12-19	12-10-56
W. G. Blessing	Power Distribution of Tower Shielding Facility Reactor (TSR)	CF-57-1-164	1-17-57
D. R. Otis	Preliminary LTSF Data Report on Experiments with Advanced Shielding Materials (Li, H, Zr, Be, Stainless Steel, H, Hevimet, Pb, and U) (Expt. 69)	CF-57-2-8	2-8-57
D. R. Otis	Neutron and Gamma-Ray Attenuation for a Fission Source in Water — Comparison of Theory With LTSF Measurements	CF-57-3-48	3-15-57

Author(s)	Title	Report Number	Publication Date
G. deSaussure	A Calculation of the Gamma-Ray Spectrum of the Bulk Shielding Facility	CF-57-7-105	8-31-57
F. N. Watson C. E. Clifford J. L. Hull	Manual of Routine and Emergency Operating Procedures for the TSF	CF-57-11-39	11-14-57
C. D. Zerby	The Effect of Anisotropic Scattering on the Neutron Flux in Air	CF-57-12-10	12-4-57
V. R. Cain C. E. Clifford F. N. Green W. E. Price C. R. Fink	Penetration of Fast Neutron Air-Scattered Dose Rate from the TSR Through the Sides of a Cylindrical Crew Compartment	CF-57-12-26	
L. A. Bowman D. K. Trubey	Stratified Slab Gamma-Ray Dose Rate Buildup Factors for Lead and Water Shields	CF-58-1-41	1-16-58
C. E. Clifford	ASTR-TSF Operation and Checking Procedures	CF-58-3-78	4-8-58
F. N. Watson	Gamma-Ray and Fast-Neutron Dose Rates in Air as a Function of Distance from the TSF Reactor	CF-58-4-6	4-15-58
Bowman, Dunn, Lessig, and Touchey	A Calculation of the Energy Spectrum and Angular Distribution of Gamma Rays at the Surface of the BSF Reactor	CF-58-4-75	4-15-58
V. R. Cain F. J. Muckenthaler C. E. Clifford	Study of Gamma Rays Produced by Neutron Interactions in Air	CF-58-4-77	5-29-58
S. K. Penny	A Monte Carlo Code for Deep Penetration of Gamma Rays	CF-58-6-30	6-4-58
L. A. Bowman	Deposition of Gamma-Ray Heating in Stratified Lead and Water Slabs	CF-58-7-99	7-28-58
J. Lewin	TSR-II Second Pass Heat Transfer	CF-59-1-111	1-28-59
V. R. Cain	Prediction of Radiation Intensities at Large Distances from the TSR-II	CF-59-3-58	3-17-59
S. C. Dominey D. R. Ward F. J. Muckenthaler	TSF Studies in Support of GE-ANP Program — Rechecks and Extension of the 2π Shield Experiments	CF-59-4-72	4-17-59
C. D. Zerby	Monte Carlo Code for the Calculation of Response Functions of Gamma-Ray Scintillation Detection	CF-59-11-90	11-24-59
G. T. Chapman T. A. Love	A Comparison of Experimental Gamma-Ray Response Measurements with Calculations for an 8-in. Right Cylindrical NaI(T*l*) Crystal	CF-59-11-93	11-24-59

Author(s)	Title	Report Number	Publication Date
F. C. Maienschein R. W. Peelle T. A. Love	Recent Fission Gamma-Ray Spectral Measurements	CF-59-11-94	11-24-59
J. Lewin	Standard Operating Procedure for TSR-II	CF-60-4-89	April 60
C. F. Zerby H. S. Moran	IBM-704 Code for Predicting the Response of Gamma-Ray Scintillation Counters	CF-60-5-72	5-19-60
T. A. Love R. B. Murray	Use of Silicon Surface Barrier Counters in Fast-Neutron Detection and Spectroscopy	CF-60-5-121	5-31-60
H. A. Todd R. D. Smiddie	Use of the DD2 Amplifier with the RIDL 200- and 400-Channel Analyzer	CF-60-9-107	9-23-60

[redacted]

Reports previously issued in this series are as follows:

ORNL-528	Period Ending November 30, 1949
ORNL-629	Period Ending February 28, 1950
ORNL-768	Period Ending May 31, 1950
ORNL-858	Period Ending August 31, 1950
ORNL-919	Period Ending December 10, 1950
ANP-60	Period Ending March 10, 1951
ANP-65	Period Ending June 10, 1951
ORNL-1154	Period Ending September 10, 1951
ORNL-1170	Period Ending December 10, 1951
ORNL-1227	Period Ending March 10, 1952
ORNL-1294	Period Ending June 10, 1952
ORNL-1375	Period Ending September 10, 1952
ORNL-1439	Period Ending December 10, 1952
ORNL-1515	Period Ending March 10, 1953
ORNL-1556	Period Ending June 10, 1953
ORNL-1609	Period Ending September 10, 1953
ORNL-1649	Period Ending December 10, 1953
ORNL-1692	Period Ending March 10, 1954
ORNL-1729	Period Ending June 10, 1954
ORNL-1771	Period Ending September 10, 1954
ORNL-1816	Period Ending December 10, 1954
ORNL-1864	Period Ending March 10, 1955
ORNL-1896	Period Ending June 10, 1955
ORNL-1947	Period Ending September 10, 1955
ORNL-2012	Period Ending December 10, 1955
ORNL-2061	Period Ending March 10, 1956
ORNL-2106	Period Ending June 10, 1956
ORNL-2157	Period Ending September 10, 1956
ORNL-2221	Period Ending December 31, 1956
ORNL-2274	Period Ending March 31, 1957
ORNL-2340	Period Ending June 30, 1957
ORNL-2387	Period Ending September 30, 1957
ORNL-2440	Period Ending December 31, 1957
ORNL-2517	Period Ending March 31, 1958
ORNL-2599	Period Ending September 30, 1958
ORNL-2711	Period Ending March 31, 1959
ORNL-2840	Period Ending October 31, 1959
ORNL-2942	Period Ending April 30, 1960
ORNL-3029	Period Ending October 31, 1960
ORNL-3144	Period Ending April 30, 1961

[redacted]

ORNL-3226

C-84 – Reactors–Special Features
of Aircraft Reactors
M-3679 (25th ed.)

Internal Distribution

1. G. M. Adamson
2. J. W. Allen
3. S. E. Beall
4. D. S. Billington
5. F. F. Blankenship
6. E. P. Blizard
7. A. L. Boch
8. G. E. Boyd
9. R. B. Briggs
10. A. D. Callihan
11. R. E. Clausing
12. W. B. Cottrell
13. F. L. Culler
14. D. A. Douglas
15. J. L. Fowler
16. A. P. Fraas
17. J. H. Frye
18. R. J. Gray
19. W. R. Grimes
20. E. Guth
21. W. O. Harms
22. T. Hikido
23. M. R. Hill
24. N. E. Hinkle
25. E. E. Hoffman
26. H. W. Hoffman
27. A. Hollaender
28. L. B. Holland
29. H. Inouye
30. W. H. Jordan
31. F. Kam
32. G. W. Keilholtz
33. C. P. Keim
34. J. J. Keyes
35. P. G. Lafyatis
36. W. R. Laing
37. C. E. Larson (K-25)
38. R. S. Livingston
39. R. N. Lyon
40. H. G. MacPherson
41. R. E. Maerker
42. F. C. Maienschein
43. W. D. Manly
44. A. J. Miller
45. K. Z. Morgan
46. E. D. Muckenthaler
47. E. L. Nelson
48. P. Patriarca
49. S. K. Penny
50. M. M. Perry
51. H. W. Savage
52. A. M. Savolainen
53. E. D. Shipley
54. O. Sisman
55. M. J. Skinner
56. G. M. Slaughter
57. A. H. Snell
58. I. Spiewak
59. B. J. Sturm
60. C. D. Susano
61. J. A. Swartout
62. D. B. Trauger
63. D. K. Trubey
64. G. M. Watson
65. A. M. Weinberg
66. J. C. White
67. C. E. Winters
68-73. Laboratory Records Department
74. Laboratory Records, ORNL R.C.
75-77. ORNL – Y-12 Technical Library
Document Reference Section
78-79. Central Research Library

[redacted]

[redacted]

External Distribution

80. Aerojet-General, Azusa (BUWEPS)
81-94. Aeronautical Systems Division
95-96. AiResearch Manufacturing Company of Arizona
97. Air Force Space Systems Division
98-99. Air Force Special Weapons Center
100. Air Technical Intelligence Center
101. Albuquerque Operations Office
102. Argonne National Laboratory
103. Army Engineer Research and Development Laboratories
104-109. Atomic Energy Commission, Washington
110. Atomics International
111. Battelle Memorial Institute
112. Brookhaven National Laboratory
113-114. Bureau of Naval Weapons
115. Chance Vought Aircraft, Inc., Dallas (BUWEPS)
116-117. Chicago Operations Office
118. Chicago Patent Group
119-121. Convair Division, Fort Worth
122. Convair Division, San Diego
123. Convair Division, San Diego (BUWEPS)
124. Defense Atomic Support Agency, Washington
125. duPont Company, Aiken
126-133. General Electric Company (ANPD)
134-136. General Electric Company, Richland
137. General Nuclear Engineering Corporation
138. Jet Propulsion Laboratory
139-140. Knolls Atomic Power Laboratory
141. Lockheed Aircraft Corporation, Burbank
142. Los Alamos Scientific Laboratory
143. Marquardt Corporation
144. Martin Company
145. Martin Company, Baltimore (BUWEPS)
146. NASA Ames Research Center
147. NASA Flight Research Center
148. NASA George C. Marshall Space Flight Center
149. NASA Langley Research Center
150-154. NASA Lewis Research Center
155-156. National Aeronautics and Space Administration, Washington
157. National Bureau of Standards
158. Naval Air Development Center
159. Naval Air Material Center
160. Naval Air Turbine Test Station
161. Naval Postgraduate School
162. Naval Radiological Defense Laboratory
163. Naval Research Laboratory
164. New York Operations Office
165. North American Aviation, Inc., Downey
166. Office of the Chief of Naval Operations

[redacted]

[redacted]

167. Patent Branch, Washington
168-169. Phillips Petroleum Company (NRTS)
170-173. Pratt and Whitney Aircraft Division
174. Public Health Service
175. RAND Corporation
176. Sandia Corporation
177-178. School of Aviation Medicine
179. Secretary of the Air Force, R&D
180. Sylvania Electric Products, Inc.
181. Technical Research Group.
182-183. United Nuclear Corporation (NDA)
184-185. University of California, Livermore
186-188. Westinghouse Bettis Atomic Power Laboratory
189-213. Division of Technical Information Extension
214. Division of Research and Development, AEC, ORO
215-216. Reactor Division, AEC, ORO

[redacted]